CHANNEL ESTIMATION TECHNIQUES FOR FILTER BANK MULTICARRIER BASED TRANSCIEVERS FOR NEXT GENERATION OF WIRELESS NETWORKS

BY

IJIGA, OWOICHO EMMANUEL (1246149)

owoicho.ijiga1@students.wits.ac.za

A dissertation submitted to the School of Electrical/Information Engineering,
Faculty of Engineering and the Built Environment,
University of the Witwatersrand,
Johannesburg, South Africa,
in fulfillment of the requirements for the degree of Master of Science in Engineering (MscEng).

28th August, 2017

DECLARATION

I, Owoicho E. **Ijiga,** declare that this dissertation is my own original work. It is been submitted for the Degree of Master of Science (in Engineering) to the University of the Witwatersrand, Johannesburg. It has not been submitted before for any degree or examination to any other university.

Signed: ……

……..…. Day of ……..... year ……

DEDICATION

The entire research work and write-up is dedicated to God, the Father Almighty and His Son, Jesus Christ together with His Holy Spirit.

PREFACE

This dissertation gives a detailed account of the research work that has been accomplished in requirement for the degree of M.Sc (Eng) at the University of the Witwatersrand, Johannesburg, South Africa and was assisted by the Center for Telecommunication Access and Services (CeTAS), University of the Witwatersrand, Johannesburg, South Africa as well as the Wits University Postgraduate Merit Award (WITS-PMA).

This research addresses the development of pilot-aided channel estimation for two filter bank multi-carrier waveforms namely orthogonal frequency division multiplexing with offset quadrature amplitude modulation and the generalized frequency division multiplexing with offset quadrature amplitude modulation based systems in fast and slow Rayleigh fading multipath channel conditions assuming near perfect reconstruction and imperfect reconstruction of prototype filter designs. To the best of my knowledge, this work is original except where acknowledgements are made to works already documented in literature.

ACKNOWLEDGEMENTS

I wish to firstly express distinctive gratitude to God, the Father almighty for his incessant inspirations, guidance and provision during the entire period of this research work.

My profound gratitude goes to my supervisor, Dr. Asad Mahmood, who consistently provided effective and beneficial advice to ensure that the objectives of this research are actualized. My sincere appreciation also goes to Professor Takawira Fambirai and Dr. Olutayo O. Oyerinde for providing me with beneficial advise and motivation in the course of this research work while also acknowledging the postgraduate coordinator (Prof. Ivan Hofsajer) and the head of school (Prof. Estelle Trengove), who provided beneficial guidance and motivation that led the completion of this research.

I give overwhelming thanks to my parents Mr. and Mrs. Eche F. Ijiga, who kept on encouraging me by providing motivation, financial support and prayers to ensure this research is completed. I also appreciate my siblings Onuh, Ooja, Onma and Amina who kept on praying for me and providing words of encouragements, not forgetting my extended family members that kept on motivating me throughout this research period.

I am grateful to all friends and family who kept on motivating me during difficult times especially; Daniel Ewim, Mr/ Mrs Edwin. S. Audu, Dr. Andrew Eloka-Eboka, Muyiwa B. Balogun, Malcolm M. Sande, Ebetsamang Thupae, Godfrey Akpakwu, Mrs E. A. Odekina, Olayinka Ogundile, Alexander Olawole, Ms. Moniera Ismail, Ms. Rose Saunders, Ms. Mumtaz Adam and all CETAS members.

I appreciate the Wits university Holy Trinity Catholic Church students choir and also give thanks to Rev. Fr. John Enslin and Rev. Fr. Graham Pugin of Holy Trinity Catholic church, Braamfontein, Johannesburg, as well as Rev. Fr. Manuel Graça for providing me with spiritual guidance during the period of this research.

Lastly, the financial support of the Wits University Center for Telecommunication Access and Services as well as the University of the Witwatersrand Postgraduate Merit Award (WITS-PMA) is highly acknowledged.

ABSTRACT

The fourth generation (4G) of wireless communication system is designed based on the principles of cyclic prefix orthogonal frequency division multiplexing (CP-OFDM) where the cyclic prefix (CP) is used to combat inter-symbol interference (ISI) and inter-carrier interference (ICI) in order to achieve higher data rates in comparison to the previous generations of wireless networks. Various filter bank multicarrier systems have been considered as potential waveforms for the fast emerging next generation (xG) of wireless networks (especially the fifth generation (5G) networks). Some examples of the considered waveforms are orthogonal frequency division multiplexing with offset quadrature amplitude modulation based filter bank, universal filtered multicarrier (UFMC), bi-orthogonal frequency division multiplexing (BFDM) and generalized frequency division multiplexing (GFDM). In perfect reconstruction (PR) or near perfect reconstruction (NPR) filter bank designs, these aforementioned FBMC waveforms adopt the use of well-designed prototype filters (which are used for designing the synthesis and analysis filter banks) so as to either replace or minimize the CP usage of the 4G networks in order to provide higher spectral efficiencies for the overall increment in data rates. The accurate designing of the FIR low-pass prototype filter in NPR filter banks results in minimal signal distortions thus, making the analysis filter bank a time-reversed version of the corresponding synthesis filter bank. However, in non-perfect reconstruction (Non-PR) the analysis filter bank is not directly a time-reversed version of the corresponding synthesis filter bank as the prototype filter impulse response for this system is formulated (in this dissertation) by the introduction of randomly generated errors. Hence, aliasing and amplitude distortions are more prominent for Non-PR.

Channel estimation (CE) is used to predict the behaviour of the frequency selective channel and is usually adopted to ensure excellent reconstruction of the transmitted symbols. These techniques can be broadly classified as pilot based, semi-blind and blind channel estimation schemes. In this dissertation, two linear pilot based CE techniques namely the least square (LS) and linear minimum mean square error (LMMSE), and three adaptive channel estimation schemes namely least mean square (LMS), normalized least mean square (NLMS) and recursive least square (RLS) are presented, analyzed and documented. These are implemented while exploiting the near orthogonality properties of offset quadrature amplitude modulation (OQAM)

to mitigate the effects of interference for two filter bank waveforms (i.e. OFDM/OQAM and GFDM/OQAM) for the next generation of wireless networks assuming conditions of both NPR and Non-PR in slow and fast frequency selective Rayleigh fading channel. Results obtained from the computer simulations carried out showed that the channel estimation schemes performed better in an NPR filter bank system as compared with Non-PR filter banks. The low performance of Non-PR system is due to the amplitude distortion and aliasing introduced from the random errors generated in the system that is used to design its prototype filters. It can be concluded that RLS, NLMS, LMS, LMMSE and LS channel estimation schemes offered the best normalized mean square error (NMSE) and bit error rate (BER) performances (in decreasing order) for both waveforms assuming both NPR and Non-PR filter banks.

Keywords: Channel estimation, Filter bank, OFDM/OQAM, GFDM/OQAM, NPR, Non-PR, 5G, Frequency selective channel.

TABLE OF CONTENTS

CHAPTER ONE

INTRODUCTION

CHAPTER TWO

DESIGN AND ANALYSIS OF FILTER BANK MULTICARRIER SYSTEMS

CHAPTER THREE

FUNDAMENTALS OF CHANNEL ESTIMATION

CHAPTER FOUR

SYSTEM MODEL DESCRIPTION

CHAPTER FIVE

SIMULATIONS AND RESULTS

CHAPTER SIX

CONCLUSIONS & FUTURE WORKS

LIST OF ABBREVIATIONS

1G	First Generation
2G	Second Generation
3G	Third Generation
4G	Fourth Generation
xG	NeXt Generation
5G	Fifth Generation Network
AWGN	Additive White Gaussian Noise
AFB	Analysis Filter Bank
BFDM	Bi-orthogonal Frequency Division Multiplexing
BER	Bit Error Rate
CFO	Carrier Frequency Offset
CE	Channel Estimation
CIR	Channel Impulse Response
CDMA	Code Division Multiple Access
CVUFB	Complex-Valued Unitary Filter Bank
CMFB	Cosine Modulated Filter Banks
CP	Cyclic Prefix
DSP	Digital Signal Processing
DVB – T	Digital Video Broadcasting – Terrestrial
DFT	Discrete Fourier Transform
DWMT	Discrete Wavelet Multitone
EMFB	Exponentially Modulated Filter Banks

ELT	Extended Lapped Transforms
FFT	Fast Fourier Transform
FMT	Filtered Multitone
FBMC	Filter Bank Multi Carrier
FIR	Finite Impulse Response
FDMA	Frequency Division Multiple Access
GFDM	Generalized Frequency Division Multiplexing
IIR	Infinite Impulse Response
ICI	Inter-Carrier Interference
ISI	Inter-Symbol Interference
IDFT	Inverse Discrete Fourier Transform
IFFT	Inverse Fast Fourier Transform
LMS	Least Mean Square
LS	Least Square
LMMSE	Linear Minimum Mean Square Error
LC-TED	Low Complexity Timing Error Detector
MTC	Machine Type Communication
MPSK	M-ary Phase-Shift Keying
ML	Maximum Likelihood
MSE	Mean Square Error
MDFT	Modified Discrete Fourier Transform
MLS	Modified Least Square
MCM	Multi-Carrier Modulation

NPR	Nearly Perfect Reconstruction
Non - PR	Non Perfect Reconstruction
NLMS	Normalized Least Mean Square
NMSE	Normalized Mean Square Error
OQAM	Offset Quadrature Amplitude Modulation
OFDM	Orthogonal Frequency Division Multiplexing
OOB	Out-of-Band
PAPR	Peak to Average Power Ratio
PR	Perfect Reconstruction
QAM	Quadrature Amplitude Modulation
RLS	Recursive Least Squares
ROF	Roll-Off Factor
SNR	Signal to Noise Ratio
SER	Symbol Error Rate
SFB	Synthesis Filter Bank
TI	Tactile Internet
TDMA	Time Division Multiple Access
UFMC	Universal Filtered Multicarrier

LIST OF NOTATIONS

λ	Delay spread index
τ_i	ith path delay spread
μ	Fixed positive step size parameter
M	Number of subcarriers used
K	Overlapping factor
L_p	Length of the FBMC prototype filter
N_P	Number of pilot symbols
f_d	ith path Doppler frequency shift
T_s	Sample period
n	OQAM preprocessing output/post processing input sample index
m	Symbol index at SFB output
l	OQAM preprocessing input/post processing output sample index
k	Subcarrier index
v	Velocity of the moving mobile
$\frac{E_b}{N_o}$	Energy per Bit to Noise Spectral Density Ratio
$p[\dot{n}, k]$	Finite impulse response of low-pass prototype filter
$g[\dot{n}, k]$	Complex modulated Synthesis filter bank channel impulse response
$w[\dot{n}, k]$	Mutually independent, zero-mean complex AWGN
$f[\dot{n}, k]$	Analysis filter bank channel impulse response
$s[\dot{n}, k]$	Received output symbols before channel estimation for OFDM/OQAM
$\vec{x}_R[n, k']$	Received output symbols before channel estimation for GFDM/OQAM
$h[n, k]$	Channel impulse responses

$x[n,k]$	Staggered OQAM input symbols
$\boldsymbol{R}_{HH}[n,k]$	Autocorrelation matrix of the channel impulse response
$\eta[n,k]$	Gaussian noise process
$\widehat{\boldsymbol{h}}_{LS}[n,k]$	Least Square channel impulse response
$\widehat{\boldsymbol{h}}_{LMMSE}[n,k]$	LMMSE channel impulse response
$\widehat{\boldsymbol{h}}_{LMS}[n,k]$	LMS adaptive channel impulse response
$\widehat{\boldsymbol{h}}_{RLS}[n,k]$	RLS adaptive channel impulse response
$\boldsymbol{e}[n,k]$	Channel estimation error
$\widetilde{\boldsymbol{g}}[k,n]$	RLS gain vector
$\tilde{\mathrm{g}}[n,k']$	RLS gain vector for GFDM/OQAM
$\mathrm{R}^{-1}[n,k']$	Inverse autocorrelation matrix for GFDM/OQAM
$\boldsymbol{e}^{*}[n,k]$	Adaptive channel estimation error for OFDM/OQAM
$\mathrm{e}^{*}[n,k']$	Adaptive channel estimation error for GFDM/OQAM

LIST OF FIGURES

LIST OF TABLES

CHAPTER ONE

INTRODUCTION

1.1 EVOLUTION OF MODERN WIRELESS COMMUNICATION SYSTEMS

Wireless communication networks are regulated by a fixed spectrum assignment policy. A huge amount of the assigned frequency spectrum is usually underutilized. This has pressed for the need to adequately exploit the scarce frequency spectrum [1 - 5]. Multiple access methods provide an efficient way for several communication users to effectively share the same spectrum resource (channel) without causing interference with one another. Three basic examples of multiple access schemes are adopted to accommodate multiple users. These access schemes are the frequency division multiple access (FDMA), time division multiple access (TDMA) and code division multiple access (CDMA) schemes [6]. In FDMA schemes, each user is allocated a frequency channel where they can transmit their respective signals at the same time over the available spectrum resource while in TDMA schemes, multiple users are allowed to transmit their signals at the same frequency over the available frequency spectrum in different time slots. Code division multiple access schemes are multiple access technologies that allow multiple users to simultaneously and asynchronously access a spectrum resource by modulating and spreading their information signals with pre-assigned signature codes (or spreading codes) which are orthogonal to one another [7]. The spread-spectrum nature of CDMA-based schemes makes them to offer some advantages over their TDMA and FDMA counterparts. These advantages include improvement in spectral efficiency, larger system capacity, higher security and better anti-interference ability, etc. [8]. The past, present and next generation of wireless networks are designed based on the basic principles of one or a hybridization of any of the above mentioned access methods. The evolution of these wireless networks is presented in subsequent subsections of this section.

1.1.1 FIRST GENERATION OF WIRELESS NETWORKS

The first generation (1G) of wireless networks became operational in 1979 [8]. The 1G of cellular systems is also known as *analog cellular systems* because the design of these cellular systems is based on FDMA and analog frequency modulation technology. The first mobile phone

system of this generation of wireless networks is called advanced mobile phone system (AMPS) and it is also the first United States of America (U.S.A.) cellular phone system which was deployed in 1983 [6].

1.1.2 SECOND GENERATION OF WIRELESS NETWORKS

Digital modulation technique was introduced as the main modulation method in the second generation (2G) of cellular systems unlike its 1G counterparts that are designed based on analog frequency modulation schemes. This is because the 2G of wireless systems are designed based on either TDMA or CDMA technology. Examples of TDMA-based cellular systems include the global system for mobile (GSM) communications (adopted in Europe), Pacific digital cellular (PDC) systems (adopted in Japan) and the U.S.A. adopted interim standard 54 (IS-54). In the 2G of wireless systems, interim standard 95 (IS-95) was also adopted in the USA and is designed based on narrowband CDMA [6]. The 2G of cellular systems were standardized in the 1990s and were upgraded subsequently to provide higher throughput rates for improvement in modern internet applications so as to realize the 2.5G standards. The 2.5G networks brought in some popular applications such as wireless application protocol (WAP), general packet radio services (GPRS), enhanced data rates for GSM evolution (EDGE) and the high speed circuit switched data (HSCSD).

1.1.3 THIRD GENERATION OF WIRELESS NETWORKS

The third generation (3G) of mobile phone standards (superseding the 2.5G standards) enabled network operators to provide users with greater network capacities by improving the spectral efficiency while providing improvement in telephone services such as video-calls, broadband wireless data and wide-area wireless voice telephony [6]. This generation of wireless networks are based on CDMA scheme where air interface standards such as wideband-CDMA (WCDMA), CMDA 2000 and time division synchronous CDMA (TD-SCDMA) were developed. WCDMA standards were adopted across Europe, Japan and Asia while CDMA 2000 (which is an upgrade version of the second generation IS-95) was adopted across North America and South Korea. The TD-SCDMA is a 3G standard adopted in China that is based on time division duplexing (TDD) unlike its WCDMA and CDMA 2000 counterparts that are all based on frequency division duplexing (FDD). The 3G of networks introduced additional features

(protocol) such as high speed downlink packet access (HSDPA) that aids the systems to achieve higher data speed communications and increased system capacity.

1.1.4 FOURTH GENERATION OF WIRLESS NETWORKS

It was predicted that by the end of 2014, the total number of connected devices will run over the total number of people in the world. It is also predicted that in 2018, the number of mobile-connected devices across the globe will exceed ten billion [9] which explains the high demand for data rates and need for efficient spectrum utilization. In order to cope with the high demand for data rates, need for lower end-to-end latency, better system throughput and lower power consumption (in comparison to previous generation of networks), the fourth generation (4G) of mobile networks has been proposed (in 2008) [10] with specifications based on the long term evolution (LTE) standards for wireless broadband communication networks [11, 12]. The LTE project was actually initiated in 2004 by the third generation partnership project (3GPP) while the specifications of its first version was documented in March 2008 (by the 3GPP) known as release 8 (REL-8) which requires a download speed of 300 Mbits/s [13, 14]. Improved LTE specifications were documented in LTE release 9 (REL-9) and the recently finalized 3GPP LTE-advanced (LTE-A) with specifications documented in release 12 (March, 2015) [15]. The 4G networks exploit technologies such as orthogonal frequency division multiple access (OFDMA), multiple input multiple output (MIMO) and single carrier-FDMA (SC-FDMA) in order to deliver higher data rates, robustness against system interference as well as better spectrum management where OFDMA is adopted for downlink transmissions while SC-FDMA is adopted for uplink transmission [15, 16]. The specification of LTE standards require an instantaneous maximum downlink data rate of 100 Mbits/s (in 4G LTE) [11] to 1000 Mbits/s in LTE-A.

1.1.5 NEXT GENERATION OF WIRELESS NETWORKS

In communication engineering, the evolution of mobile phones into smartphones designed with very high screen resolutions and cameras has led to further increase demand for very high data rates. The future fifth generation (5G) networks is specified to offer 10 to 100 times higher user data rates in comparison to the current 4G networks [17], however this emerging generation of networks have been designed with several other requirements that go far beyond higher data rates [11, 15, 16]. Some main scenarios for this generation of networks are *machine type communication* (MTC) [18, 19], *tactile internet* (TI) [20] and *wireless regional area networks*

(WRAN) [21] while requirements such as ultra-low latency (for TI), low power consumption (for MTC communications) and low out-of-band (OOB) emission are put into paramount consideration for this emerging generation of communication systems [22]. These requirements (of 5G networks) make it difficult for OFDM schemes to be considered as the main multiplexing technology for the next generation (xG) networks because the low power consumption requirements which MTC requires may not be sufficient to maintain the orthogonality of OFDM subcarriers as continuous and accurate synchronizations are required for this scheme [23]. It is a well-known fact that the CP of OFDM based schemes reduces the spectral efficiency of the wireless communication system, thus resulting into poor utilization of the scarce and expensive bandwidth [24 - 30]. The rectangular pulse shaping adopted in these schemes (OFDM) can also cause extensive spectral leakage to the adjacent frequency bands. Another demerit of CP-OFDM based schemes is the introduction of large sidelobes that may result into the creation of ISI and ICI as well as the introduction of large out-of-band (OOB) emissions which may cause interference [31, 32]. This can lead to energy wastage while giving rise to possible timing offsets (arising from poor carrier synchronizations) [33, 34]. The modulated signals obtained in these schemes usually exhibit very high peak-to-average power ratio (PAPR) [23, 35]. Furthermore, the requirements of future generation networks (for instance TI applications), require short data bursts which make the poor bandwidth utilization of CP-OFDM based systems unsuitable for this generation of networks [5]. The poor bandwidth utilization of these systems makes them unsuitable for WRAN applications as the duration of the CIR is in the range of tenths of microseconds [36]. All these shortcomings of OFDM transmission technology make it not to be the most promising multiplexing scheme for the xG networks. Alternative filter bank MCM technologies have been proposed as promising candidates to address these shortcomings (of CP-OFDM based schemes) for the next generation of mobile systems. These filter bank technologies include *orthogonal frequency division multiplexing based on offset quadrature amplitude modulation* (OFDM/OQAM), *universal filtered multicarrier* (UFMC) [37], *bi-orthogonal frequency division multiplexing* (BFDM) [38, 39], and *generalized frequency division multiplexing* (GFDM) [40] based schemes. An introduction to these waveforms for 5G networks is given in Section 1.2.

1.2 INTRODUCTION TO MCM AND WAVEFORMS FOR 5G NETWORKS

The speedy growth of wireless communication in recent years has placed huge demands on available frequency spectrum, making it a scarce resource [41]. In multicarrier modulation (MCM) schemes, data can easily be transmitted simultaneously over a set of multiple narrowband subcarriers. In these schemes, a wideband signal is split (at high symbol rate) into multiple lower rate signals where each low rate signal is modulated onto a narrowband subchannel (also known as subcarrier) [42] as illustrated in Fig. 1.1 (a). Multicarrier modulation schemes offer several advantages over their single carrier modulation (SCM) counterparts. One notable advantage is in their ability to offer higher spectral efficiency as compared to SCM schemes due to the overlapping of subcarriers [43]. The basic design principle of SCM schemes is shown in Fig 1.1 (b).

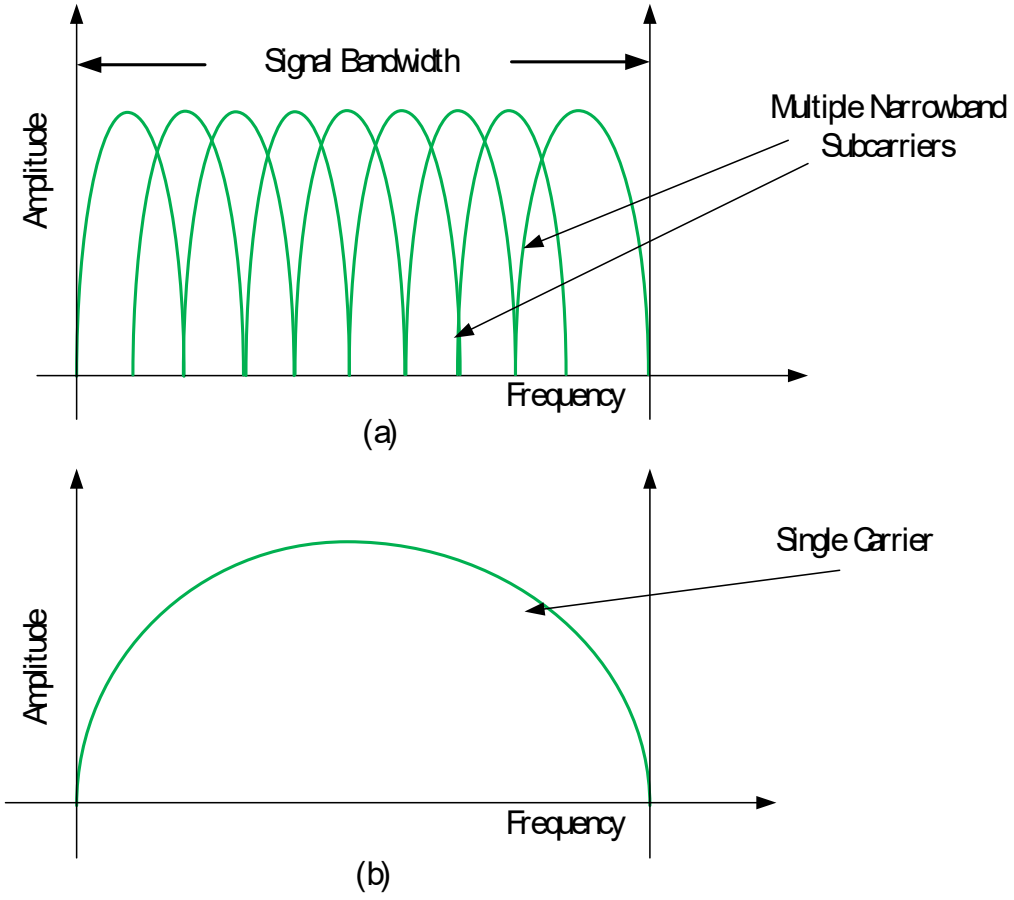

Fig. 1.1 Illustration of (a) single carrier vs (b) multicarrier modulation schemes

Three main multiplexing techniques have been identified in literature for the efficient sharing of a communication channel among several users. The techniques are the frequency division multiplexing (FDM) (which is based on FDMA method), time division multiplexing (TDM) (based on TDMA) and code division multiplexing (CDM) (based on CDMA scheme). The FDM scheme adopted in 1G networks is known to exhibit insufficient spectral efficiency as the total signal bandwidth are divided into multiple non-overlapping subchannels (with guard bands) that results into excessive bandwidth wastage [44]. Recently, an improved version of FDM scheme (which is one of the most reliable and efficient multiplexing technology in telecommunication engineering designed to offer higher data rates and spectral efficiency) named *orthogonal frequency division multiplexing* (OFDM) with *cyclic prefix* (CP) (i.e. CP-OFDM) has been proposed to deal with the bandwidth wastage of the 1G FDM schemes [44, 45] by overlapping the subchannels where the sidebands of individual carriers overlap without creating ICI as individual subcarriers are made to be orthogonal to one another. This transmission technology (which adopts the use of rectangular pulse shaping [46]) offers robustness against multipath fading [23, 47] as a result of the CP insertion while providing easy implementation based on inverse fast Fourier transform/fast Fourier transform (IFFT/FFT) [23, 47 - 49]. Due to these improvements, CP-OFDM is recommended as the main multiple access method for the 4G of wireless communication systems based on long term evolution (LTE).

Despite these improvements of CP based OFDM transmission technology, it is not considered as the most promising multiplexing scheme for the neXt generation (xG) of wireless networks (as highlighted in Subsection 1.1.5). Currently, the xG of wireless networks is the emerging fifth generation (5G) wireless network and its design is based on filter bank multicarrier (FBMC) technology. Filter bank multicarrier based schemes with offset quadrature amplitude modulation (FBMC/OQAM) provide an alternative modulation scheme that limits the short comings of CP-based OFDM systems by the elimination of CP. Hence, this results in higher spectral efficiency including provision of enhanced robustness to synchronization errors [50]. One good example of the FBMC/OQAM scheme is OFDM/OQAM. Generalized frequency division multiplexing is considered as a flexible filter bank multicarrier modulation waveform and it is the most promising candidate for the emerging 5G networks [23, 51]. This is because it combines the qualities of CP-OFDM and filter bank OFDM/OQAM-based systems by employing the use of CP and well-designed prototype filters. Each subcarrier is modulated onto a well-designed pulse

shaped filter in GFDM-based schemes where subcarriers' orthogonality may be lost. In compensation, this research adopts the near orthogonality properties of OQAM schemes to improve the throughput of GFDM-based systems. In literature, the structure of GFDM systems has been fairly considered specifically for GFDM systems based on QAM (GFDM/QAM) while GFDM schemes based on OQAM (GFDM/OQAM) is not well studied in literature. More details of the GFDM scheme are given in Chapter 4, Section 4.3. Fig. 1.2 presents the FBMC waveforms that are been considered for the xG of wireless networks. Chapter 2 elaborates more on this classification.

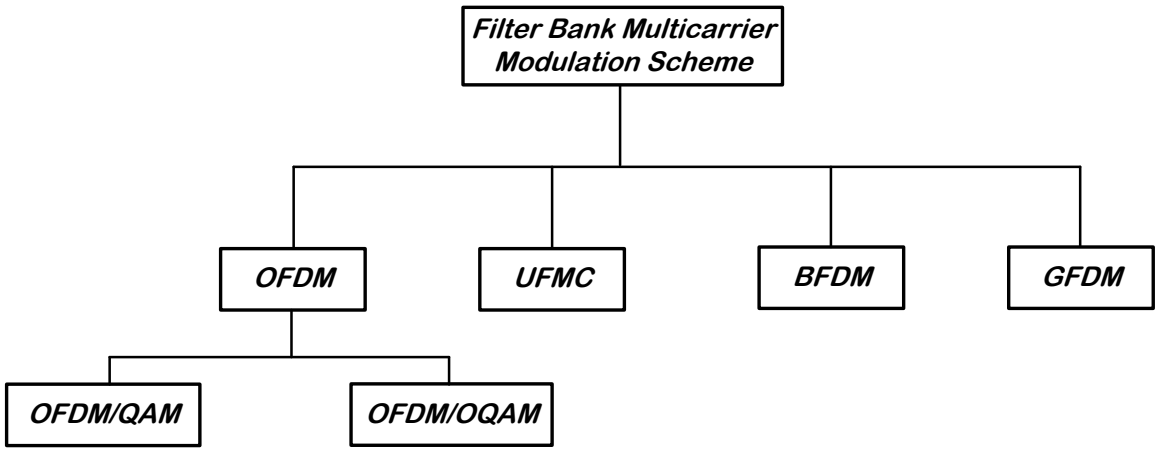

Fig. 1.2 Possible MC modulation schemes under consideration for the emerging 5G

1.3 INTRODUCTION TO CHANNEL ESTIMATION

The transmitted symbols of a baseband signal are usually corrupted by noise as they propagate through the communication channel. They usually experience detrimental effects such as *multipath propagation* and *fading* which eventually makes it difficult for accurate detection of the transmitted symbols. For accurate detection of the transmitted symbols, accurate *channel estimation* (CE) is required [52]. Channel estimation makes it possible for the receiver to approximate the channel impulse response (CIR) of the communication channel and to predict/understand the effects of the communication channel on the transmitted symbols. It is needed for perfect reconstruction of the transmitted symbols. Several channel estimation algorithms have been proposed in literature for general wireless communication systems (including filter bank OFDM/OQAM systems). Some of these algorithms are briefly highlighted

in Chapter 3, Section 3.4. Some linear and adaptive CE schemes have not been analysed for OFDM/OQAM-based systems. Furthermore, no channel estimation scheme has been considered for GFDM/OQAM -based systems. In this dissertation, some existing CE algorithms are adopted to predict the channel impulse response of the time varying frequency selective Rayleigh fading channel for OFDM/OQAM and GFDM/OQAM-based transceivers under near perfect reconstruction (NPR) and Non-perfect reconstruction (Non-PR) of filter banks. These CE algorithms include the least squares (LS), linear minimum mean square error (LMMSE), least mean square (LMS), normalized LMS (NLMS) and recursive least square (RLS) based CE schemes. These CE algorithms are properly described in Chapter 4, Section 4.4 and in the appendix.

1.4 RESEARCH BACKGROUND AND MOTIVATION

A number of channel estimation schemes have been proposed for filter bank OFDM/OQAM in literature, however the performances of LMMSE and all the proposed adaptive channel estimators presented in this dissertation have not been analysed before for this waveform. Similarly, few works have been reported in literature to investigate the performances of channel estimation in GFDM-based transceivers (usually QAM-based GFDM). The performances of channel estimation schemes have not been analysed for filter bank GFDM/OQAM in literature. It is also important to note that the techniques deployed so far for these filter bank waveforms are implemented assuming NPR design of the analysis and synthesis filter banks. In Non-PR of filter banks (which is not considered in literature), the synthesis and analysis filters are designed with different prototype filters. A random error is introduced to the analysis filter impulse response so as to yield non perfection as proposed in this dissertation. The performances of these proposed channel estimation schemes (as highlighted in Section 1.3) are then analyzed and compared with one another under both design conditions of NPR and Non-PR at different Doppler rates for the filter bank structures in frequency selective Rayleigh fading channel.

1.5 RESEARCH QUESTIONS

The main question to be addressed in this dissertation is “how well can the proposed channel estimation schemes (i.e. LS, LMMSE, LMS, NLMS and RLS) perform in comparison with one another for filter bank OFDM/OQAM and GFDM/OQAM-based transceivers in both slow and fast frequency selective Rayleigh fading channel under assumptions of NPR and Non-PR design

of finite impulse response prototype filter in terms of normalized mean square error (NMSE) and bit error rate (BER) at various levels of signal to noise ratio (SNR)?"

Two sub-questions that partly address the main question can be itemized as:

i) How well will the linear channel estimators perform in comparison to each other under slow and fast fading frequency selective Rayleigh channel in conditions of Non-PR and NPR filter design for both filter bank OFDM/OQAM and GFDM/OQAM waveform?

ii) What will be the performance of the adaptive CE schemes in comparison to the linear schemes under the same conditions mentioned above?

1.6 METHODOLOGY

The following methodologies are employed to address the research questions.

a) Intensive literature survey to identify channel estimation techniques that have not been adopted for filter bank OFDM/OQAM and GFDM/OQAM-based systems.

b) System model designed for the filter bank OFDM/OQAM and GFDM/OQAM-based systems assuming NPR and Non-PR under time varying channel conditions.

c) Development of well-designed mathematical models that describe the proposed filter bank systems (i.e. OFDM/OQAM and GFDM/OQAM).

d) Performance analysis of proposed channel estimation schemes via software-based computer simulations (using MATLAB programming language) for filter bank OFDM/OQAM and GFDM/OQAM-based transceivers under both assumptions of NPR and Non-PR.

1.7 DISSERTATION ORGANIZATION

The remaining chapters of this dissertation are structured as follows: Chapter 2 gives the basic structure of FBMC systems and also identifies and classifies the waveforms for next generation of wireless networks. It gives an overview of filter bank designs. In Chapter 3, a literature review analysis of channel estimation techniques that have been adopted for general wireless communication systems as well as for FBMC/OQAM-based systems is presented. This chapter also reviews mechanisms of propagation in wireless communication channels while Chapter 4 presents a comprehensive system model description and system analysis of the two investigated

FBMC waveforms (OFDM/OQAM and GFDM/OQAM). In Chapter 5, simulation results are presented to answer the research questions as implemented using MATLAB programming language, while Chapter 6 concludes the works presented in this dissertation.

The appendix section of this dissertation contains extra information that can help interested readers to further understand detailed derivations of the proposed channel estimation schemes. This presents a broad mathematical and technical description of the proposed channel estimation schemes that are applicable for estimating fading channel coefficients in the filter bank multicarrier waveforms.

CHAPTER TWO

DESIGN AND ANALYSIS OF FILTER BANK MULTICARRIER SYSTEMS

2.1 INTRODUCTION

In this dissertation, two filter bank multicarrier waveforms (as briefly introduced in Chapter 1) are identified and selected for investigation for the emerging next generation of wireless networks. These waveforms are the orthogonal frequency division multiplexing schemes based on offset quadrature amplitude modulation and generalized frequency division multiplexing with offset quadrature amplitude modulation. Since the fundamental building blocks of these waveforms are based on filtering, Section 2.2 of this dissertation gives a general overview of filter design while Section 2.3 describes the conventional design of FBMC-based systems. It presents the elementary structure of FBMC-based transceivers and also gives a comprehensive classification of FBMC waveforms in literature (including potential waveforms for the emerging fifth generation of wireless systems). It is important to note that a meticulous review of "analysis and synthesis" filter banks of FBMC schemes is paramount in making explicit designs of these schemes. These filter banks (analysis and synthesis) are usually designed based on some FBMC structures such as exponentially and cosine modulated filter banks which are also expatiated in this chapter.

2.2 OVERVIEW OF FILTER DESIGN

One of the most fundamental building blocks of filter bank multicarrier waveforms is a well-designed prototype filter. A review of filter design will provide more understanding to the basic design requirements of FBMC waveforms (which are already potential air interfaces for the emerging 5G networks). A filter can be defined as a frequency selective circuit that is designed to pass signals of a particular frequency band while attenuating signals of other frequencies [53]. Filters are generally employed to eliminate (or minimize) unwanted system features such as interference, noise and distortions. Filters are classified in many ways which could depend on the functions they are required to perform or based on their physical structures (i.e. components used). Hence, filters may be broadly classified as analog/digital filters (based on function) or active/passive filters (based on structure), etc. Passive filters are filters that are designed with the use of passive components such as resistors, capacitors, inductors, relays, etc., while active filters

are designed with the aid of active components (such as transistors, integrated circuits, diodes) and passive components.

Digital filters (also known as discrete-time filters) are employed in digital signal processing (DSP) mainly for the separation of digital signals that are combined together and for the restoration of distorted signals. The implementation of digital filters can be realized by convolution or by recursion. Convolution filters are known as finite impulse response (FIR) filters while recursion filters are known as infinite impulse response (IIR) filters. All filters are classified based on their frequency response characteristics [53 - 55]. In the design of digital filters, the frequencies that are allowed to pass through are known as pass-band frequencies [54], whereas, the rejected (or attenuated) frequencies can be referred to as stop-band frequencies. Based on this information, filters are classified as *low-pass* filters, *high-pass* filters, *band-pass* filters, *band-stop* filters (also known as *band-reject* filters) and *all-pass* filters. Low-pass filters allow signals of low frequencies to pass through while rejecting signals above its cut-off frequencies and high-pass filters eliminate frequencies below its cut-off frequency while allowing signals of high frequencies to pass through. Band-pass filters allow signals within a certain range of frequencies to pass through while attenuating all other frequencies. On the other hand, band-stop filters allow all frequencies to pass through while attenuating a certain range of frequencies. Finally, all-pass filters are used to allow all frequencies to pass through, however they change the phase of the passing signals without changing their amplitude.

2.2.1 REVIEW OF DIGITAL FILTERS

As mentioned in Section 2.2, digital filters can be classified into FIR and IIR filters depending on the method of design or their characteristics [53, 56]. An FIR filter is a digital filter that has a finite duration of impulse response. These filters are reverse cases of the IIR filters since there is no feedback of output signals into input, hence can be named non-recursive filters [53, 57]. The impulse responses of these filters are finite because of the absence of feedback. The structure of FIR filters consist of series of multipliers, delays and adders coupled together to give an output. This design makes these filters suitable for designing *multirate* filters. Some methods (or techniques) used for designing FIR filters include windowing, frequency sampling and equiripple approximation [53, 58]. The finite length impulse response of the FIR filters is obtained by truncating an infinite length impulse response. The truncation of an infinite duration sequence to

yield a finite response is termed *windowing*. Some functions are used to perform windowing. Examples of such functions include rectangular, Barlett, Hanning, Hamming and Blackman windowing functions. Infinite impulse response filters are digital filters that have an infinite duration of impulse response. They are also called recursive filters because they are designed to use the feedback signals obtained from the system output. These types of filters have nonlinear phase and are usually unstable. Some examples are [53, 57, 59], Butterworth filters, Chebyshev type I and Chebyshev type II filters, Elliptic filters and Bessel filters.

2.2.2 OVERVIEW OF MULTIRATE FILTERS

One basic concept that is adopted in DSP is the concept of sampling rate [60]. Sampling rate conversion involves the conversion of a signal from a given rate to a different rate. It is worthy to note that systems that adopt multiple sampling rates in DSP are known as *multirate* digital signal processing systems. These systems employ the use of multirate filters which are classified into hybrid and polyphase filters. Polyphase filters have demonstrated good performances, hence proving to be an excellent multirate filter that can be effectively adopted to solve wireless communication problems [60]. Multirate filters find useful applications in digital audio and video processing, speech coding, image compression, adaptive signal processing, scrambling and software define radios, etc. [60 - 63].

Multirate filtering is adopted in modern DSP systems to connect two digital systems together that have different sampling rates. It is based on two filtering techniques namely decimation and interpolation [64 - 67].

2.2.2.1 INTERPOLATION IN MULTIRATE FILTERING

In multirate systems, interpolation is a sampling rate conversion technique that is adopted to remove the effects of *imaging* through the use of an interpolation filter while increasing the sampling rate of the signal using an interpolator (also known as upsampler or expander). Upsampling is used to increase the sampling rate of a signal by the insertion of an integral number of samples (zeros) between consecutive samples of input signals. Fig. 2.1 shows a simple diagrammatic representation of an interpolation process that consist of an expander (of factor M) and an interpolation filter (with response ($g[n,k]$)) while Fig. 2.2 shows a simple illustration of interpolation where zeros are inserted between consecutive samples.

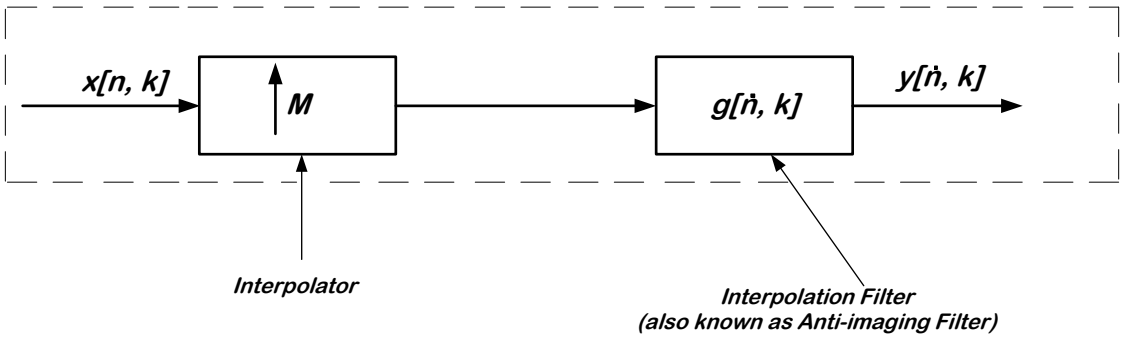

Fig. 2.1 Structure of interpolation in multirate filtering

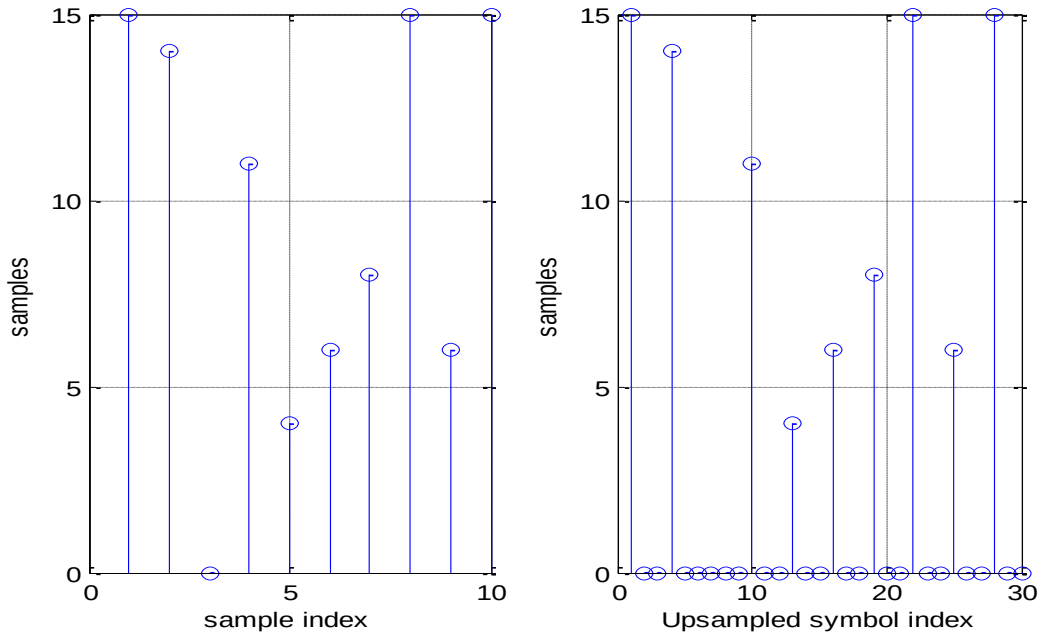

Fig. 2.2 Time domain plot showing the process of signal Interpolation for $M = 2$

2.2.2.2 DECIMATION IN MULTIRATE FILTERING

Decimation is a sampling rate conversion technique that is usually adopted at the receiver of a communication system to suppress *aliasing* by the use of a decimation filter and a downsampler [68]. Other names for downsamplers are sub-samplers, compressors and decimators. They are used to reduce the sampling rate of a signal by a factor M as shown in Fig. 2.3. The process of decimation is illustrated in Fig. 2.4.

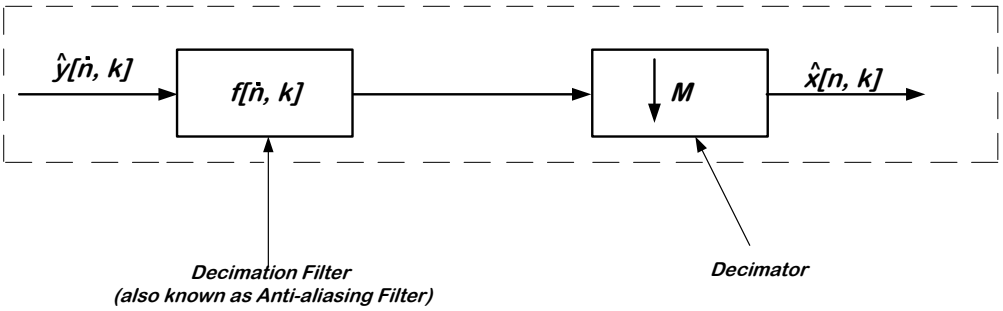

Fig. 2.3 Structure of decimation in multirate filtering

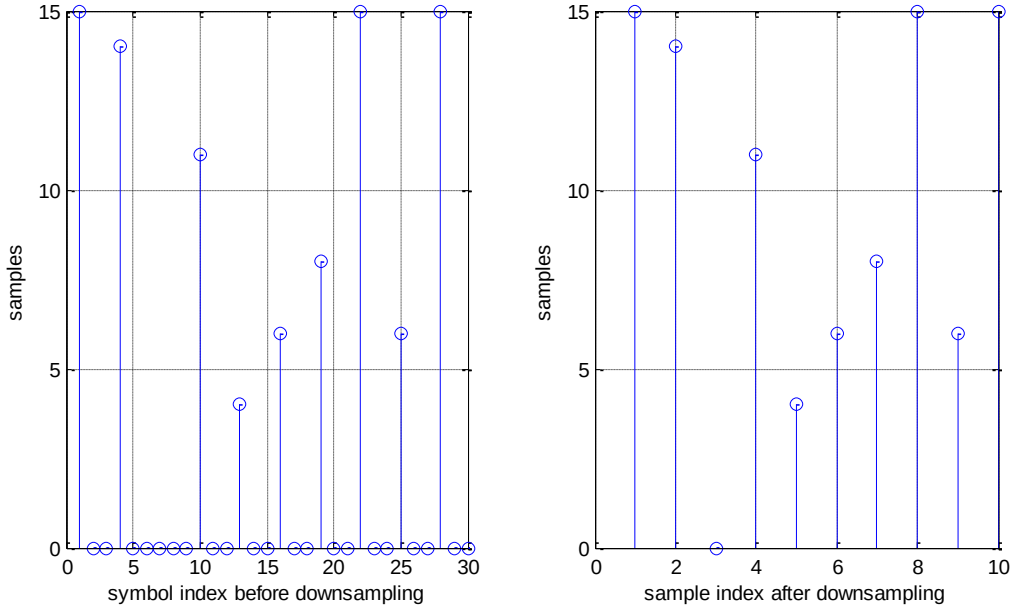

Fig. 2.4 Time domain plot showing the process of signal decimation for $M = 2$

2.2.2.3 DESIGN OF POLYPHASE FILTERS

When designing an FBMC system, the first step is to design a low-pass prototype filter that meets the requirements of NPR or PR. For filter bank systems, the frequency response of the filter at various subcarriers is shown in Fig. 2.5 where the subcarrier spacing Δf equals $1/T$ with T being the signaling period.

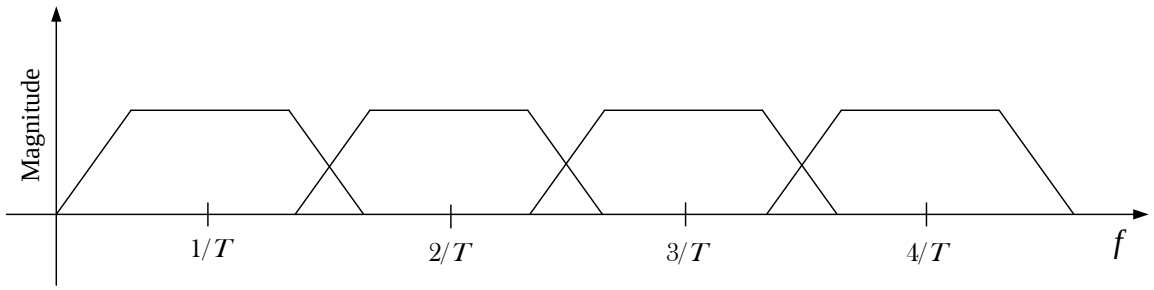

Fig. 2.5 Typical frequency response of a uniform filter bank

In [69], three kinds of prototype filters are analyzed and compared for the design of FBMC-based systems. The author's proposed prototype filter model (in this paper) named *Farhang* offers the best performance when it comes to sidelobe suppression in comparison to the widely used square-root raised-cosine (SRRC) filter as well as another discrete-time square root Nyquist filter model designed in [70]. The prototype filters are adopted for designing interpolation and decimation filters. It has earlier been mentioned that Fig. 2.1 depicts the basic structure of implementing interpolation in FBMC systems which is usually incorporated into the system with the aim of prevent imaging. This figure can be further developed to form the basic structure of interpolation in polyphase filter banks over M subcarriers as shown in Fig. 2.6 [71]. The discrete, real input signal $x[n,k]$ of Fig. 2.1 is split to yield M sub-band signals by use of synthesis bandpass filters whose impulse response is given as $g[n,k]$ in order to realize the polyphase representation shown in Fig. 2.6.

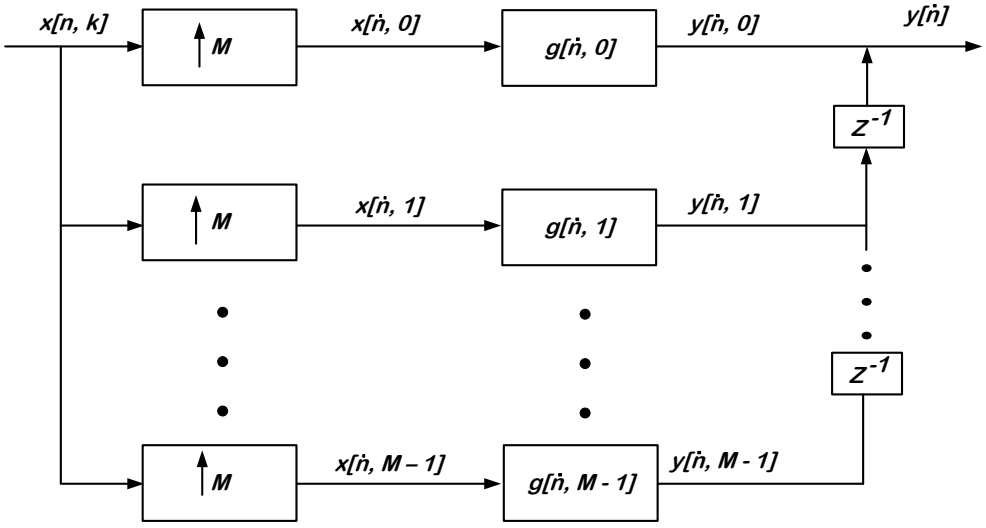

Fig. 2.6 Basic structure of interpolation in polyphase filters

In a similar manner, Fig. 2.3 shows the process of decimation in multirate systems that are usually adopted for combating the effects of aliasing. This figure can be used as a foundation to develop an efficient implementation structure for polyphase decimation as shown in Fig. 2.7.

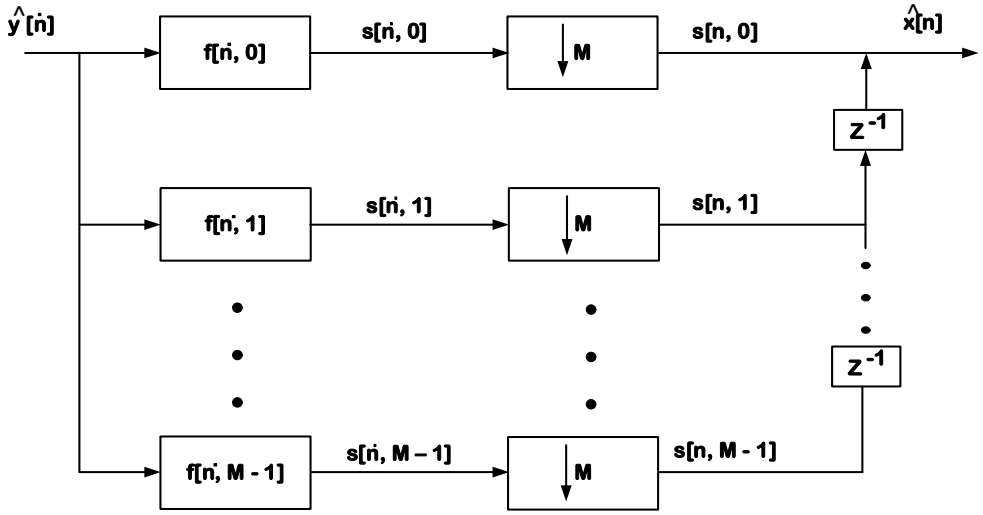

Fig. 2.7 Basic structure of Decimation in polyphase filters

2.3 INTRODUCTION TO FILTER BANK MULTICARRIER SYSTEMS

One good application of multirate filters in communication engineering is in the design of filter bank multicarrier-based transceivers. In this section, the general structure of FBMC systems (which is based on multirate filtering) is discussed in Subsection 2.3.1. Subsection 2.3.2 identifies and classifies the waveforms for next generation of wireless systems. These waveforms can be built (or designed) using FBMC structures, such as exponentially or cosine modulated filter banks.

2.3.1 GENERAL STRUCTURE OF FBMC SYSTEMS

A digital filter bank multicarrier-based transceiver is made up of two filter banks namely synthesis filter bank (SFB) and analysis filter bank (AFB) [64, 72]. The synthesis filter bank is positioned at the transmitter while the analysis filter bank is found at the receiver. It is designed with M digital filters arranged in a parallel configuration [64, 72]. The synthesis filter combines M signals at the transmitter into a single signal that is ready for transmission over a channel. This single signal can be referred to as the *reconstructed* signal. In perfect reconstruction of filter banks, the output signal is a delayed replica of the input signal [73]. In practical applications, the

output signal is designed to achieve nearly perfect reconstruction. Just like the design of decimation and interpolation filters discussed in Subsection 2.2.2.1 and 2.2.2.2, the synthesis filter bank is designed with an interpolation filter and an upsampler while the analysis filter is designed with a decimation filter and a downsampler. This makes multirate filters to be linear periodically time-varying systems because they are made up of linear filters and also perform time varying linear operations (such as decimation) [74]. A diagrammatic representation of the basic structure of digital filter banks is shown in Fig. 2.8 [50, 75]. This figure is an FBMC system because it is designed to offer multi-rate filtering where the sampling rate of the input symbols $x[n,k]$ (at transmitter) is increased using an interpolator and then filtered with a low-pass anti-imaging filter $g[n,k]$ so as to remove images of the input spectrum. In other words, this system is adopted to connect and transmit the input symbols ($x[n,k]$) over the fading channel by converting the symbols into higher rates using an SFB so as to enhance efficient data transmission over the frequency selective multipath fading channel for higher data rates and spectral efficiency. This upsampling of input symbols at SFB is performed in order to ensure that the sampling rate of the signals at receiver input is the same which is subsequently decimated at the AFB by filtering the received signals using the anti-aliasing filter ($f[n,k]$) for the purpose of combating aliasing where the signal is then downsampled appropriately to obtain $\hat{x}[n,k]$ in order to ensure efficient demodulation and detection of the received symbols. Fig. 2.6 and 2.7 are combined via a communication channel to realize this general structure of FBMC systems.

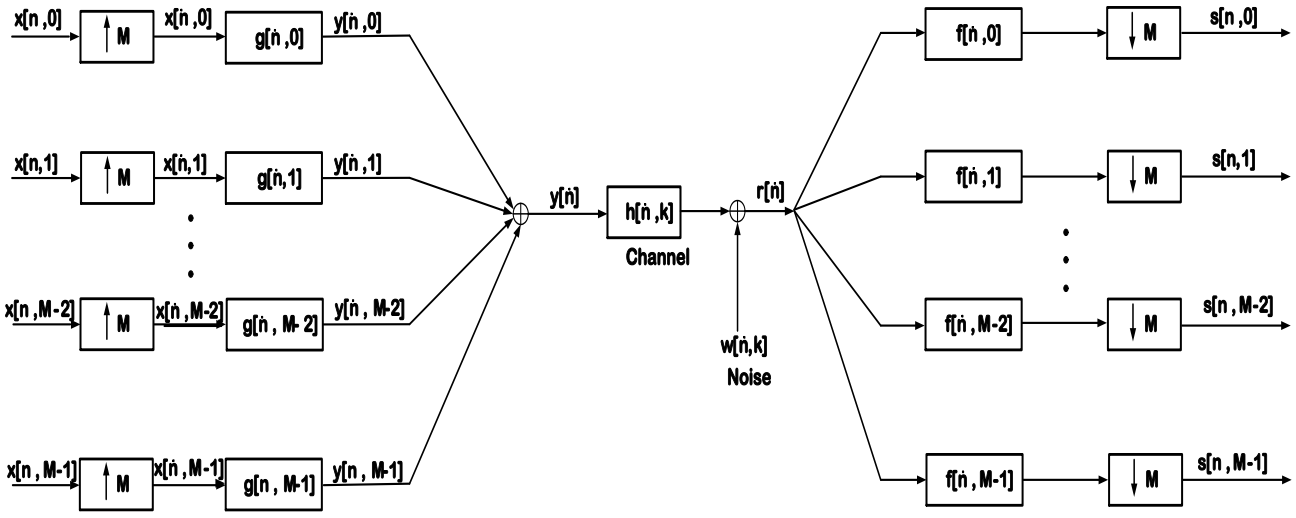

Fig. 2.8 General structure of FBMC-based transceivers

One effective way of implementing FBMC-based schemes assuming NPR is by realizing the system through the use of DFT-based polyphase filter bank model. The IFFT block is used to transform the input signal from the frequency domain to the time domain. Fig. 2.9 presents the basic structure of DFT-based filter bank that is realized through polyphase filtering. This system is adopted and analyzed in the filter bank OFDM/OQAM system model described in Chapter 4.

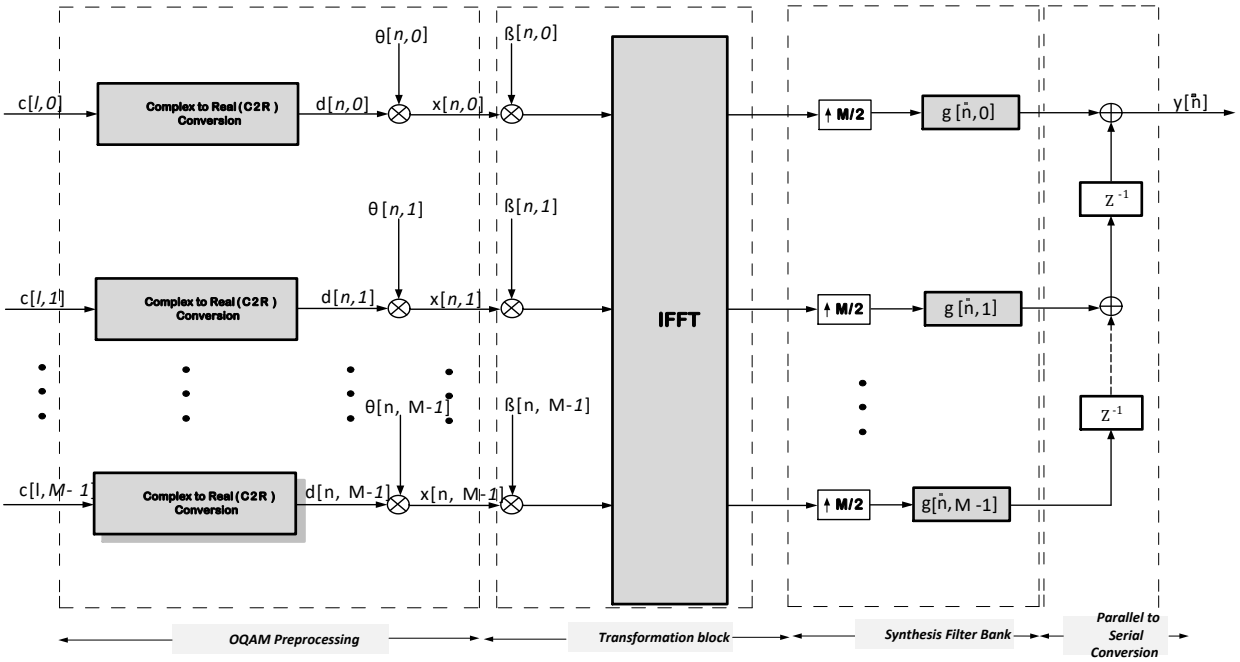

Fig. 2.9 Polyphase realization of DFT-based FBMC transmitter

When polyphase filtering structures are employed to implement the FBMC-based system, the type 1 synthesis polyphase filter at SFB is given as [76, 77]:

$$g[\dot{n}, k] = p[k + \dot{n}M] \tag{2.1}$$

where $g[\dot{n}, k]$ is the synthesis filter impulse response of the kth subcarrier at time $\dot{n}$. The symbol M is the total number of subcarriers while p is the FIR of the low-pass prototype filter.

The type 2 polyphase filters realized at the receivers SFB is given as [76, 77]:

$$f[\dot{n}, k] = g[\dot{n}, M - 1 - k]$$

$$= p[M - 1 - k + \dot{n}M] \tag{2.2}$$

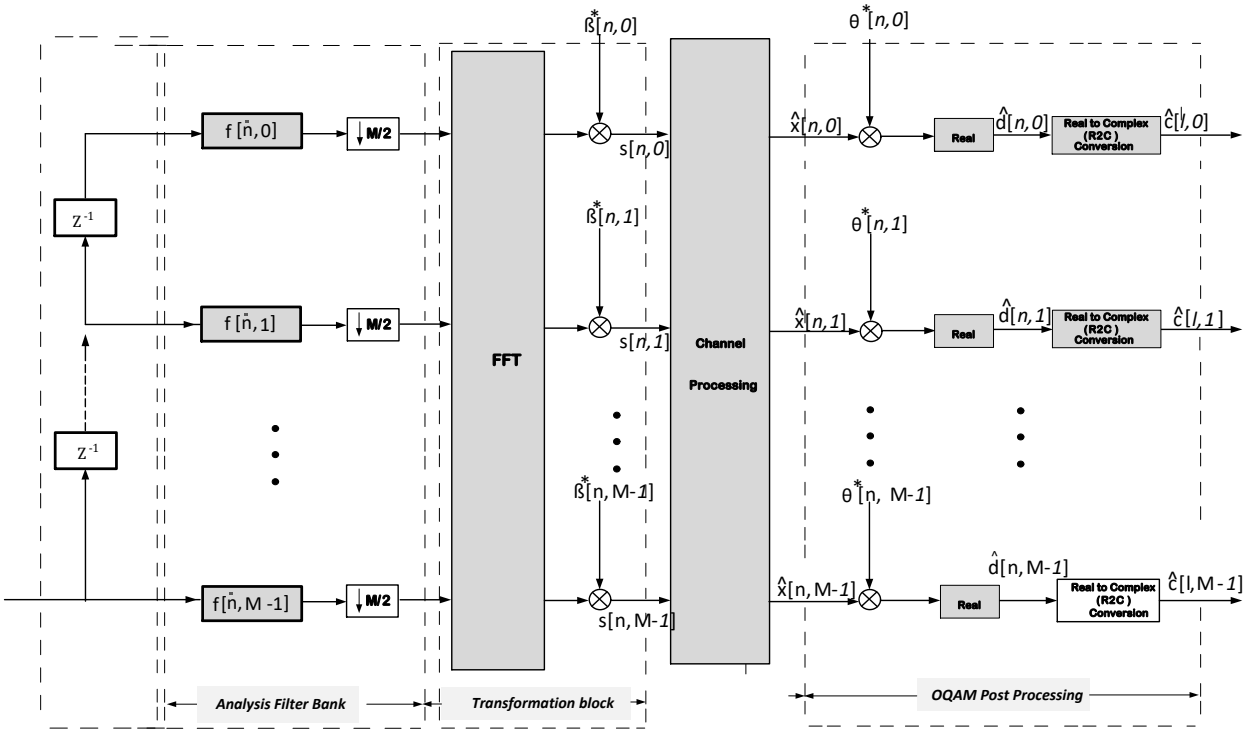

Fig. 2.10 Polyphase realization of DFT based FBMC receiver

The FBMC scheme can be implemented using OQAM pre-processing at the transmitter. This is achieved to maintain the orthogonality of subcarriers at all-time instants [78] where the complex QAM input symbols are staggered into real and imaginary parts by a delay, thus increasing the sample rate by a factor of 2. Fig. 2.11 shows the OQAM staggering for even indexed subcarriers [78] while the delay z^{-1} is located at the upper branch having the imaginary parts.

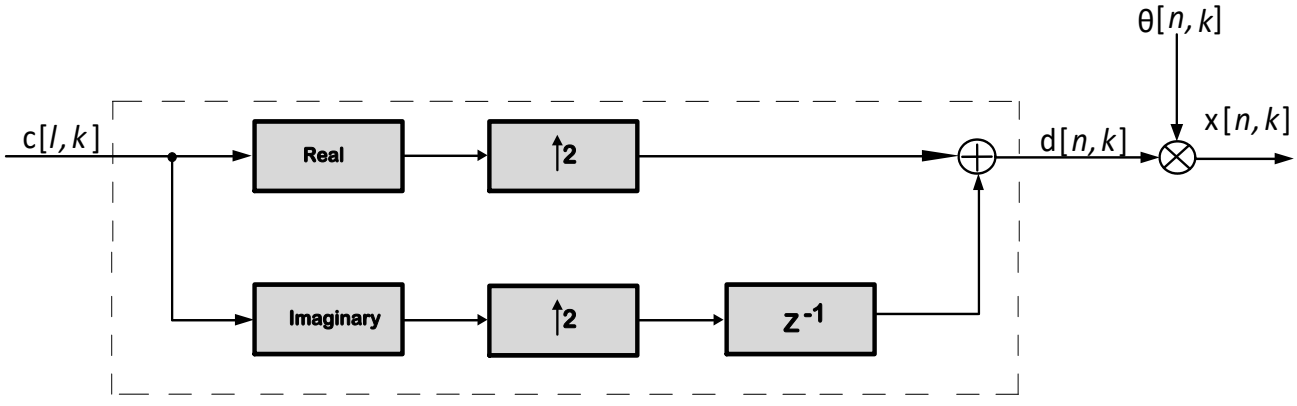

Fig. 2.11 OQAM staggering for even indexed subcarriers

2.3.2 WAVEFORMS FOR 5G NETWORKS

The waveforms under current investigation and consideration for the emerging 5G networks include *orthogonal frequency division multiplexing with offset quadrature amplitude modulation*, *universal filtered multicarrier* [37], *bi-orthogonal frequency division multiplexing* [38, 39], and *generalized frequency division multiplexing* [23] based schemes. These schemes are all examples of FBMC transmission technology and are usually based on discrete Fourier transform (DFT). Hence, they are also classified as DFT-based FBMC systems. Other FBMC transmission technologies include discrete wavelet multitone (DWMT) [79, 80], filtered multitone (FMT) [47] and cosine modulated multitones [81] which are built based on discrete wavelet transforms (DWT). Fig. 2.12 shows the FBMC schemes based on modulation type.

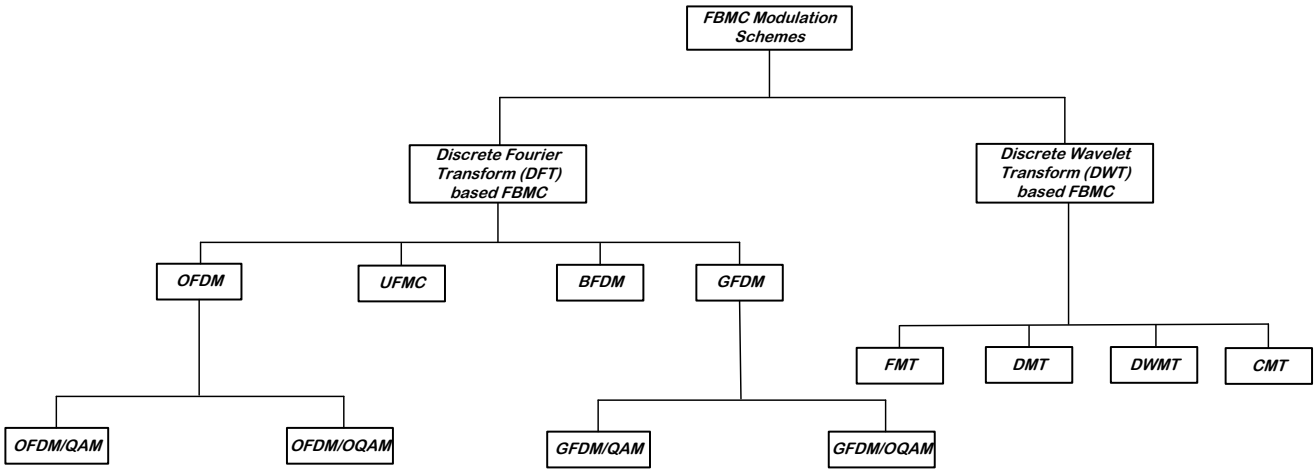

Fig. 2.12 Classification of FBMC schemes based on modulation

The DWT-based FBMC systems employ the use of wavelet packet transforms (WPT) unlike the DFT-based FBMC systems. In wavelet transform, a particular signal of interest is decomposed into a set of waveforms known as wavelets [82]. When DFT is employed, two sets of functions associated with low pass and high pass filtering namely scaling and wavelet function are incorporated [82]. In this system, the time domain signal is decomposed into different frequency bands using high-pass and low-pass filters. The incoming signal is passed through a half-band high-pass filter and a half-band low-pass filter where the former removes all frequencies below half of the highest frequency of incoming signal and the latter removes frequencies that are below half of the highest frequency of the incoming signal [82].

As shown in Fig. 2.12, OFDM/QAM is an FBMC system based on DFT while DWMT is an FBMC system based on DWT [83]. Their respective transceiver structures are very similar except that DFT is used as transformation in the receiver of the former while DWT is adopted as transformation for the latter. Inverse DFT (IDFT) and inverse DWT (IDWT) are implemented in their respective transmitters. The block diagrams of Fig. 2.13 (a) and (b) clearly show the main difference in structure of these two FBMC-based transceivers (i.e. OFDM/QAM and DWMT) using QAM modulation scheme. It is observed from this figure that the basic difference between DFT and DWT-based systems can be found at the transformation block.

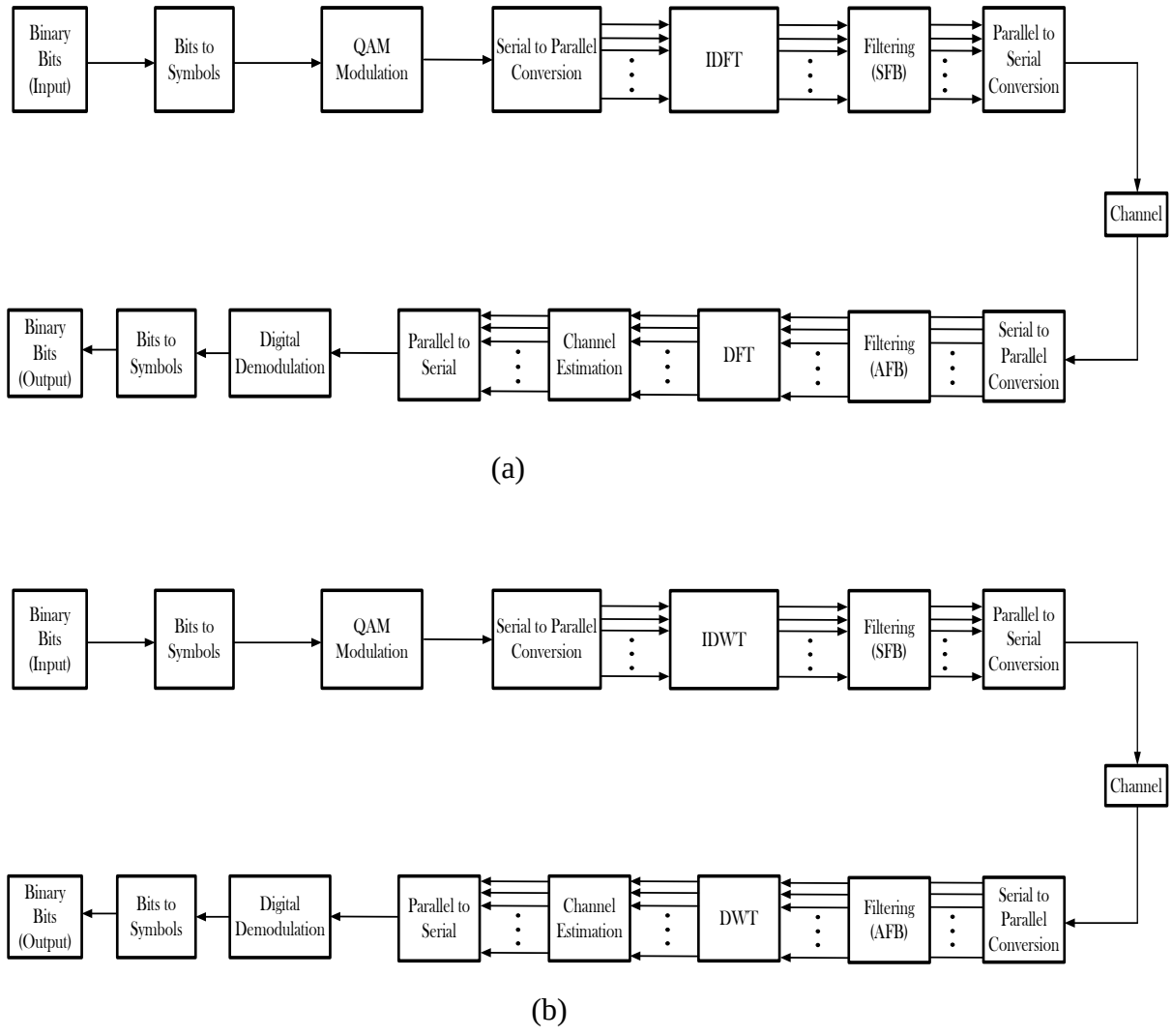

Fig. 2.13 Block diagram of (a) DFT vs. (b) DWT based FBMC systems

The low-pass FIR prototype synthesis and analysis filters of the FBMC schemes mentioned in Fig. 2.12 (for both DFT and DWT-based FBMC systems) can be implemented using various FBMC structures such as exponentially modulated filter banks (EMFB) [84], cosine modulated filter banks (CMFB) [85, 86], modified discrete Fourier transform (MDFT) [87] and extended lapped transforms (ELT) [88]. The structures of these FBMC systems are presented in Subsection 2.3.3.

2.3.3 TYPES OF FBMC STRUCTURES

The FBMC schemes considered for 5G networks can be designed based on discrete Fourier transforms. The synthesis and analysis filter banks for these schemes can be implemented using FBMC structures such as EMFB, CMFB and MDFT. Fig. 2.14 shows the classification of these FBMC structures.

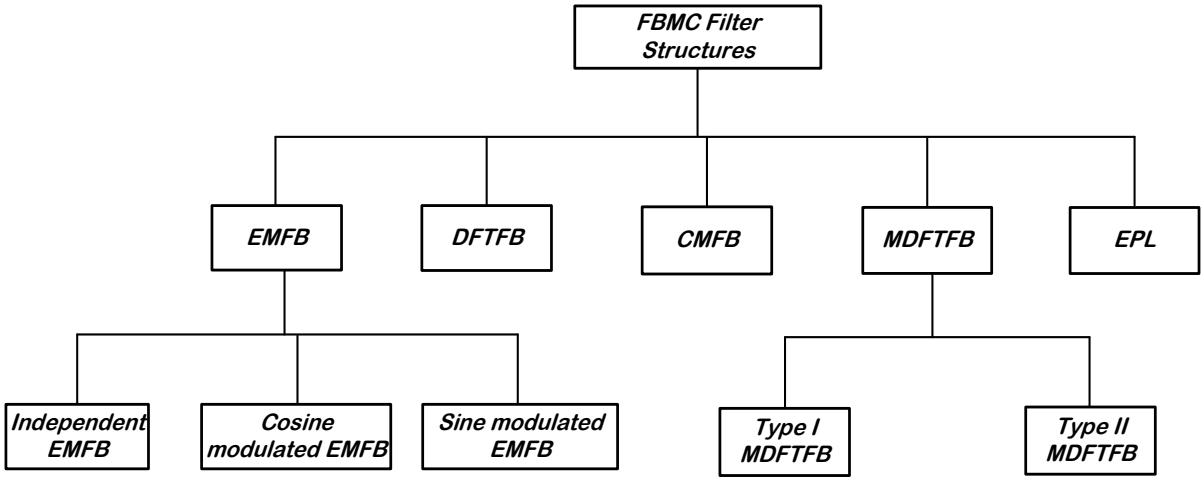

Fig. 2.14 Classification of FBMC filter structures

2.3.3.1 DISCRETE FOURIER TRANSFORM FILTER BANKS

An appropriate complex modulation of low-pass prototype filter can be used to realize linear-phase analysis and synthesis filters. The implementation of filter banks by use of complex modulation results in DFT filter banks which is implemented based on IDFT/DFT and use of polyphase filters [53, 65]. DFT filter banks can be referred to as special kinds of EMFB, however, they differ in the way they are sampled and in the way their channels are stacked [53]. The general block diagram of discrete Fourier transform filter banks is given in Fig. 2.8.

In realizing the synthesis and analysis filters for a DFT-based filter bank, all the subchannel filters are generated from the symmetrical, zero-phase, real-valued low-pass prototype filter $p[n]$ using complex modulation as shown in (2.3) [80, 89]:

$$g[n,k] = p[n] \exp\left(j\frac{2\pi kn}{M}\right) \tag{2.3}$$

where k is the subcarrier index, $k = 0, 1, \ldots, M - 1$ and M is the number of subcarriers.

To realize the time domain expression for the causal (or delayed) analysis filters, the prototype filter $p[n]$ is delayed by $(L_p - 1)/2$ samples as given in (2.4) [89]:

$$f[n,k] = p\left[\left(n - \frac{(L_p - 1)}{2}\right), k\right] \tag{2.4}$$

Comparing (2.3) with (2.4), equation (2.5) is obtained as:

$$f[n,k] = p\left[\left(n - \frac{(L_p - 1)}{2}\right)\right] \exp\left(j\frac{2\pi k}{M}\left(n - \left(\frac{L_p - 1}{2}\right)\right)\right) \tag{2.5}$$

where $n = 0, 1, \ldots, L_p - 1$, $k = 0, 1, \ldots, M - 1$ and L_p is the length of prototype filter impulse response. The synthesis and analysis filters for this system (phase delayed filters) are identical, hence, the synthesis filter bank impulse response is given as:

$$g[n,k] = f[n,k] = p\left[\left(n - \frac{(L_p - 1)}{2}\right)\right] \exp\left[j\frac{2\pi k}{M}\left(n - \left(\frac{L_p - 1}{2}\right)\right)\right] \tag{2.6}$$

2.3.3.2 MODIFIED DISCRETE FOURIER TRANSFORM FILTER BANKS

Due to the fact that discrete Fourier transform-based complex modulated filter banks suffer from aliasing [53, 89], a modified version of DFT named MDFT is proposed to cancel the aliasing effects of DFT-based filter banks. The MDFT filter bank can be defined as a complex modulated M channel filter bank that has two step downsampling of the subband signals where decimation by two is accomplished with and without delay after subsampling the sampling rate (by $M/2$) has been achieved [76].

The modifications of the DFT filter banks to yield the MDFT filter banks are as follows:

i) MDFT consists of complex modulated M-channel filter banks having two-step compression of the subband signals. The received signal is decimated by $M/2$ while another down sampling is performed by a factor of two, with and without delay of one sampling period.

ii) The input signal is complex valued. The real or imaginary part is used in the *2M* sub-bands.

The MDFT filter banks can be classified as *Type I* and *Type II* MDFT filter banks based on the expressions of the synthesis and analysis filter bank impulse responses. The impulse response of the synthesis and analysis filter banks for *Type I MDFT*-based filter banks is given as (2.7) and (2.8) respectively [53].

$$g[n,k] = \sqrt{2}p[n]\exp\left(j\frac{2\pi k}{2M}\left(n-\frac{D}{2}\right)\right) \tag{2.7}$$

$$f[n,k] = \sqrt{2}p[n]\exp\left(j\frac{2\pi k}{2M}\left(n-\frac{D}{2}\right)\right) \tag{2.8}$$

where D is the delay of the system and $k = 0, 1, \ldots, 2M-1$.

Fig. 2.15 shows the structure of Type I MDFT filter banks which is achieved from the DFT filter bank structure with modifications on the subsampling stages of this filter bank [86, 90, 91].

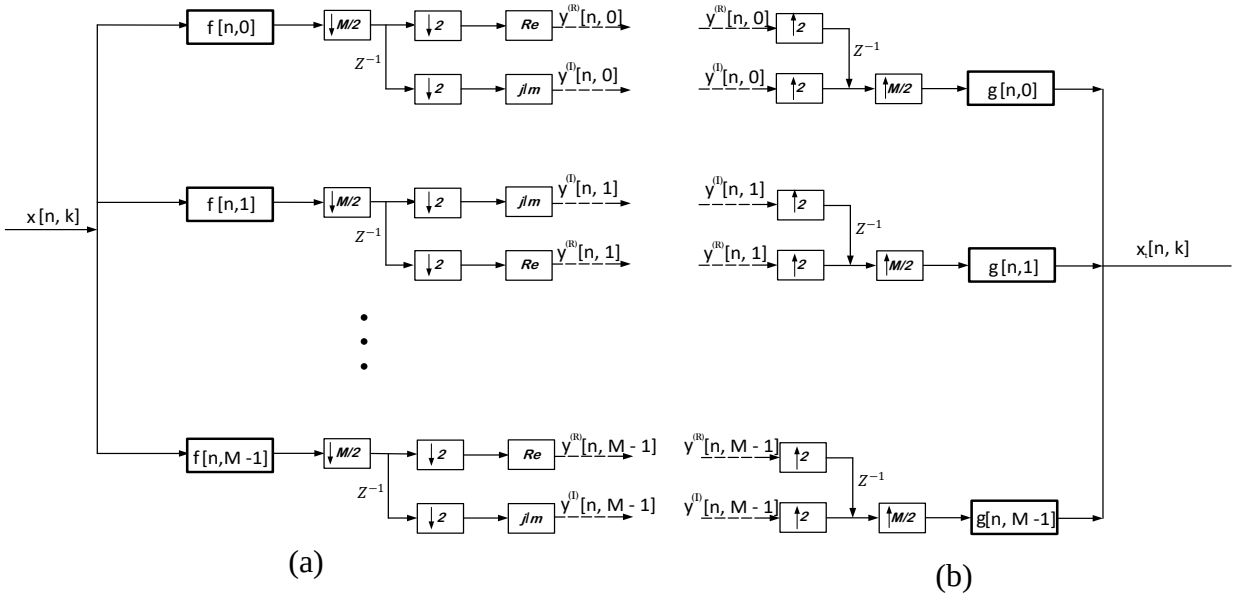

Fig. 2.15 Basic structure of (a) type I and (b) type II MDFT filter banks

Type II MDFT filter banks also have similar structure, however the analysis and synthesis filter banks are modelled differently as [53]:

$$g[n,k] = \sqrt{2}p[n]\exp\left(j\frac{2\pi k}{2M}\left(n - \left(\frac{D+M}{2}\right)\right)\right) \tag{2.9}$$

$$f[n,k] = \sqrt{2}p[n]\exp\left(j\frac{2\pi k}{2M}\left(n - \left(\frac{D-M}{2}\right)\right)\right) \tag{2.10}$$

where $k = 0, 1, \ldots, 2M - 1$. In this structure, the imaginary part in the delayed branch and the real part in the direct branch of the sub-band are chosen. They find more application in block filtering and sub-band coding [53, 92].

2.3.3.3 EXPONENTIALLY MODULATED FILTER BANKS

When the prototype filter impulse responses are modulated exponentially, the resulting filter banks are known as exponentially modulated filter banks. These filter banks can either be implemented independently or from a combination of both cosine and sine modulated filter banks and also from ELT [88, 93]. If independent modulation is considered, the synthesis and analysis filter bank impulse response are given as [77, 94]:

$$g[n,k] = p[n,k]\exp\left(j\frac{2\pi kn}{M}\right) \tag{2.11}$$

$$f[n,k] = g^*\left[L_p - 1 - n, k\right] = p\left[L_p - 1 - n, k\right]\exp\left(j\frac{2\pi k}{M}\left(n - \left(\frac{L_p - 1}{2}\right)\right)\right) \tag{2.12}$$

where $p[n,k]$ is the real-valued low-pass prototype filter impulse response, k is the subcarrier index for $k = 0, 1, \ldots, M - 1$, M is the number of subcarriers while n is the time index given as $n = 0, 1, \ldots, L_p$. L_p is the length of the prototype filter impulse response.

From this complex modulation of filter impulse response in EMFB, it is evident that the synthesis filter bank impulse responses given in (2.11) are complex valued. If these filter banks are implemented using DFT, they are known as complex-modulated DFT filter banks. Another efficient implementation of EMFB is given by the two times oversampled EMFB [95]. Based on

this filter bank structure, the synthesis filter impulse response of the $2M$ channel EMFB is given using cosine and sine modulate sub-filters as [88]:

$$g[n,k] = \sqrt{\frac{2}{M}}\, p[n,k]\, \exp\left(j\, \left(n + \left(\frac{M+1}{2}\right)\right)\left(k + \frac{1}{2}\right)\frac{\pi}{M}\right) \tag{2.13a}$$

$$= \begin{cases} g_{cos}[n,k] + j\, g_{sin}[n,k], & k \in [0, M-1] \\ -\left[g_{cos}[n,2M-1-k] - j\, g_{sin}[n,2M-1-k]\right], & k \in [M, 2M-1] \end{cases} \tag{2.13b}$$

where

$$g_{cos}[n,k] = \sqrt{\frac{2}{M}}\, p[n,k]\, \cos\left(\left(n + \left(\frac{M+1}{2}\right)\right)\left(k + \frac{1}{2}\right)\frac{\pi}{M}\right) \tag{2.14}$$

$$g_{sin}[n,k] = \sqrt{\frac{2}{M}}\, p[n,k] \sin\left(\left(n + \left(\frac{M+1}{2}\right)\right)\left(k + \frac{1}{2}\right)\frac{\pi}{M}\right) \tag{2.15}$$

where $n = 0, 1, \ldots, L_p$, k is earlier defined as in (2.3) and $j = \sqrt{-1}$.

The analysis filter is a time-reversed and complex-conjugated version of the corresponding synthesis filter given as [95]:

$$f[n,k] = \sqrt{\frac{2}{M}}\, p[n,k]\, \exp\left(-j\, \left(L_p - n + \frac{M+1}{2}\right)\left(k + \frac{1}{2}\right)\frac{\pi}{M}\right) \tag{2.16}$$

$$= \begin{cases} f_{cos}[n,k] - j\, f_{sin}[n,k], & k \in [0, M-1] \\ -\left[f_{cos}[n,2M-1-k] + j\, f_{sin}[n,2M-1-k]\right], & k \in [M, 2M-1] \end{cases} \tag{2.17}$$

2.3.3.4 COSINE MODULATED FILTER BANKS

In CMFBs, subcarrier filters with real coefficients are derived from single low-pass prototype filters through the use of cosine modulation [88, 96], hence filter banks that are designed based on cosine modulation are known as CMFB [53]. CMFB can be implemented to achieve near perfect reconstruction [96 - 98] or perfect reconstruction [99 - 101] and one useful way of implementing CMFB is by modifying EMFB. The coefficients of the output filter banks in CMFB are real unlike in EMFB where the filter coefficients are complex. The most common

way of implementing CMFBs involve the use of low-pass FIR prototype filter $p[n]$. If L_p is the length of the prototype filter $p[n]$ given as $L_p = 2KM - 1$, where K and M are the overlapping factor and number of channels respectively, then the synthesis and analysis filter banks for this design of CMFB is obtained using cosine modulation of the prototype filter $p[n]$ as given in (2.18) and (2.19) as [88, 96, 101 - 103]:

$$g_{cos}[n,k] = 2p[n]\cos\left((2k+1)\frac{\pi}{2M}\left(n - \frac{L_p}{2}\right) - (-1)^k\frac{\pi}{4}\right) \tag{2.18}$$

$$f_{cos}[n,k] = 2p[n]\cos\left((2k+1)\frac{\pi}{2M}\left(n - \frac{L_p}{2}\right) + (-1)^k\frac{\pi}{4}\right) \tag{2.19}$$

where k is the subcarrier index, $k = 0, 1, \ldots, M - 1$ and n is the symbol index, $n = 0,1, \ldots, L_p$.

Equations (2.18) and (2.19) imply that the synthesis filters are time reversed versions of the analysis filters given as [75, 96, 104]

$$g_{cos}[n,k] = f_{cos}[L_p - n, k] \tag{2.20}$$

2.4 CHAPTER SUMMARY

In this chapter, an overview of the basic concepts of digital filtering is presented. Due to the fact that multirate digital signal processing has attracted the interests of researchers over the last two decades as a result of the current need for higher data rates and spectral efficiency, a brief review of multirate filtering has been discussed (in this chapter) since the building blocks of future generation networks are designed based on the fundamental principles of multirate filtering. The general structure of various types of FBMC systems has been highlighted as they provide the elementary principles and operation that the waveforms under consideration for xG of wireless networks are based. The potential waveforms for the emerging 5G networks are also mentioned and briefly discussed since their structures are built on the fundamental principles and operations of multirate filtering. The two proposed waveforms for xG networks in this dissertation (filter bank OFDM/OQAM and GFDM/OQAM) also have their structures built on the basics of multirate filtering.

CHAPTER THREE

FUNDAMENTALS OF CHANNEL ESTIMATION

3.1 INTRODUCTION

As transmitting symbols propagate through the wireless communication channel, they experience several harmful effects such as *multipath propagation* and signal *attenuation* (fading). Channel estimation is a useful wireless communication technique that is adopted to ensure accurate detection of the transmitting signals. In this dissertation, two promising filter bank multicarrier waveforms (which are potential candidates for the emerging next generation of wireless networks (5G)) have been identified and investigated. These FBMC waveforms are OFDM/OQAM and GFDM/OQAM-based systems. For eminent understanding of the basic concepts and need to deploy channel estimation in the proposed transceivers, a good understanding of propagation of signals (in wireless channel) is required, hence the mechanisms of propagation in wireless channels are reviewed in this chapter.

The structure of this chapter is outlined as follows. Section 3.2 reviews the mechanism of propagation in wireless channels, while Section 3.3 gives a detailed review on the basics of multipath propagation and fading in general wireless communication systems. Section 3.4 presents an introduction to the basic concepts of CE while providing reviews of CE schemes that have been reported in literature for some useful communication technologies. Section 3.5 gives a review of CE schemes that have been reported for the two proposed FBMC waveforms under investigation in this dissertation while Section 3.6 summarizes and concludes this chapter.

3.2 MECHANISM OF PROPAGATION IN WIRELESS CHANNEL

In the design of typical mobile-radio systems, there is need for information to be transmitted from a fixed base station to the moving mobile unit. The information to be sent are modulated and transmitted in waveforms over a wireless channel. As the signals travel via the wireless channel to the receiver, terrain objects such as cars, buildings, trees, mountains and hills, etc. obstruct the line of sight (LOS) path of propagation which makes the propagating symbols to experience some undesirable effects. Due to the harmful effects of these obstructions, the signals experience *reflection*, *diffraction* and *scattering* (as shown in Fig. 3.1) making them to arrive at

the receiver via multiple reflective paths with different *time delays*, *amplitudes* and *phases* in a propagation phenomenon described as *multipath propagation* [105 - 109].

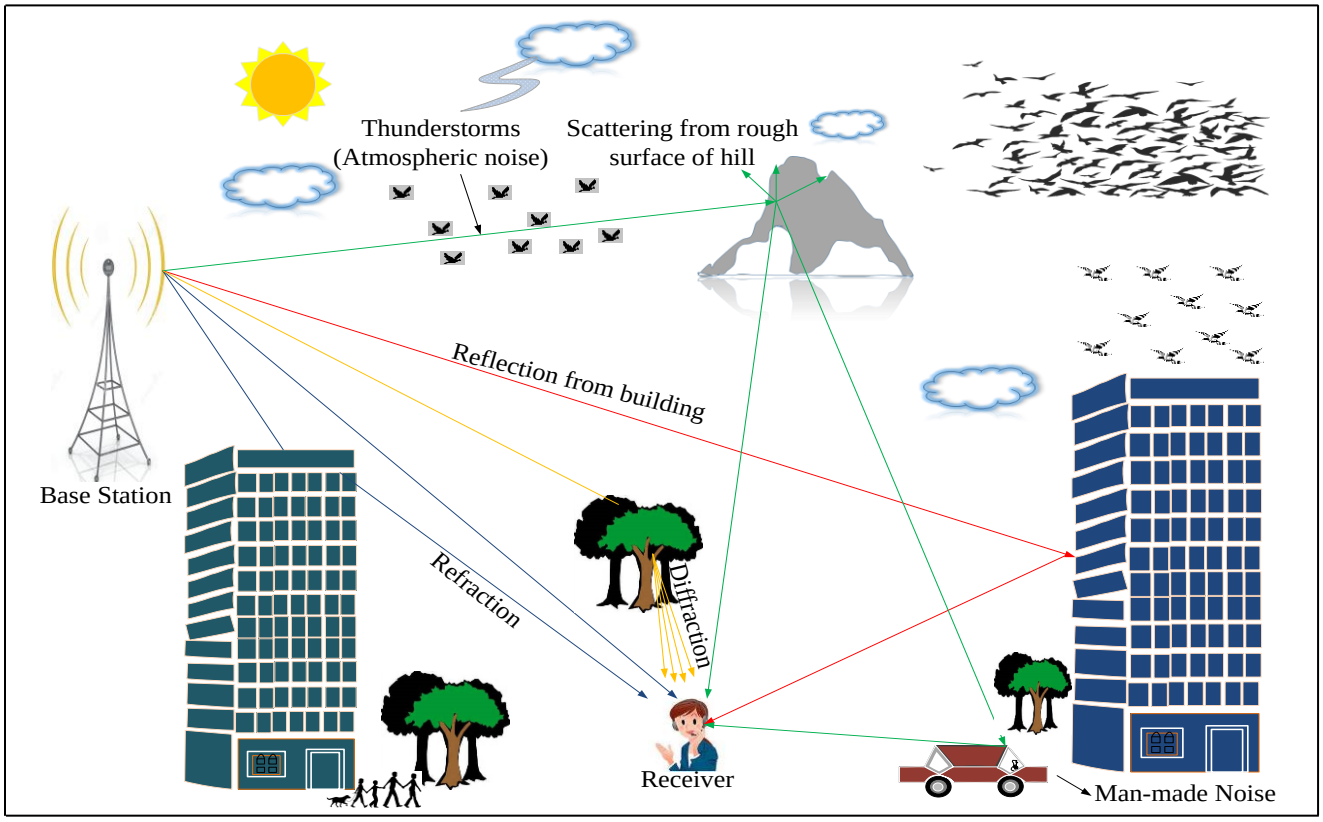

Fig. 3.1 Basic concept of signal propagation in wireless channel

3.3 MULTIPATH PROPAGATION AND FADING IN WIRELESS CHANNELS

As mentioned in Section 3.2, transmitting signals can experience multipath propagation and fading. This section gives a more detailed description of these propagation mechanisms as presented in Subsections 3.3.1 and 3.3.2 respectively.

3.3.1 THE CONCEPT OF MULTIPATH PROPAGATION

As described in Section 3.2, propagation mechanisms such as reflection, diffraction and scattering can make the propagating symbols arrive via several paths in a phenomenon termed multipath propagation. These mechanisms are briefly described in subsequent subsections.

3.3.1.1 REFLECTION OF PROPAGATING SYMBOLS

In mobile communication systems, reflection is a basic propagation mechanism (having negative impact on propagating symbols) that occurs when the transmitting electromagnetic signal impinges on terrains with very large dimensions in comparison to the wavelength of the travelling waves [105]. It usually occurs when the propagating wave strikes the ground surface, walls and furniture (for indoor), etc. Reflection leads to partial refraction of the propagating waves [105].

3.3.1.2 DIFFRACTION OF PROPAGATING SYMBOLS

Diffraction is a propagation phenomenon that occurs when the transmission path between the transmitter and receiver is interrupted by surfaces with sharp edges [105]. In this propagation phenomenon, the travelling electromagnetic waves are bent around the obstacle even when there is no LOS path between the transmitter and the receiver, hence causing secondary waves to be formed behind the obstructing body [108] as shown in Fig. 3.1.

3.3.1.3 SCATTERING OF PROPAGATING SYMBOLS

This phenomenon occurs when travelling radio waves impinge upon large rough surfaces (i.e. when number of obstacles per unit volume is large). If the channel consists of objects with very small dimensions as compared to the wavelength of the wave, scattering is bound to occur [108] causing the reflected energy to scatter (spread out) in all directions. In urban centres, environmental objects like lampposts, foliage and street signs and hills can cause transmitting symbols to scatter.

3.3.2 FADING TYPES IN WIRELESS CHANNELS

The received signal is usually attenuated as it encounters various environmental obstacles in the wireless radio channel leading to fading of the transmitted signals. Several kinds of fading can be experienced. The kind of fading experienced by the transmitting signals as they propagate through the wireless channel depends on channel characteristics and the nature of the transmitted signal [108]. Based on this, fading may be classified as large or small scale.

3.3.2.1 LARGE SCALE FADING

Large scale fading results from the average signal power attenuation (or path loss) due to motion over large areas [108]. Factors affecting this type of fading include prominent terrain contours

such as forests, hills, buildings, bill boards, etc. that are positioned between the base station and the receiver. These obstructions result into shadowing of the propagating signals.

3.3.2.2 SMALL SCALE FADING

Small scale fading on the other hand results from changes in the signal amplitude and phase experienced from small changes in the spatial separation between the transmitter and receiver. Fig. 3.2 shows the various types of signal fading as mentioned.

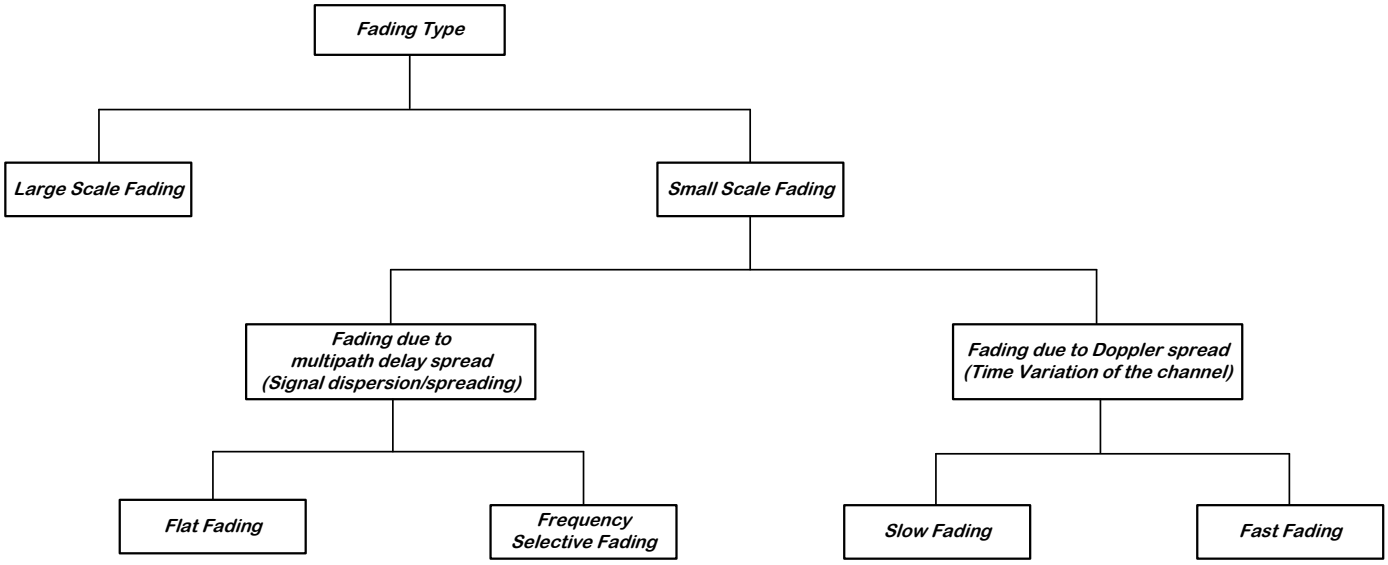

Fig. 3.2 Types of fading in mobile communication systems

As shown in Fig. 3.2, small scale fading may be due to *multipath delay spread* or based on *Doppler spread*. Multipath delay spread fading results into time spreading of the signal (i.e. *signal dispersion*) which gives rise to *frequency selective* and *flat fading* while fading based on Doppler spread results into *time variance* of the channel [107]. The channel is time variant because there are propagation path variations as a result of the motion between the base station transmitter and the moving receiver, hence leading to either *slow* or *fast* fading.

The received signal experiences *frequency selective fading* if the bandwidth of the transmitted signal is larger than the bandwidth of the channel at constant gain and linear phase response [107]. In this type of fading, the received signals are scattered (or dispersed), attenuated and time delayed and contain several versions of the transmitted signal resulting into *Inter-symbol Interference* (ISI). The received signal on the other hand experience flat fading if the bandwidth

of the transmitted signal is less than the bandwidth of the channel at constant gain and linear phase response. It is the most common fading type experienced in practice where the signal strength varies with time as a result of changes in the channel gain. It is basically caused by the detrimental effects of multipath propagation.

A channel may either experience *fast fading* or *slow fading* as a result of Doppler spread. This is subject to how fast or slow the transmitting baseband signal varies in comparison to the time rate of change of the channel. Fast fading channels are characterized by a rapid change in CIR within symbol duration. In other words, fast fading deals with the rate of change of the channel due to motion. In this fading, the symbol period of the transmitted baseband signal is much greater than the coherence time of the channel. This eventually leads to distortion of the transmitted signal [107]. The CIR varies at a much slower rate when compared to the symbol period of the transmitted baseband signal in slow fading channel conditions. The Doppler spread of the channel is considered far less than the bandwidth of the transmitted baseband signal when viewed in the frequency domain.

3.4 OVERVIEW OF CHANNEL ESTIMATION

As described in Section 3.2 and 3.3, the transmitting symbols propagating through the frequency selective Rayleigh fading channel are usually corrupted by the channel in a random manner through fading that result from its interaction with environmental objects and also from the addition of noise that could be additive thermal noise, man-made noise or atmospheric noise (e.g. thunder storms). The signal then experiences multipath fading and Doppler spread due to reflection, diffraction, scattering and interference as illustrated in Fig. 3.1. Due to these harmful effects, limitations are placed on the performance of the communication system as transmitting symbols propagating towards the receiver arrive in multiple reflective paths and are usually attenuated and phase shifted. In order to mitigate the negative effects of these propagation phenomena and for proper signal reconstruction, appropriate channel estimation is required [52].

In wireless systems, channel estimation is a challenging problem [110], however, the need for carrying out accurate channel estimation techniques for these systems cannot be overemphasized since it is needed for predicting the behavior of the frequency selective channel and also to ensure excellent reconstruction of the transmitted symbols. Several CE schemes have been proposed in literature which can be adopted for estimating the fading channel coefficients in

different wireless communication systems that includes single carrier communication systems and multi-carrier communication systems such as single-input single-output (SISO) CP based OFDM (SISO-OFDM), non-contiguous OFDM (NC-OFDM), MIMO-OFDM systems and most FBMC schemes like filter bank OFDM/OQAM and GFDM-based schemes. Channel estimation schemes can be broadly classified into *non-blind*, *semi-blind* and the *blind* channel estimation schemes. These schemes are elaborated in Subsections 3.4.1, 3.4.2 and 3.4.3 respectively while Fig. 3.3 shows the classification of channel estimation schemes that have been adopted in literature.

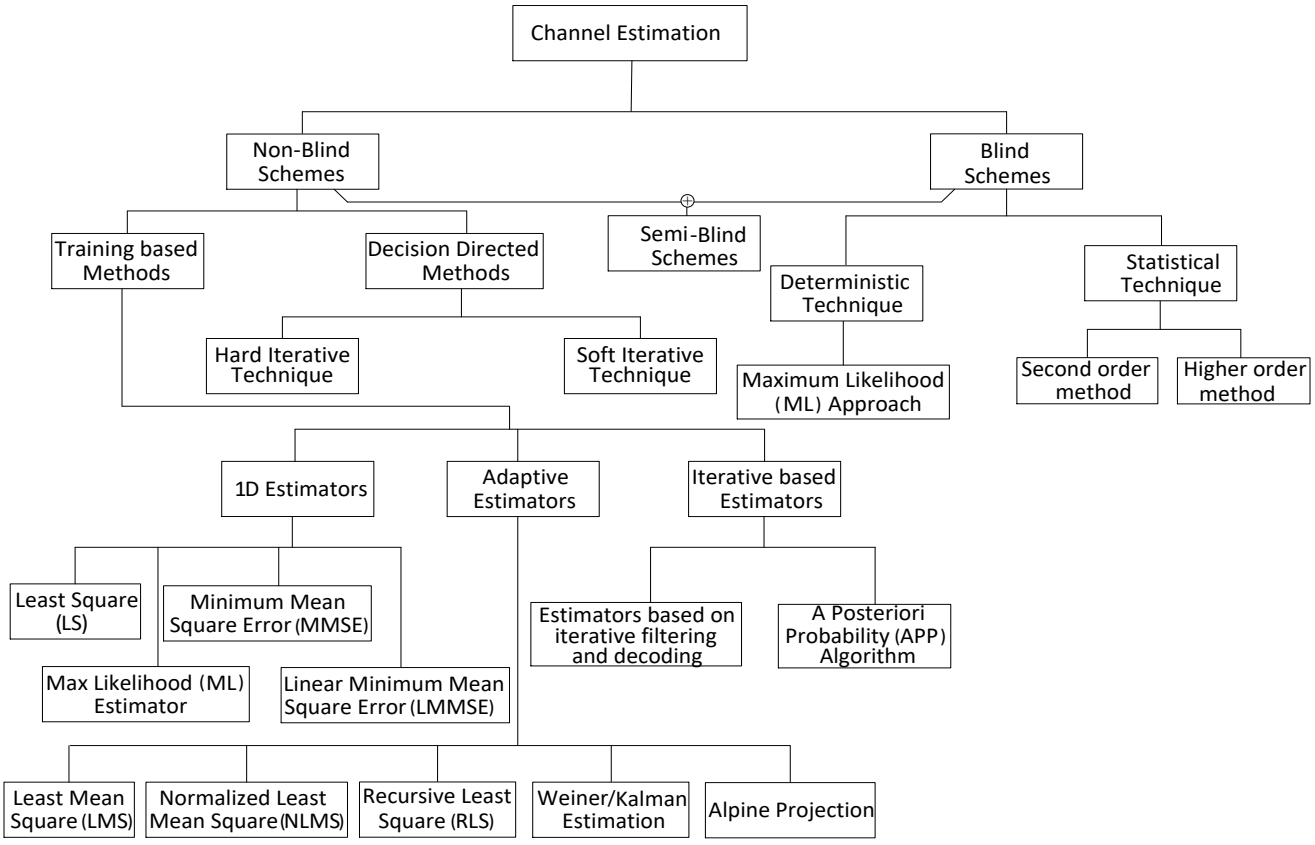

Fig. 3.3 Classification of channel estimation techniques adopted in literature

3.4.1 NON-BLIND CHANNEL ESTIMATION SCHEMES

Non-blind channel estimation can either be data-aided (training-based) or decision directed channel estimation as depicted in Fig. 3.3. In training-based channel estimation (also known as pilot-assisted channel estimation), training sequences (or pilot symbols) which are known to the receiver are transmitted so as to enable the receiver to easily estimate the radio channel by

demodulating the samples received [110, 111]. If the density of the training symbols used is high, the system channel estimation accuracy improves tremendously, however the spectral efficiency of the system is decreased due to the introduction of overhead by the pilot symbols [110]. A number of works have been reported in literature that addresses the challenges of pilot-assisted channel estimation schemes for various telecommunication techniques such as SISO-OFDM, NC-OFDM and MIMO-OFDM schemes.

In [112] the performances of two time-domain CE techniques named LS and minimum mean square error (MMSE) channel estimation schemes are investigated for OFDM systems in a slow fading multipath channel. In this paper, the basic LS and MMSE channel estimates are modified and estimated through multi-path fading channel assuming different number of taps. It is observed from results obtained that the MMSE CE scheme demonstrated superior performances over LS in terms of mean square error (MSE) and symbol error rate (SER) at various levels of SNR. In [113], the performances of three CE schemes (i.e. LS, LMMSE and LMS) are investigated for SISO-OFDM-based transceivers under two channel types named auto-regressive based fading channel and multi-path Rayleigh fading channel assuming different kinds of pilot arrangements under 16 quadrature amplitude modulation (16-QAM), quadrature phase shift keying (QPSK), binary phase shift keying (BPSK) and differential QPSK (DQPSK) modulation schemes. In [114], the challenges of pilot-aided CE in OFDM systems are addressed using time-domain channel statistics under additive white Gaussian noise (AWGN) channel where CE techniques such as LS, MMSE and DFT-CE are deployed. The autocorrelation matrix of the channel and the noise variance are obtained using noise suppressed channel impulse response where results are analyzed in terms of MSE and SER. The MMSE estimation scheme demonstrated the best performance in comparison to LS and DFT-based CE schemes with LS offering the worst performance. A comparison of two pilot-aided CE techniques are analyzed in [115] for OFDM systems where the performances of maximum likelihood estimator (MLS) and Bayesian MMSE estimator (BMMSEE) are investigated. The MLE does not require information of the SNR and channel statistics while BMMSEE exploits prior information about the channel. This makes the MLE simpler to implement, however BMMSEE demonstrates better accuracy at low SNR. It is concluded that at higher and intermediate SNR, the performances of both schemes are comparable.

In recent times, NC-OFDM has been proposed for higher data rates transmission in cognitive radio context [45, 116]. This technology (born out of OFDM) employs the use of continuous (or contiguous) blocks of subcarriers for the transmission of data symbols. In these systems, the subcarriers been utilized by the primary users (PUs) are deactivated by the secondary users (SUs) [117] with the sole aim of avoiding license users (LUs) interference [118]. Channel estimation is not well studied for NC-OFDM [118], however some channel estimation algorithms have been proposed and implemented in literature by many researchers to improve the performance of the NC-OFDM system. According to [119], it has been proven that equispaced and equipowered pilot tones yields the optimal pilot design for conventional OFDM, on the other hand, this does not hold true for an NC-OFDM system. A new pilot symbol design for channel estimation in NC-OFDM-based cognitive radio systems is proposed in [120]. In this proposed method, convex optimization and cross entropy optimization are adopted for designing of pilot symbols with the purpose of minimizing the MSE of the channel estimate for frequency selective fading channels. In [45], a new LS channel estimation algorithm is proposed for NC-OFDM systems in cognitive radio context. In this proposed scheme, LS channel estimation is adopted and modified for obtaining the channel fading coefficient of subcarriers that transmits the pilot symbols. LS channel estimation with IDFT-based noise reduction is proposed to improve channel estimation accuracy while pilot-block average-based noised reduction (PBANR) is proposed to further improve the performance of CE for slow time-varying channels. Simulation results showed that these proposed algorithms offered better performance than the conventional LS channel estimation method. An improved time domain channel estimation method based on the principles of spectrum sensing adopted at transmitter and receiver is proposed in [116] to improve the performance and reduce noise for NC-OFDM systems. This proposed method (which offered superior performance) is compared with the DFT-based and conventional LS channel estimation methods. In recent times, active research has been taking place in the field of compressive sensing (CS) which finds many applications in mathematics and signal processing communities [121]. The application of CS techniques to sparse CE employs less pilot symbols (or shorter training sequences) for channel estimation. Two main classes of algorithms are considered for CE based on CS [122] which are *convex optimizers* and *greedy* algorithms. The *linear programming* method is based on *Basic Pursuit* (BP) and *Gradient Projection for Sparse Reconstruction* (GPRSR) algorithms while the greedy algorithms include *Matching Pursuit*

(MP), *Orthogonal Matching Pursuit* (OMP), *Stagewise Orthogonal Matching Pursuit* (StOMP), *Regularized Orthogonal Matching Pursuit* (ROMP), *Compressive Sampling Matching Pursuit* (CoSaMP), *Subspace Pursuit* (SP) and *Sparsity Adaptive Matching Pursuit* (SAMP) algorithms. For NC-OFDM systems, sparse channel estimation techniques have been implemented using OMP and SAMP algorithms. In [123], channel estimation based on CS is investigated while the subspace pursuit algorithm is implemented. Results are compared with LS-based CE for both wideband and narrowband interference cases. Min Jia et al. investigates channel estimation based on compressive sensing in [122] where OMP, SAMP and MAMP algorithms are adopted to estimate the channel for NC-OFDM-based transceivers. Results obtained are compared in terms of MSE vs. SNR where MAMP, SAMP, OMP and LS showed superior performances respectively (in decreasing order).

Channel estimation has also been investigated for MIMO systems based on CS in [124]. In this paper, two pilot allocation methods are proposed for CS-based CE. The first method is designed to minimize the largest element in a mutual coherence set. The elements of the coherence set are simply values of mutual coherence that corresponds to the pilot patterns for all the multiple antenna ports. The second proposed method is based on the genetic algorithm (GA) and shifting mechanism. This method demonstrated superior performance in comparison to the first method in terms of MSE and BER while both proposed methods showed better performances as compared with the method proposed in [125]. In [125 - 128], optimal pilot designs for MIMO-OFDM systems are documented.

In decision directed channel estimation (DDCE), training symbols are adopted for channel estimation as well as the re-modulated detected message symbols [111]. In these CE schemes, CE of previous symbols is used for data detection of the current estimates after which the newly detected data is used for estimating the current channel. The detection of data in DDCE can be achieved either by hard or soft decision where bitwise detection is adopted for soft decision while a specific constellation is forced for hard decision [110]. An MSE expression for DFT-based DDCE schemes in M-ary phase shift keying (MPSK) for LTE-A downlink transmission system is proposed in [129]. Simulation results from this scheme are compared with practical systems based on LTE-A downlink standards. It is observed that the results obtained match each other while in [130], a novel soft DDCE technique is proposed which estimates the channel of interfering signals based on demodulation reference signal (DM-RS) using virtual pilot signals

(VPS) for multiuser-MIMO OFDM (MU-MIMO OFDM) based transmission scheme. In this algorithm, reliable data tones are chosen from the desired and interfering signals as VPS after which the quality of CE is improved by using iterative detection and decoding (IDD) scheme. The proposed algorithm showed superior performance gain over conventional approaches that adopt either single user detection (SUD) or multiuser detection (MUD) such as the conventional MMSE for both SUD and MUD assuming 16-QAM and QPSK modulation schemes.

3.4.2 SEMI-BLIND CHANNEL ESTIMATION SCHEMES

In semi-blind methods, information from the transmitted signal's statistical properties as well as training sequences are incorporated to estimate the CIR of the channel. This means that semi-blind methods are hybridization of the pilo-based techniques and blind methods. In [131], semi-blind iterative space-alternating generalized expectation maximization (SAGE) CE algorithm is proposed for massive MIMO systems that makes use of data symbols for CE. In this system, the base station is assumed to have knowledge of its own cell's large scale fading coefficients without being aware of interfering cells. This novel CE algorithm is designed to update the training-based MMSE CE iteratively using SAGE algorithm where the initial estimate is improved by employing pilot symbols and soft information of the transmitted data. This proposed algorithm demonstrated superior performance in comparison with other semi-blind and blind CE schemes reported in literature. In [132], a low-complexity precoding and semi-blind CE scheme is proposed for a two-way multi-relay networks under frequency selective fading channels. The proposed method makes use of a rotation-based matrix for precoding while the composite CIR of each source relay-destination link is estimated using second order statistics of the received signals. Small number of pilot symbols is adopted to eliminate the ambiguity in the proposed CE which is caused by the channel information of the direct link. Results obtained showed that the MSE of the channel estimates varies inversely to the number of training blocks and the SNR as the number of data blocks approaches infinity. A quasi-Newton method for semi-blind CE named Brayben, Fletcher, Goldfarb and Shanno (BFGS) estimation scheme is proposed for uplink cloud radio access networks (C-RANs) that utilizes unknown data symbols and known training sequence for CE in [133]. The maximum likelihood (ML) principle is adopted to improve the performance of CE. Simulation results showed that the proposed algorithm decreases the overhead of bandwidth without sacrificing the MSE performance. The

semi-blind algorithm demonstrated high data throughput and spectral efficiency for C-RAN as compared to the pilot aided CE scheme investigated in this work.

3.4.3 BLIND CHANNEL ESTIMATION SCHEMES

The blind channel estimation scheme requires a lot of data and it is known for exploiting the statistical and mathematical properties of the transmitted data [110, 134, 135]. Two techniques can be adopted assuming blind CE named deterministic and statistical blind CE as shown in Fig. 3.3. Deterministic CE schemes offer better performance in comparison to statistical CE schemes [111] at the expense of very high computational complexity which increases further as the constellation order in the transmitter's modulator increases. Blind CE schemes are known to be bandwidth efficient since they do not require training symbols in order to perform CE, however they are known for their very high computational complexities. However, they only offer superior performances in slow time-varying channels which make them applicable to fast fading channels [111].

Some works have been reported in literature which adopts several blind CE techniques for different wireless communication technologies. A new subspace-based blind channel estimation (SBCE) algorithm that is not affected by null subspace CE errors caused by noise and fading algorithm is proposed in [136] for CP-OFDM schemes named inverse-channel-based blind channel estimation (ICBCE). The performance of this new algorithm is compared with two conventional SBCE CE algorithms named repetition-based blind channel estimation (RPBCE) scheme and re-modulation-based blind channel estimation (RMBCE) scheme. It is known that RPBCE scheme has very high computational complexity. The RMBCE scheme is then designed to offer lower computational complexity in comparison to RPBCE schemes, however the performances of both schemes are similar. The newly proposed ICBCE algorithm outperforms both conventional SBCE schemes (i.e. RMBCE and RPBCE) in terms of MSE at low SNR values while also providing lower computational complexity. Several orthogonal space-time block codes (OSTBC)-based MIMO-OFDM schemes have been reported in literature and are designed to exploit the OSTBC structure together with the inter-subcarrier relationships caused by the FIR channel model. These CE schemes are known for their very high computational complexities. Some works have been reported (such as the sub-channel grouping technique) that proposes methods capable of reducing the computational complexities of existing OSTBC CE

schemes. Most blind CE algorithms are usually applicable to a single block of OSTBC-OFDM data and are only efficient in flat fading channels especially in MIMO-OFDM schemes. In [137], a new blind CE scheme is proposed for OSTBC-OFDM schemes that takes advantage of structural properties of OSTBCs where processing across all subcarriers are processed coherently. This new proposed scheme is efficient in time-varying channels and has no limitations on the numbers of transmit and receive antennas in comparison to other schemes. The algorithm proposed in this paper exploits a semi-definite relaxation (SDR) technique for converting the blind CE problem to a convex semi-definite programming (SDP) form. Substantial simulation performance is demonstrated in comparison with several conventional blind MIMO-OFDM based CE schemes.

3.5 CHANNEL ESTIMATION TECHNIQUES FOR FBMC/OQAM SYSTEMS

The two FBMC waveforms under investigation in this research are filter bank OFDM/OQAM and GFDM/OQAM-based transceivers. This section identifies the channel estimation schemes that have been reported for both waveforms in literature as highlighted in Subsections 3.5.1 and 3.5.2 respectively.

3.5.1 CHANNEL ESTIMATION TECHNIQUES FOR OFDM/OQAM

This subsection presents a literature review of the channel estimation techniques that have been proposed and implemented for OFDM/OQAM-based systems.

In [138], pilot aided channel estimation schemes are implemented for estimating channel coefficients in OFDM/OQAM-based communication system. A new preamble aided estimation scheme named *modified interference approximation method* (MIAM) is developed from the original *interference approximation method* (IAM) scheme [138] for estimating channel conditions. Results are compared with existing methods such as the *wide* and *narrow auxiliary pilot* (AP) schemes. The proposed scheme (MIAM) is designed to solve the suffering of pilot symbol imaginary interference. However, from the results obtained, AP scheme achieves better estimation performance in terms of mean square error and bit error rate.

In [139], a preamble-based CE scheme is proposed to improve the existing IAM estimation method. The IAM channel estimation technique depends on the knowledge of pilot neighborhood for the approximation of interference in order to improve CE performance. This technique (IAM) consists of *IAM-R* and *IAM-C* where R and C are real and imaginary pilot

symbols respectively. In IAM-C, the pilot symbols are imaginary (complex) as shown in Fig. 3.4 where offset quadrature phase shift keying (OQPSK) is assumed with $M = 8$ subcarriers.

0	1	0	0	1	0	j	1	-j
0	-1	0	0	-j	0	-1	-j	1
0	-1	0	0	-1	0	-j	-1	j
0	1	0	0	j	0	1	j	-1
0	1	0	0	1	0	j	1	-j
0	-1	0	0	-j	0	-1	-j	1
0	-1	0	0	-1	0	-j	-1	j
0	1	0	0	j	0	1	j	-1
	(a)			(b)			(c)	

Fig. 3.4 Pilot arrangements for (a) IAM-R, (b) IAM-C, (c) E-IAM-C for *M* = 8 using OQPSK [136]

In these IAM schemes, pseudo-pilots are obtained by restructuring the training symbols of maximum magnitude. The interference weights follow a specific pattern for all frequency k and time n indices**.**

$$\begin{matrix} (-1)^k\delta & -\beta & (-1)^k\delta \\ -(-1)^k\gamma & x[n,k] & (-1)^k\gamma \\ (-1)^k\delta & \beta & (-1)^k\delta \end{matrix} \tag{3.1}$$

where $x[n,k]$ represents the training symbols surrounding the pilot while β, γ are chosen to be greater than δ and are given as:

$$\beta = \sum_{\dot{n}\,=\,0}^{L_p-1} p^2(\dot{n}) \exp\left(j\frac{2\pi}{M}\left(\dot{n} - \frac{L_p-1}{2}\right)\right) \tag{3.2}$$

$$\gamma = \sum_{\dot{n}\,=\,\frac{M}{2}}^{L_p-1} p(\dot{n})\, p\left(\dot{n} - \frac{M}{2}\right) \tag{3.3}$$

$$\delta = -j \sum_{\dot{n}=\frac{M}{2}}^{L_p-1} p(\dot{n})\, p\left(\dot{n} - \frac{M}{2}\right) \exp\left(j \frac{2\pi}{M}\left(\dot{n} - \frac{L_p - 1}{2}\right)\right) \tag{3.4}$$

In (3.2)**,** (3.3), and (3.4)**,** p represents the impulse response of the prototype filter, while L_p is the length of the prototype filter. The proposed algorithm in this paper extends the IAM pilot-based algorithms (which have nulls at neighbouring time instants) and is built into a structure that consists of significantly larger pseudo-pilots. This new structure is called *extended IAM-C* (E-IAM-C). From this work, the proposed E-IAM-C algorithm provided a better estimation performance when compared to IAM-R and IAM-C. In [140], a short preamble-based CE algorithm is developed where the preamble consists of only one pilot FBMC symbol for highly frequency selective channels in OFDM/OQAM systems. Simulation results demonstrate the effectiveness of this algorithm in both frequency and time domain IAM-C channel estimation methods for mildly and highly frequency selective channels.

A novel pilot design scheme named *composite pilot pair* (CPP) which takes advantages of the filter's localization properties for a simple CE method at receiver is proposed in [142]. It captures the major part of channel induced distortions. Results are compared with existing AP schemes in terms of MSE and un-coded BER. The proposed CCP demonstrated superior performance in comparison to the existing AP schemes.

In [143], a novel preamble-based algorithm is proposed for narrowband per-subcarrier maximum likelihood (ML) channel estimation as shown in (3.11). This new method is based on the ML channel estimator. The major extension in this method involves the assumption that only the training sequence transmitted in the observed subcarrier is known while unknown (data) symbols are transmitted in two neighboring subcarriers that are immediately adjacent to themselves. This new CE method is improved using the expectation maximization (EM) algorithm and it is designed to iteratively approach and improve the ML estimator's performance as shown in (3.14). The EM-ML channel estimator is known for providing an increase in spectral efficiency as only a few numbers of subcarriers are filled with training symbols. Fig. 4 in [143] describes the subcarrier model for the FBMC system. From this figure, if the synthesis and analysis filters are respectively represented by $\boldsymbol{g}_k[n]$ and $\boldsymbol{f}_k[n]$, then the received signal $\boldsymbol{s}_k[n]$ at a given

subcarrier k when input OQAM symbols $\boldsymbol{x}_k[n]$ are transmitted across the channel $\boldsymbol{h}_k[n]$ is represented as

$$\boldsymbol{s}_k[n] = \left(\boldsymbol{X}_k[n]\boldsymbol{G}_{k,k} + \boldsymbol{X}_{k-1}[n]\boldsymbol{G}_{k,k-1} + \boldsymbol{X}_{k+1}[n]\boldsymbol{G}_{k,k+1}\right)\boldsymbol{h}_k + \mathbf{F}_k\boldsymbol{\eta}[\dot{n}] \tag{3.5}$$

where $\boldsymbol{X}_k[n]$, $\boldsymbol{X}_{k-1}[n]$ and $\boldsymbol{X}_{k+1}[n]$ are Hankel matrices obtained from the input OQAM symbols while $\boldsymbol{G}_{k,k}$, $\boldsymbol{G}_{k,k-1}$ and $\boldsymbol{G}_{k,k-1}$ are Toeplitz matrices containing the impulse responses of the synthesis filters. The CIR are contained in $\boldsymbol{h}_k$ and $\mathbf{F}_k$ is a matrix containing the impulse response of the analysis filter bank while $\boldsymbol{\eta}$ contains AWGN samples with zero mean and variance σ_η^2. From (3.5), let $\boldsymbol{D}_k[n] = \boldsymbol{X}_k[n]\boldsymbol{G}_{k,k}$, $\boldsymbol{Q}_k[n] = \boldsymbol{X}_{k-1}[n]\boldsymbol{G}_{k,k-1} + \boldsymbol{X}_{k+1}[n]\boldsymbol{G}_{k,k+1}$ and ύ $= \mathbf{F}_k\boldsymbol{\eta}[\dot{n}]$, if the time and subcarrier index are neglected for notation simplicity, then (3.5) reduces to

$$\boldsymbol{s} = (\boldsymbol{D} + \boldsymbol{Q})\boldsymbol{h} + \acute{\upsilon} \tag{3.6}$$

The covariance matrix $\boldsymbol{R}_{\acute{\upsilon}\acute{\upsilon}}$ of the noise according to (3.6) is given as

$$\boldsymbol{R}_{\acute{\upsilon}\acute{\upsilon}} = \sigma_\eta^2\mathbf{F}\mathbf{F}^{\boldsymbol{H}} \tag{3.7}$$

while the per-subcarrier ML channel estimate is then given by

$$\widehat{\boldsymbol{h}}_{\boldsymbol{ML}} = \underset{h}{\operatorname{argmax}}\, p(\boldsymbol{s}|\boldsymbol{h}) = \underset{h}{\operatorname{argmin}}\, J(\boldsymbol{h}) \tag{3.8}$$

where

$$\begin{aligned} J(\boldsymbol{h}) &= (\boldsymbol{s} - (\boldsymbol{D} + \boldsymbol{Q})\boldsymbol{h})^H \boldsymbol{R}_{\acute{\upsilon}\acute{\upsilon}}{}^{-1}(\boldsymbol{s} - (\boldsymbol{D} + \boldsymbol{Q})\boldsymbol{h}) \\ &= (\boldsymbol{s}^H - (\boldsymbol{D} + \boldsymbol{Q})^H\boldsymbol{h}^H)\ \boldsymbol{R}_{\acute{\upsilon}\acute{\upsilon}}{}^{-1}(\boldsymbol{s} - (\boldsymbol{D} + \boldsymbol{Q})\boldsymbol{h}) \\ &= \left(\boldsymbol{s}\boldsymbol{s}^H - \boldsymbol{s}^H(\boldsymbol{D} + \boldsymbol{Q})\boldsymbol{h} - \boldsymbol{s}(\boldsymbol{D} + \boldsymbol{Q})^H\boldsymbol{h}^H + ((\boldsymbol{D} + \boldsymbol{Q})^H\boldsymbol{h}^H)\left((\boldsymbol{D} + \boldsymbol{Q})\boldsymbol{h}\right)\right)\boldsymbol{R}_{\acute{\upsilon}\acute{\upsilon}}{}^{-1} \end{aligned} \tag{3.9}$$

The per-subcarrier ML channel estimate is finally obtained by differentiating $J(\boldsymbol{h})$ with respect to $\boldsymbol{h}^H$ and equating the expression to zero. Hence,

$$\frac{\partial J(\boldsymbol{h})}{\partial \boldsymbol{h}^H} = -\boldsymbol{s}(\boldsymbol{D} + \boldsymbol{Q})^H\boldsymbol{R}_{\acute{\upsilon}\acute{\upsilon}}{}^{-1} + ((\boldsymbol{D} + \boldsymbol{Q})^H(\boldsymbol{D} + \boldsymbol{Q})\boldsymbol{h})\,\boldsymbol{R}_{\acute{\upsilon}\acute{\upsilon}}{}^{-1} = 0 \tag{3.10}$$

The expression for the per-subcarrier ML channel estimate of the narrowband multipath fading channel (as derived in this paper) is then obtained from (3.10) as:

$$\widehat{\boldsymbol{h}}_{\boldsymbol{ML}} = \frac{(\boldsymbol{D} + \boldsymbol{Q})^{H} \boldsymbol{R}_{\acute{u}\acute{u}}{}^{-1}\boldsymbol{s}}{\left((\boldsymbol{D} + \boldsymbol{Q})^{H}(\boldsymbol{D} + \boldsymbol{Q})\right) \boldsymbol{R}_{\acute{u}\acute{u}}{}^{-1}} \tag{3.11}$$

The system model is improved by the introduction of EM-ML channel estimation where an interference term $\boldsymbol{u}$ with improper statistics is considered. In EM algorithm, a rough estimate of the channel (which ignores interference) is obtained before the first iteration given by

$$\widehat{\boldsymbol{h}} = \frac{\boldsymbol{D}^{H} \boldsymbol{R}_{\acute{u}\acute{u}}{}^{-1}\boldsymbol{s}}{\left(\boldsymbol{D}^{H} \boldsymbol{R}_{\acute{u}\acute{u}}{}^{-1}\boldsymbol{D}\right)} \tag{3.12}$$

As the iterative process (with index i) begins, the EM algorithm is divided into two steps named E-step and M-step. In the E-step, the ML function is approximated by taking the average (or expected) value shown as:

$$E_{\boldsymbol{u}|\boldsymbol{s},\boldsymbol{h}_i}\left[\frac{\partial J(\boldsymbol{h}_i)}{\partial \boldsymbol{h}_i{}^{H}}\right] = \left(\boldsymbol{D}^{H} \boldsymbol{R}_{\acute{u}\acute{u}}{}^{-1}(\boldsymbol{D} + E[\boldsymbol{Q}]) + E[\boldsymbol{Q}]^{H} \boldsymbol{R}_{\acute{u}\acute{u}}{}^{-1}\boldsymbol{D} + E\left[\boldsymbol{Q}^{H}\boldsymbol{R}_{\acute{u}\acute{u}}{}^{-1}\boldsymbol{Q}\right]\right)\boldsymbol{h}_i - (\boldsymbol{D} + E[\boldsymbol{Q}])^{H} \boldsymbol{R}_{\acute{u}\acute{u}}{}^{-1}\boldsymbol{s} \tag{3.13}$$

Equation (3.13) is then solved using M-step to yield the new ML channel estimate $\boldsymbol{h}_i$ over the ith iteration based on EM by minimizing $J(\boldsymbol{h}_i)$ which gives

$$\widehat{\boldsymbol{h}}_{i+1} = \frac{\left(\boldsymbol{D} + \widehat{\boldsymbol{Q}}_{\boldsymbol{i}}\right)^{H} \boldsymbol{R}_{\acute{u}\acute{u}}{}^{-1}\boldsymbol{s}}{\left(\boldsymbol{D} + \widehat{\boldsymbol{Q}}_{\boldsymbol{i}}\right)^{H}\left(\boldsymbol{D} + \widehat{\boldsymbol{Q}}_{\boldsymbol{i}}\right) \boldsymbol{R}_{\acute{u}\acute{u}}{}^{-1} + \boldsymbol{\Psi}_{\boldsymbol{i}}} \tag{3.14}$$

More details on the derivation of this EM-based ML channel estimate as well as $\boldsymbol{\Psi}_{\boldsymbol{i}}$ in (3.14) is obtainable in this paper.

In [141], a performance comparison between two models for the received subcarrier signals is made. This includes a per-subcarrier *broadband* channel model as well as its *narrowband* equivalent. Three cases of interference embedded CE schemes are considered and applied to both the broadband and narrowband channel models. These interference embedded CE techniques involve CE in the presence of ISI only, ICI only and in situations of both ICI and ISI. From results obtained, both broadband and narrowband-based models offered the best normalized mean square error (NMSE) performances when ISI only was considered. ICI came next in estimation performance while estimation in the presence of both ICI and ISI offered the worst CE performance.

In [144] a new way of designing training sequences based on per-subcarrier ML-CE algorithm is introduced. The use of both transmitter and receiver prototype filters are adopted for calculation of pilot sequences in this novel method where gradient projection algorithm is assumed for finding the optimum sequences while targeting the minimum mean square error (MMSE) of the CE scheme.

Estimation of time-varying channels is adopted in [77] where dual optimal Kalman filters are introduced for estimating fading channel statistics as well as their unknown pth order autoregressive parameters in an OFDM/OQAM-based wireless system. The optimal dual Kalman fading process is modelled in state-space form as

$$\boldsymbol{h}_k = \boldsymbol{\phi}\boldsymbol{h}_{k-1} + \boldsymbol{g}\boldsymbol{v}_k \tag{3.15}$$

where

$$\boldsymbol{\phi} = \begin{bmatrix} -a_1 & -a_2 & \cdots & -a_p \\ 1 & 0 & \cdots & 0 \\ \vdots & \vdots & \vdots & \vdots \\ 0 & \cdots & 1 & 0 \end{bmatrix} \tag{3.16}$$

$$\boldsymbol{g} = [1 \quad 0 \quad . \quad . \quad . \quad 0]^T \tag{3.17}$$

The symbol a_p in (3.16) represents the autoregressive parameters while the received signal is given as

$$\boldsymbol{s}_k = \boldsymbol{x}_k{}^T\boldsymbol{h}_k + \boldsymbol{\eta}_k \tag{3.18}$$

where $\boldsymbol{x}_k$ are the transmitted OQAM pilots and $\boldsymbol{\eta}_k$ is the AWGN noise with variance σ_η^2. In this CE algorithm, the a posteriori channel estimate is given as

$$\widehat{\boldsymbol{h}}_{k|k} = \boldsymbol{\phi}\,\widehat{\boldsymbol{h}}_{k-1|k-1} + \boldsymbol{K}_k\boldsymbol{\alpha}_k \tag{3.19}$$

where $\boldsymbol{K}_k$ is known as the Kalman gain given by

$$\boldsymbol{K}_k = \mathbf{P}_{k|k-1}\boldsymbol{x}_k\mathbf{C}_k{}^{-1} \tag{3.20}$$

In (3.20), $\mathbf{P}_{k|k-1}$ is termed a priori error covariance matrix and is obtained recursively as

$$\mathbf{P}_{k|k-1} = \phi\mathbf{P}_{k|k-1}\phi^H + \boldsymbol{g}\sigma_v^2\boldsymbol{g}^T \tag{3.21}$$

The state vector in (3.19) and the error covariance matrix in (3.20) are initially assigned zeros and the identity matrix respectively. This proposed method shown in (3.19) estimates the fading coefficients at pilot symbol positions, while linear, spline and low-pass interpolation are adopted for estimating data position fading coefficients. Simulation results demonstrated the superior performance of the proposed method to existing adaptive schemes. Fig. 3.5 displays the channel estimation techniques that have been adopted for FBMC/OQAM systems in literature.

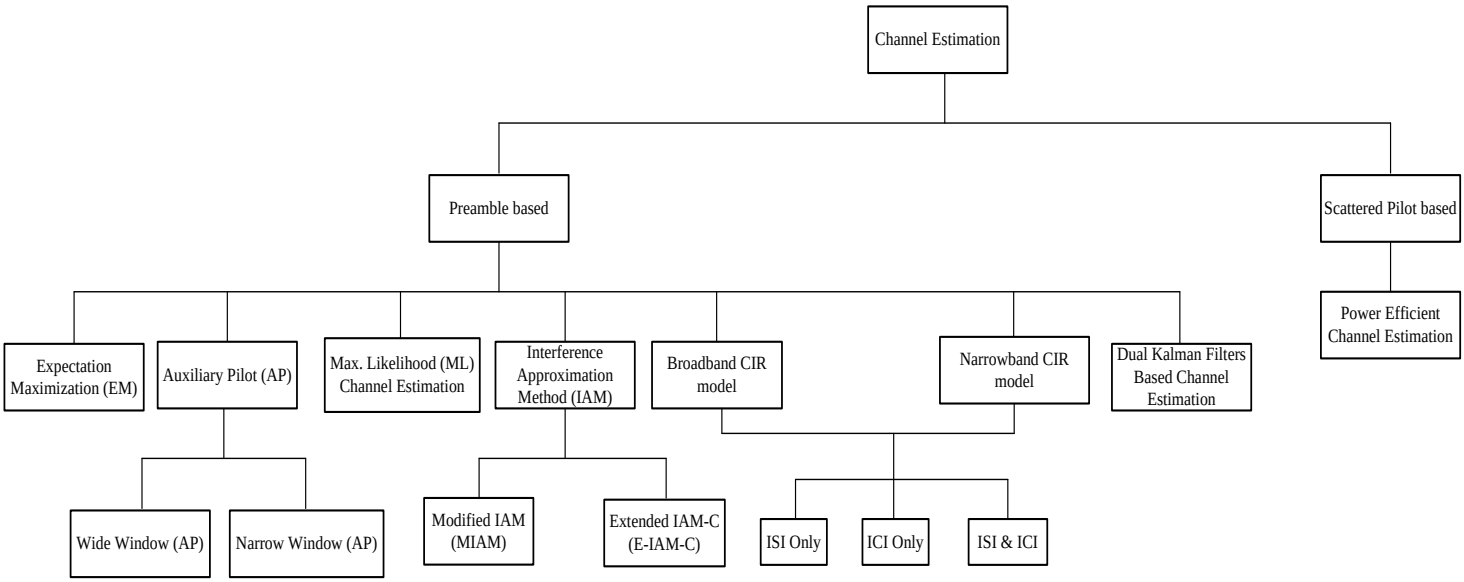

Fig. 3.5 Channel estimation techniques adopted for OFDM/OQAM based transceivers in literature

3.5.2 CHANNEL ESTIMATION TECHNIQUES FOR GFDM/OQAM

The work presented in [144] is the only one, to the best of our knowledge, reported in literature that has proposed channel estimation scheme for GFDM-based transceivers (i.e. GFDM/QAM). There is no work reported in literature that has investigated CE for GFDM/OQAM-based systems. Fig. 3.6 shows a diagrammatic classification of channel estimation schemes that have been proposed for the conventional filter bank (GFDM/OQAM) system in literature.

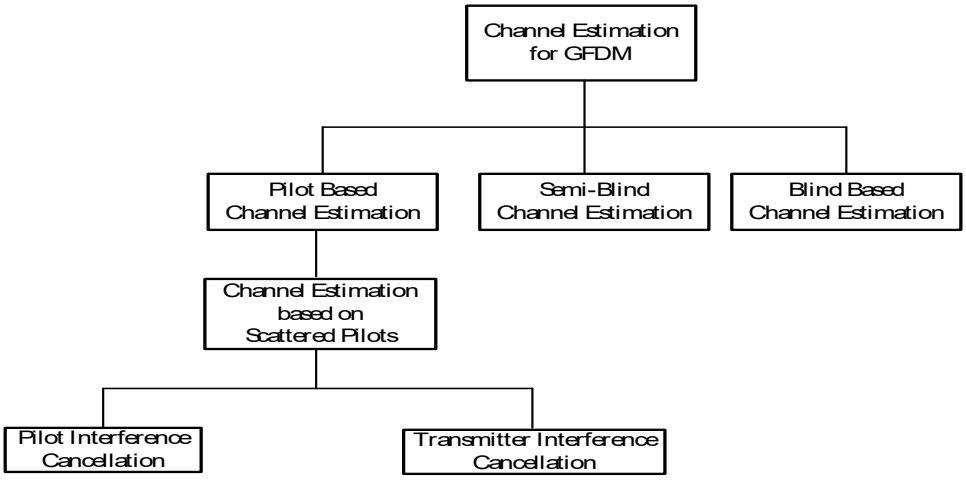

Fig. 3.6 Channel estimation schemes adopted for conventional GFDM system in literature

In [144], two novel pilot-based CE methods namely *pilot interference cancellation* (Pilot–IC) and *transmitter interference cancellation* (Tx-IC) are proposed for estimating the fading channel coefficients for GFDM-based transceivers with QAM modulation (i.e. GFDM/QAM). In Pilot-IC, interference is only pre-cancelled at pilot symbols while interference is simultaneously pre-cancelled at both pilot and data symbols for Tx-IC. These estimation algorithms are realized with scattered pilots over time and frequency grid ensuring a reduction in overhead, thus making it possible for the estimation of frequency selective and time-varying channels. In this paper, $K \times M$ complex valued data symbols (where K is the total number of subcarriers and M is the number of sub-symbols) are considered for transmission such that the symbols to be transmitted are collected into a vector given as

$$\mathbf{d} = \left[d_{0,0}\, d_{1,0} \ldots d_{K-1,0}\, d_{0,1}\, d_{1,1} \ldots\ d_{K-1,1} \ldots d_{0,M-1}\, d_{1,M-1}\, d_{K-1,M-1}\right]^T \tag{3.22}$$

The symbols in (3.22) are circularly convolved with a pulse shaping filter $\boldsymbol{g}_{k,m}[n]$ whose impulse response are formed into a $KM \times KM$ transmitter modulation matrix denoted as $\boldsymbol{A}$. The signal to be transmitted is then represented as

$$\mathbf{x} = \boldsymbol{A}\mathbf{d} \tag{3.23}$$

Cyclic prefix is added to the transmitted signal which is then transmitted over the multipath fading channel. The received signal is given by

$$\boldsymbol{y}[\mathrm{n}] = \boldsymbol{x}[\mathrm{n}] * \boldsymbol{h}[\mathrm{n}] + \boldsymbol{w}[\mathrm{n}] \tag{3.24}$$

where * denotes linear convolution, $\boldsymbol{x}[\mathrm{n}]$ is the transmitted signal given in (3.23) with added CP while $\boldsymbol{h}[\mathrm{n}]$ is the channel impulse response and $\boldsymbol{w}[\mathrm{n}]$ is the AWGN with zero mean and variance σ_w^2.

For CE to be evaluated for this waveform, the interference that is introduced due to pulse shaping at transmitter is pre-cancelled with pre-coded transmitted data given as

$$\mathbf{d}^{"} = (\boldsymbol{A}\boldsymbol{A}^H)^{-1}\mathbf{d} \tag{3.25}$$

Equation (3.25) describes the proposed Tx-IC scheme where the transmitted data is given as

$$\mathbf{x} = \boldsymbol{A}\mathbf{d}^{"} \tag{3.26}$$

The received signal $\mathbf{z}_{k_p,\, m_p}$on the kth subcarrier and mth sub-symbol obtained from the matched filter (MF) receiver at pilot symbols is represented as

$$\mathbf{z}_{k_p,\, m_p} = \boldsymbol{A}^H\mathbf{y} \tag{3.27}$$

Hence, the channel estimate $\hat{\mathbf{h}}_{k_p,\, m_p}$ on the kth subcarrier and mth sub-symbol at time n located at pilot positions due to Tx-IC is given as

$$\hat{\mathbf{h}}_{k_p,\, m_p} = \frac{\mathbf{z}_{k_p,\, m_p}}{\mathbf{d}_{k_p,\, m_p}} \tag{3.28}$$

where $\mathbf{z}_{k_p,\, m_p}$ is the received signal given in (3.27) while $\mathbf{d}_{k_p,\, m_p}$ are the transmitted data on the kth subcarrier and mth sub-symbol at pilot location.

In Pilot–IC CE, the generated interference (due to pulse shaping filter) is only pre-cancelled at pilot symbol locations in the transmitter. This interference $\boldsymbol{a}_{(\Delta k,\Delta m)}$ at pilot symbols is calculated as

$$\boldsymbol{a}_{(\Delta k,\Delta m)} = \boldsymbol{g}_{k,m}[n]\boldsymbol{g}^*_{k-\Delta k\,,m-\Delta m}[n] \tag{3.29}$$

where $\boldsymbol{g}_{k,m}[n]$ is the impulse response of the pulse shaping filter formulated into the $KM \times KM$ transmitter modulation matrix $\boldsymbol{A}$. The values of Δk and Δm provides information on ICI generated by neighboring data from Δk subcarriers away and also ISI that is created by neighboring data from Δm sub-symbols away. In this scheme (i.e. Pilot–IC CE), the pilot symbols at k_pth subcarrier and m_pth sub-symbol is represented as

$$\mathbf{d}^{"}_{k_p, m_p} = \mathbf{d}_{k_p, m_p} - \mathbf{d}^{IC,nb}_{k_p, m_p} \tag{3.30}$$

where $\mathbf{d}^{IC,nb}_{k_p, m_p}$ is the interference term that is generated by neighbor symbols expressed in (3.30) while $\mathbf{d}_{k_p, m_p}$ is the intended pilot symbols.

$$\mathbf{d}^{IC,nb}_{k_p, m_p} = \sum_{(k,m)_{nb} \neq (k_p, m_p)} \mathbf{d}_{k,m} \boldsymbol{a}_{(k-k_p, m-m_p)} \tag{3.31}$$

At the MF receiver, the received signal associated with pilot signals $\boldsymbol{y}_p[\mathrm{n}]$ according to (3.24) is filtered with $\boldsymbol{g}^*_{k_p, m_p}[n]$ to yield

$$\begin{aligned} \mathbf{z}_{k_p, m_p} &= \sum_n \boldsymbol{y}_p[\mathrm{n}] \boldsymbol{g}^*_{k_p, m_p}[n] \\ &= \mathbf{h}_{k_p, m_p} \mathbf{d}^{"}_{k_p, m_p} + \sum_n \mathbf{h}_{k_p, m_p} \mathbf{d}_{k,m} \boldsymbol{a}_{(k-k_p, m-m_p)} + \boldsymbol{I}_f \cong \mathbf{h}_{k_p, m_p} \mathbf{d}_{k_p, m_p} \end{aligned} \tag{3.32}$$

where $\boldsymbol{I}_f$ in (3.32) is the negligible interference term caused from the rest of the data symbols excluding the neighboring ones. Based on this information, the channel coefficients at pilot locations is similarly estimated according to Pilot–IC CE algorithm using (3.28) where $\mathbf{z}_{k_p, m_p}$ in this case is obtained from (3.32).

The performances of the two proposed CE schemes are analyzed in terms of MSE and un-coded BER for time-invariant frequency selective pedestrian B (PB) channels where pilot symbols are scattered over the subcarriers of one GFDM symbol with interpolation performed in frequency domain. The CE performances of the two proposed algorithms are compared with the CE performance of conventional OFDM. Initial results obtained showed that the two proposed algorithms demonstrated the same MSE performance having comparable performance with OFDM. The performances of both CE techniques are analyzed for MF and zero forcing (ZF) receivers using same PB channel. It is observed from un-coded BER performances that both pilot-IC and Tx-IC have the same BER performance which is also comparable to OFDM systems. The BER performance of the two proposed CE algorithms for GFDM system is analyzed for various transmitter-receiver settings over AWGN channel. It is observed that GFDM systems using Tx-IC transmitter as well as MF receiver (with Tx-IC channel estimation) performs relatively the same as GFDM system with Pilot-IC transmitter and zero forcing

receivers (with Pilot-IC CE). Since the two proposed CE schemes demonstrated similar performances, it is concluded in this paper that interference can either be cancelled at either the transmitter or the receiver.

3.6 CHAPTER SUMMARY

In general wireless communication systems, transmitting signals propagating through a wireless channel can experience several undesirable effects such as multipath propagation and fading as a result of the physical properties of the communication channel. The multipath propagation and fading experienced result into attenuation, distortion, delay as well as phase shifting of the received symbols. To compensate for these detrimental effects (experienced by the propagating signals), perfect and up-to-date estimates of the channel is carried out through the process of channel estimation which consists of methods such as pilot (or training) based techniques, semi blind or blind methods. In this chapter, the basic mechanisms of propagation in general wireless communication systems is described with detailed description and illustration of the effects of multipath propagation as well as the types of fading experienced by transmitting signals as they propagate across the wireless channels. An overview of the basic concepts and types of channel estimation techniques is also presented while the channel estimation schemes that have been reported in literature for estimating the channel in filter bank OFDM/OQAM and GFDM/OQAM-based transceivers are reviewed and documented.

.

CHAPTER FOUR

SYSTEM MODEL DESCRIPTION

4.1 INTRODUCTION

In this chapter, the proposed waveforms under investigation (in this dissertation) are analyzed. The two filter bank multicarrier waveforms considered are OFDM/OQAM and GFDM/OQAM-based transceivers. An introduction to the basic concepts of these waveforms is given while system model diagram and elaborate mathematical analysis for these systems are presented assuming conditions of near perfect reconstruction and non-perfect reconstruction design of prototype filters. In NPR, the distortion of signals is minimized from accurate design of an FIR low-pass prototype filter which also reduces amplitude distortions. For Non-PR (i.e. imperfect reconstruction), aliasing and amplitude distortions are more prominent which may reduce system efficacy. Section 4.2 of this chapter gives an introduction to the filter bank OFDM/OQAM system while providing system description of this filter bank transceiver assuming both conditions of NPR and Non-PR. In Section 4.3, the system model of GFDM/OQAM is described while Section 4.4 describes the adopted channel estimation schemes for both waveforms with Section 4.5 concluding the chapter.

4.2 FILTER BANK OFDM/OQAM-BASED TRANSCEIVER

Filter bank multicarrier is proposed to be an alternative MCM scheme that improves on the shortcomings of OFDM-based systems while emphasis is made on spectral efficiency improvement [145, 146]. FBMC systems employ the use of finite impulse response prototype filters that possess longer impulse response than the symbol period (T) [72, 147]. In other words, the length of the prototype filter (L_p) is greater than the total number of subcarriers (M). The prototype filter reduces signal side lobes that result into ICI, ISI and energy wastage. A higher spectral efficiency is achieved by FBMC-based schemes in comparison to CP-OFDM systems because of the absence of CP, hence making it a suitable technique for cognitive radio systems [148].

Filter bank multicarrier-based on offset quadrature amplitude modulation is a special type of FBMC scheme that yields high data rates as result of the absence of cyclic prefix. Unlike

traditional CP-OFDM systems, the real and imaginary parts of the quadrature amplitude modulation (QAM) symbols are separately processed with two times the symbol rate in filter bank OFDM/OQAM [146]. In other words, elimination of ICI and ISI in this MCM system involves staggering the real and imaginary parts of the input symbols by $T/2$ hence the name 'offset QAM (OQAM)' [78], also referred to as staggered QAM [149].

4.2.1 SYSTEM MODEL DESCRIPTION OF OFDM/OQAM-BASED SCHEME

The general stages of the proposed OFDM/OQAM scheme consist of a transmitter, channel and a receiver structure. The OFDM/OQAM structure is made up of the synthesis filter bank at the transmitter and the analysis filter bank at the receiver. In Chapter 2, Subsection 2.3.1, the general structure of FBMC-based transceivers has been described. This structure is adopted and further developed in order to realize the design of the OFDM/OQAM system where the input QAM symbols are pre-processed and transformed at the transmitter. The reverse process is implemented at the receiver to ensure proper demodulation of the transmitted signal as shown in the block representation of the OFDM/OQAM system model illustrated in Fig. 4.1.

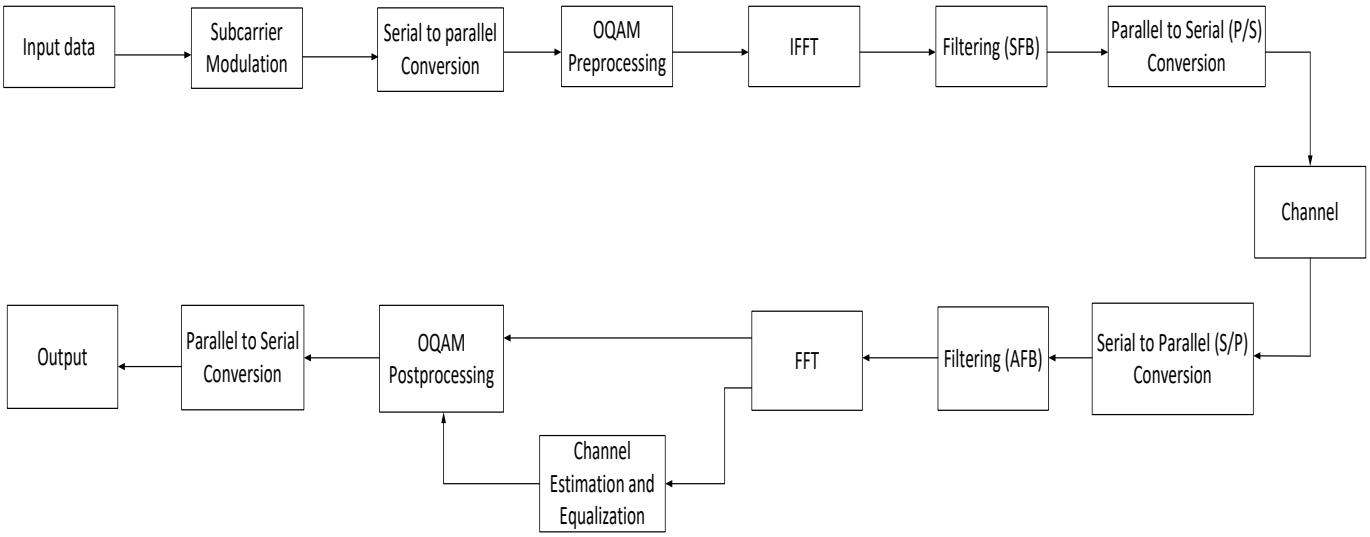

Fig. 4.1 General structure of filter bank OFDM/OQAM system

The stages of the system diagram depicted in Fig. 4.1 consist of OQAM pre-processing/post processing, transform blocks, filtering, channel estimation and signal conversions (i.e. serial/parallel and parallel/serial conversions). In Subsection 4.2.1.1, a detailed description of the transmitter of the proposed filter bank OFDM/OQAM-based system is described. Subsections

4.2.1.2 and 4.2.1.3 give the respective description of the channel and receiver for this system assuming NPR. The system model assuming Non-PR is given in Subsection 4.2.1.4.

4.2.1.1 TRANSMITTER DESCRIPTION OF PROPOSED OFDM/OQAM SYSTEM

At the transmitter of the filter bank OFDM/OQAM system model, the complex valued QAM symbols at the input ($c[l,k]$) usually have their real and imaginary parts interleaved by a time offset of $T/2$ where T is the signaling period. After the bits are mapped into symbols, OQAM pre-processing is performed on the QAM symbols where the complex-valued input symbols are mapped into real-valued data symbols $d[n,k]$ at k subcarrier index (representing the in-phase components of ($c[l,k]$) and are transmitted at a rate $2/T$ where $T = 1/\Delta f$ while Δf is the subcarrier spacing. The quadrature components of the input symbols $c[l,k]$ are represented as $d[n+1,k]$ in an entire process termed "complex to real conversion". The system model shown in Fig. 4.2 gives a diagrammatic representation of the transmitter of the OFDM/OQAM-based system while equations corresponding to each block are derived according to [77].

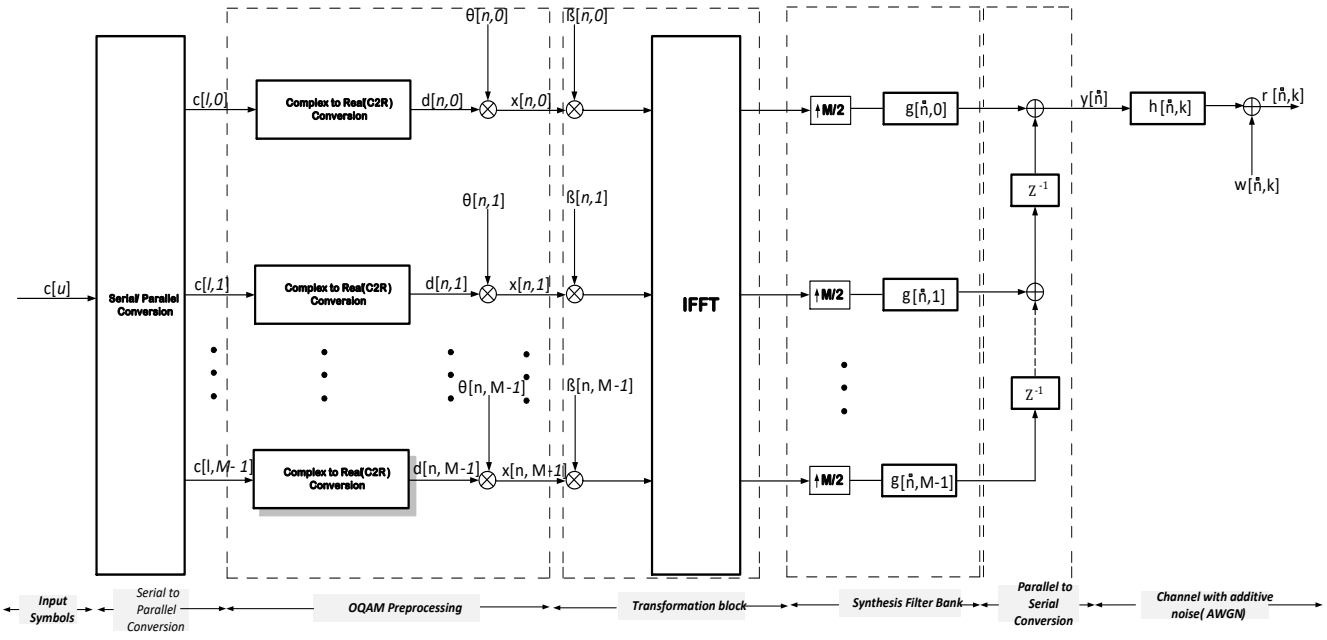

Fig. 4.2 Structure of a filter bank OFDM/OQAM transmitter

The conversion of the complex valued input symbols to real symbols is mapped mathematically as [46, 77]:

$$d[n,k] = \begin{cases} R_e(c[l,k]); & k\ even \\ I_m(c[l,k]); & k\ odd \end{cases} \quad (4.1a)$$

$$d[n+1,k] = \begin{cases} I_m(c[l,k]); & k\ odd \\ R_e(c[l,k]); & k\ even \end{cases} \quad (4.1b)$$

In (4.1), l represents the OQAM preprocessing input/post processing output sample index while n is the OQAM preprocessing output/post processing input sample index. R_e and I_m signifies the real and imaginary parts of the complex valued input symbols respectively. To ensure orthogonality of subcarriers, $\theta[n,k]$ is multiplied by $d[n,k]$ [74, 98]. This results in

$$x[n,k] = d[n,k]\theta[n,k] \quad (4.2)$$

where $x[n,k]$ is the OQAM preprocessing output symbols and

$$\theta[n,k] = j^{k+n} \quad (4.3)$$

Before inverse fast Fourier transform is implemented, $x[n,k]$ undergoes a transformation process where it is multiplied by the factor β as

$$\beta[n,k] = (-1)^{kn} \exp\left(-j\frac{2\pi k}{M}\left(\frac{L_p-1}{2}\right)\right) \quad (4.4)$$

where M is the IFFT size or the total number of subcarriers, k is the subcarrier index for $k = 0,1,2,\dots,M-1$, and L_p is the length of the FBMC prototype filter $p[n,k]$ given as:

$$L_p = KM \quad (4.5)$$

In (4.5), K is the overlapping factor that determines the number of symbols that superpose each other in time. The use of complex modulated filter banks are employed to ensure high spectral efficiency. The sub-channel synthesis filter bank impulse response $g[\dot{n},k]$ is expressed as [77, 78, 81, 143, 150]:

$$g[\dot{n},k] = p[\dot{n}] \exp\left(j\frac{2\pi k}{M}\left(\dot{n} - \frac{L_p-1}{2}\right)\right) \quad (4.6)$$

where $\dot{n}$ in (4.6) is the symbol index at SFB output and AFB input for $\dot{n} = 0,1,2,\ldots,L_p - 1$. To achieve nearly perfect reconstruction prototype filters, the finite impulse response of the low-pass prototype filter $p[\dot{n}]$ is defined as [46, 77, 150]:

$$p[\dot{n}] = \tilde{P}[0] + 2\sum_{k=1}^{\frac{L_p-1}{2}} (-1)^k \tilde{P}[k] \cos\left(\omega[k]\left(\dot{n} + \frac{KM - (L_p - 1)}{2}\right)\right) \tag{4.7}$$

where $\omega[k]$ is the uniformly spaced frequency points given as:

$$\omega[k] = \frac{2\pi k}{KM} \tag{4.8}$$

for $\dot{n} = 0,1,2,\ldots,L_p - 1$ and $\tilde{P}[0] = 1$. $p[\dot{n}]$ is designed such that the following expression is achieved:

$$\tilde{P}[c]^2 + \tilde{P}[K - c]^2 = 1 \tag{4.9}$$

where $c = 1,2,\ldots,\lfloor K/2 \rfloor$ and $\tilde{P}[0] = 0$ for $k = K, K+1, \ldots, \frac{(L_p-1)}{2}$.

These requirements can be summarized as follows in situations where polyphase filtering structures are employed for the proposed OFDM /OQAM-based system.

$$\begin{cases} \tilde{P}[0] = 1 \\ \tilde{P}[c]^2 + \tilde{P}[K - c]^2 = 1, & for\ c = 1,2,\ldots,\lfloor K/2 \rfloor \\ \tilde{P}[0] = 0, & for\ k = K, K+1, \ldots, \dfrac{(L_p - 1)}{2}, \end{cases} \tag{4.10}$$

For this system, the values of $\tilde{P}[c]$ are initialized and designed as shown in Table 4.1 for different values of overlapping factors (K).

Table 4.1 Prototype filter impulse response for different values of overlapping factor (K)

Overlapping Factor (K)	4				3			2		1
Filter Impulse ($\tilde{P}[c]$)	$\tilde{P}[0]$	$\tilde{P}[1]$	$\tilde{P}[2]$	$\tilde{P}[3]$	$\tilde{P}[0]$	$\tilde{P}[1]$	$\tilde{P}[2]$	$\tilde{P}[0]$	$\tilde{P}[1]$	$\tilde{P}[0]$
	1	0.9720	$\frac{\sqrt{2}}{2}$	0.2351	1	0.9114	0.4114	1	$\frac{\sqrt{2}}{2}$	1

Fig. 4.3 illustrates the simulated prototype impulse response ($p[\dot{n}]$) at different overlapping factors (K) according to (4.7). It shows that at $K = 1$, the FBMC scheme adopts the rectangular pulse shaping of OFDM systems.

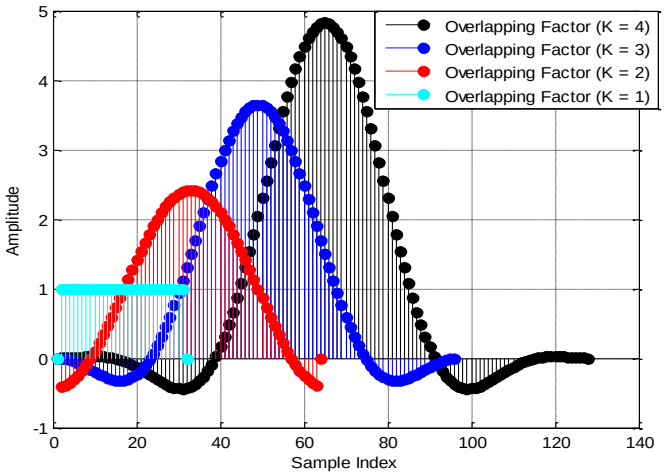

Fig. 4.3 Plot of prototype filter impulse response for different K at $(M, L_p) = (32, KM - 1)$

4.2.1.2 CHANNEL DESCRIPTION

The frequency domain channel transfer function (FD-CTF) fading coefficients $H[k]$ can be described by two properties namely power spectral density (PSD) and the autocorrelation function (ACF). The PSD is expressed by [77, 151]:

$$s|f| = \begin{cases} \dfrac{1}{\pi f_d \sqrt{1-(f/f_d)^2}}, & |f| \leq f_d \\ 0, & \text{elsewhere} \end{cases}, \tag{4.13}$$

If L_{ch} represents the length of the channel, then the corresponding normalized discrete-time ACF is expressed by (4.14) under the assumption that the channel is repeated for a frame [77, 152].

$$a[k] = J_0\left(2\pi f_d T_s \left(\frac{M}{L_{ch}}\right)|k|\right) \qquad k = 0,1,2,\ldots,(L_{ch}-1) \tag{4.14}$$

Equation (4.13) is the u-shaped band limited Jakes spectrum where f_d is the maximum Doppler frequency of the moving channel given as $f_d = \frac{v}{\lambda}$, v is the velocity of the moving mobile and λ is the wavelength of the carrier wave. A plot of the u-shaped Jakes power spectrum for $f_d = 10\text{Hz}$ and $f_d = 200\text{Hz}$ is given in Fig. 4.4. $J_0(\cdot)$ in (4.14) is the zero-order Bessel function of the first kind, T_s is the symbol period while $f_d T_s$ can be referred to as the normalized Doppler frequency (or Doppler rate). A plot of the ACF corresponding to $f_d T_s = 0.001$ and $f_d T_s = 0.02$ is shown in Fig. 4.5.

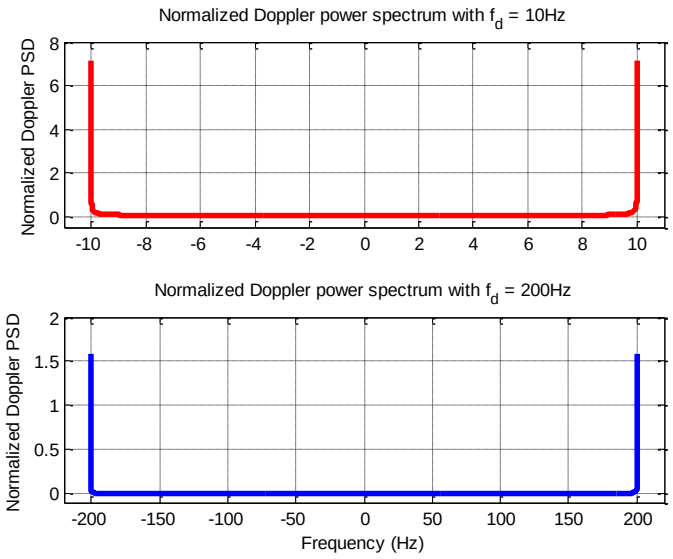

Fig. 4.4 Jakes Doppler Spectrum for $f_d = 10\text{Hz}$ and $f_d = 200\text{Hz}$

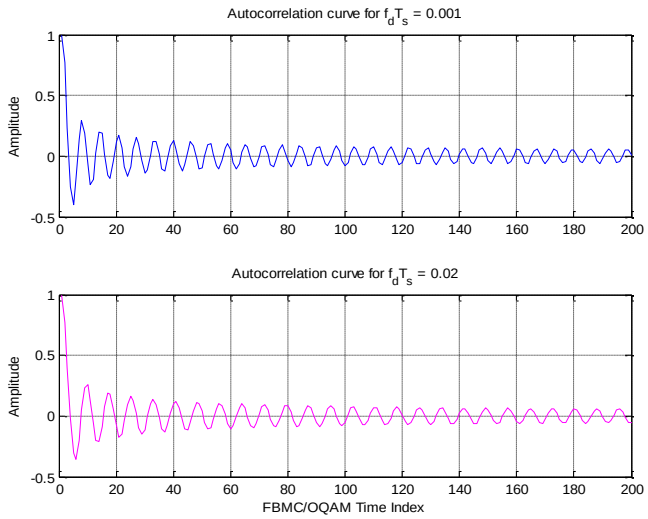

Fig. 4.5 A plot of ACF corresponding to $f_d T_s = 0.001$ and $f_d T_s = 0.02$

The correlation matrix ($\boldsymbol{R}_{HH}[k]$) is given in expanded form in (4.15) as a function of ACF according to [151 - 154] as:

$$\boldsymbol{R}_{HH}[k] = \begin{bmatrix} a[0] & a[1] & \cdots & a[(L_{ch}-1)] \\ a[1] & a[0] & \cdots & a[(L_{ch}-2)] \\ \vdots & \vdots & \ddots & \vdots \\ a[(L_{ch}-1)] & a[(L_{ch}-2)] & \cdots & a[0] \end{bmatrix} \tag{4.15}$$

The FD-CTF fading channel coefficients $H[k]$ can be generated via an L_{ch}th order autoregressive (AR) process represented as $AR(L_{ch})$. This is given as [77, 152 - 154]:

$$H[k] = \sum_{i=1}^{L_{ch}} z[i]H[k-i] + \Omega[k] \qquad k = 0,1,2,\ldots,(L_{ch}-1) \tag{4.16}$$

where $H[k]$ represents the channel fading coefficient over the kth subcarrier ($k = 0,1,2,\ldots,L_{ch}-1$) while $z[i]$ and $\varphi[i]$ are respectively expressed as:

$$z[i] = -\varphi[i] \tag{4.17}$$

$$\varphi[i] = \left[\varphi[1], \varphi[2], \ldots \varphi[L_{ch}]\right]^T \tag{4.18}$$

In (4.18), T is the transpose operator, $\Omega[k]$ in (4.16) is a zero mean white Gaussian noise process with variance σ_{Ω}^{2} given as [152, 153 p.83]:

$$\sigma_{\Omega}^{2} = a[0] + \sum_{k=0}^{L_{ch}-1} \varphi[k]a[k], \tag{4.19}$$

while $\varphi[k]$ are the coefficients of the AR model parameters and can be obtained by computing the Yule-Walker (YW) equation expressed as:

$$\varphi[k] = -\boldsymbol{R}_{HH}{}^{-1}[k]b[k], \tag{4.20}$$

where

$$b[k] = \left[a[0]\, a[1] \ldots a[(L_{ch}-1)]\right]^{T} \tag{4.21}$$

Based on the channel expression in (4.16), the channel coefficients are realized to be equal for a given frame length $F_L = \frac{M}{L_{ch}}$. For instance, the fading coefficients at $H[0]$ is given as:

$$H[0] = z[1]H[-1] + \Omega[0] \tag{4.22}$$

In (4.22), $H[-1]$ is initialized. The channel coefficients across all frequencies at a given time for a frame length $\frac{M}{L_{ch}}$ are chosen to be the same for all M subcarriers. For instance, if $\dot{H}[\ddot{k}]$ represents the channel coefficients across the $\ddot{k}$th subcarrier for $\ddot{k} = 0,1, \ldots, M-1$, then $\dot{H}[0]$ to $\dot{H}[F_L - 1]$ (one frame length) are chosen to equal $H[0]$ that is obtained from (4.16). Algorithm 4.1 gives the implementation procedure for obtaining the fading channel coefficients $\dot{H}[\ddot{k}]$ at the $\ddot{k}$th subcarrier for all M subcarriers. The coefficients change across one frame length as shown in Algorithm 4.1.

ALGORITHM 4.1: Frequency domain channel realization for proposed OFDM/OQAM

01 **Start**
02 **Input**: M, L_{ch}, $z[i]$, $\Omega[k]$
03 **Output**: $\{\dot{H}[\ddot{k}]\}$
04 $H[-1] = \text{rand}(1,1) + j\text{rand}(1,1)$ % Initialize $H[-1]$ by random generation.
05 ***for*** $k \leftarrow 0:1:L_{ch}-1$
06 calculate $H[k]$ using (4.16) % The vector $H[k]$ has length L_{ch}
07 ***end for*** *(in line 05)*
08 $\dot{H} = zeros(1, M)$ % Generate $(1 \times M)$ $\dot{H}$ vector
09 ***for*** $\ddot{k} \leftarrow 0:1:M-1$
10 ***if*** $mod(\ddot{k}, (M/L_{ch})) == 0$ % where (M/L_{ch}) is the frame length.
11 $\dot{H}[\ddot{k}] = H\left[\frac{\ddot{k}}{L_{ch}}\right]$ (4.16)
12 ***else***
13 $\dot{H}[\ddot{k}] = \dot{H}[\ddot{k}-1]$
14 ***end if*** *(in line 10)*
15 ***end for*** *(in line 09)*
16 ***return*** $\{\dot{H}[\ddot{k}]\}$
17 ***Stop***

4.2.1.3 DESCRIPTION OF FILTER BANK OFDM/OQAM RECEIVER ASSUMING NPR

The received signal over the kth subcarrier, after passing through the fading channel under conditions of near perfect reconstruction is given by [146]:

$$s[n,k] = \ddot{\boldsymbol{H}}x[n,k] + \eta[n,k] \tag{4.23}$$

where $\ddot{\boldsymbol{H}}$ is an $M \times M$ diagonal matrix that contains the fading channel coefficients $\dot{H}[\ddot{k}]$ obtained as described in Algorithm 4.1 while $\eta[n,k]$ is a Gaussian noise process with variance (σ_η^2) expressed by:

$$\eta[n,k] = w[n,k] * f[n,k] \tag{4.24}$$

In (4.24), $w[n,k]$ signifies the mutually independent, zero-mean complex AWGN process with equal variances $(\sigma_{w,k}^2)$ while the variance of η $\left(\sigma_{\eta,k}^2\right)$ is given as:

$$\sigma_{\eta,k}^2 = \sigma_{w,k}^2 \sum_{j=0}^{L_p-1} f^2[j,k] \tag{4.25}$$

The derivation of (4.25) is given in Appendix A.

The receiver analysis filter bank (AFB) impulse response is defined as [46, 150]:

$$f[\dot{n},k] = g^*\big[L_p - 1 - \dot{n},k\big] \tag{4.26}$$

The expression in (4.26) can be further simplified as follows [94]. If $g[\dot{n},k]$ is given by (4.6), then $g\big[L_p - 1 - \dot{n},k\big]$ can be obtained from (4.6) by substituting $\dot{n}$ for $(L_p - 1 - \dot{n})$ in the entire expression. This is given as

$$g\big[L_p - 1 - \dot{n},k\big] = p\big[L_p - 1 - \dot{n}\big]\exp\left(j\frac{2\pi k}{M}\left(\big(L_p - 1 - \dot{n}\big) - \left(\frac{L_p - 1}{2}\right)\right)\right) \tag{4.27}$$

$$= p\big[L_p - 1 - \dot{n}\big]\exp\left(j\frac{2\pi k}{M}\left(\frac{2\big(L_p - 1 - \dot{n}\big) - \big(L_p - 1\big)}{2}\right)\right)$$

$$= p\big[L_p - 1 - \dot{n}\big]\exp\left(j\frac{2\pi k}{M}\left(\frac{\big(2\,L_p - 2 - 2\dot{n}\big) - \big(L_p - 1\big)}{2}\right)\right)$$

$$= p\big[L_p - 1 - \dot{n}\big]\exp\left(j\frac{2\pi k}{M}\left(\frac{\big(2\,L_p - L_p - 2 + 1 - 2\dot{n}\big)}{2}\right)\right)$$

$$= p\big[L_p - 1 - \dot{n}\big]\exp\left(j\frac{2\pi k}{M}\left(\frac{\big(L_p - 1 - 2\dot{n}\big)}{2}\right)\right)$$

$$= p\big[L_p - 1 - \dot{n}\big]\exp\left(j\frac{2\pi k}{M}\left(\frac{L_p - 1}{2} - \dot{n}\right)\right)$$

$$g\big[L_p - 1 - \dot{n},k\big] = p\big[L_p - 1 - \dot{n}\big]\exp\left(-j\frac{2\pi k}{M}\left(\dot{n} - \frac{L_p - 1}{2}\right)\right) \tag{4.28}$$

Hence,

$$g^*\big[L_p - 1 - \dot{n},k\big] = p^*\big[L_p - 1 - \dot{n}\big]\,exp^*\left(-j\frac{2\pi k}{M}\left(\dot{n} - \frac{L_p - 1}{2}\right)\right)$$

$$f[\dot{n},k] = g^*\big[L_p - 1 - \dot{n},k\big] = \; p\big[L_p - 1 - \dot{n}\big]\exp\left(j\frac{2\pi k}{M}\left(\dot{n} - \frac{L_p - 1}{2}\right)\right) \tag{4.29}$$

A diagrammatic representation of the receiver is illustrated in Fig. 4.6.

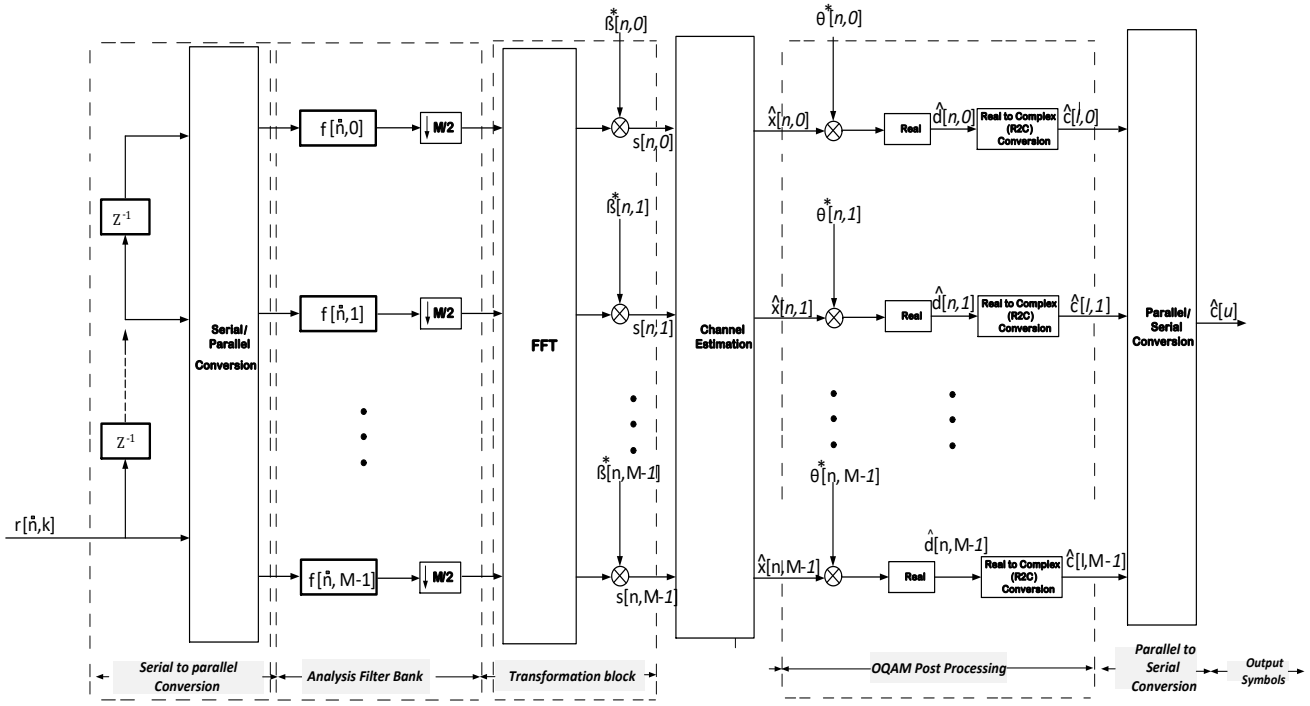

Fig. 4.6 Structure of an OFDM/OQAM receiver

4.2.1.4 DESCRIPTION OF THE OFDM/OQAM-BASED SYSTEM ASSUMING NON-PR

This subsection discusses the system description of filter bank OFDM/OQAM system assuming non-perfect reconstruction design of the analysis filter bank prototype filter. In Non-PR (or imperfect reconstruction) conditions of filter banks, the impulse response of the analysis filter bank FIR prototype filter is different from that of the synthesis filter bank, hence the analysis filter bank is not directly a time-reversed version of the corresponding synthesis filter bank due to the difference in prototype filter impulse response. In order to achieve this imperfection, an error $\overline{\delta}$ is randomly introduced to the analysis filter FIR prototype filter such that $-\overline{\Delta} < \overline{\delta} < +\overline{\Delta}$, where $\overline{\Delta}$= 0.1. Hence, the filter bank prototype filter according to (4.7) is modified by the introduction of an error $\left(\overline{\delta}[k]\right)$ so as to yield the non-perfect reconstructed FIR analysis prototype filter bank formulated as:

$$p'[\dot{n}] = \tilde{P}[0] + 2\sum_{k=1}^{\frac{L_p-1}{2}} (-1)^k \left(\tilde{P}[k] + \overline{\delta}[k]\right) \cos\left(\frac{2\pi k}{KM}\left(\dot{n} + \frac{KM - (L_p - 1)}{2}\right)\right) \tag{4.30}$$

where $\overline{\delta}[k]$ is the introduced error as described above.

After complex to real conversion as in $(4.1a)$ and $(4.1b)$, the transmitted symbols after pre-processing is also given as (4.2) while the exponentially modulated synthesis filter bank, assuming Non-PR condition of filter bank $(g[\dot{n}, k])$, is given as (4.6).

The transmitted filtered OFDM/OQAM symbol $y[\dot{n}, k]$ over the kth subcarrier for the $\dot{n}$th symbol, assuming Non-PR, is obtained by convolving the synthesis filter bank impulse response $(g[\dot{n}, k])$ with the up sampled transmitted signal $(x[\dot{n}, k])$ given as:

$$y[\dot{n}, k] = (x[\dot{n}, k] * g[\dot{n}, k]) = \sum_{l=0}^{L_p-1} x[\dot{n} - l, k] g(l, k) \tag{4.31}$$

In Non-PR, since the analysis filter bank is not directly a time-reversed version of the corresponding synthesis filter bank due to the difference in prototype filter impulse response $p'[\dot{n}]$, the analysis filter bank impulse response $(f'[\dot{n}, k])$ obtained from error introduction is:

$$f'[\dot{n}, k] = p'[\dot{n}] \exp\left(j\frac{2\pi k}{M}\left(\dot{n} - \frac{L_p - 1}{2}\right)\right) \tag{4.32}$$

where L_p is given by (4.5).

The $\dot{n}$th filter bank OFDM/OQAM symbol received over the kth subcarrier is given as [67]:

$$r[\dot{n}, k] = y[\dot{n}, k] h[\dot{n}, k] + w[\dot{n}, k] \tag{4.33}$$

In (4.33), $h[\dot{n}, k]$ is the frequency selective Rayleigh fading channel impulse response while $w[\dot{n}, k]$ signifies the mutually independent, zero-mean complex AWGN process with variance $\sigma_{w,k}^2$ given as:

$$\sigma_{w,k}^2 = E\left[x^2[\dot{n}, k]\right] 10^{-\gamma_{dB}/10} \tag{4.34}$$

where $E\left[x^2[\dot{n},k]\right]$ is the average energy of the input symbols while γ_{dB} (also represented as $\left(\frac{E_s}{N_o}\right)_{dB}$) is the ratio of energy per symbol to noise power spectral density in decibels (dB).

The received signal $s[n,k]$, after $r[\dot{n},k]$ has been processed with the analysis filter bank, is given as [74]:

$$s[n,k] = \left[r[\dot{n},k] * \ f'[\dot{n},k]\right]_{\downarrow M/2} \tag{4.35a}$$

$$= \left[x[\dot{n},k].\left(h[\dot{n},k]g[\dot{n},k] * \ f'[\dot{n},k]\right) + \ \eta[\dot{n},k]\right]_{\downarrow M/2} \tag{4.35b}$$

where $*$ denotes the convolution operator and

$$q[\dot{n},k] = \left[h[\dot{n},k]g[\dot{n},k] * \ f'[\dot{n},k]\right] \tag{4.36}$$

Hence,

$$s[n,k] = \left[x[\dot{n},k].q[\dot{n},k] + \ \eta[\dot{n},k]\right]_{\downarrow M/2} \tag{4.37}$$

while $\eta[\dot{n},k]$ in (4.37) is a Gaussian noise process expressed by:

$$\eta[\dot{n},k] = \left[w[\dot{n},k] * f'[\dot{n},k]\right] \tag{4.38}$$

with variance $\left(\sigma^2_{\eta,k}\right)$ given as:

$$\sigma^2_{\eta,k} = \ \sigma^2_{w,k} \sum_{j=0}^{L_p-1} f'^2[j,k] \tag{4.39}$$

4.3 GFDM/OQAM BASED SYSTEM DESCRIPTION

The generalized frequency division multiplexing scheme addresses the challenges of large out-of-band emission in OFDM systems (in order to avoid interference) [35] while providing flexible signal bandwidth. It is considered to be the most promising candidate for the air interface of 5G networks [51, 155, 156]. One of the most distinguishing characteristic properties of GFDM-based systems is the introduction of flexible pulse shaping across each individual subcarrier [33, 156]. The filtering of these subcarriers by well-designed prototype filters reduces the harmful effects of ICI while providing robustness to the system against the harmful effects of

synchronization errors [32, 157]. GFDM introduces the CP extension properties of OFDM to combat inter-carrier interference (ICI) as well as well-designed pulse shaping [158, 159]. However, the modulation of each subcarrier by non-rectangular pulse shaped filters lead to non-orthogonality of subcarriers in GFDM-based schemes [144, 160]. Due to this non-orthogonal nature of the GFDM-based system, ISI and ICI are expected to occur whose effects can be mitigated by exploiting the near orthogonality properties of the offset quadrature amplitude modulation scheme. The GFDM scheme based on OQAM (GFDM/OQAM) is proposed in this dissertation to combat the expected detrimental effects of ISI and ICI where each subcarrier block is modulated against real-valued symbols, unlike the subcarrier modulation of the complex-valued symbols of GFDM/QAM-based systems.

Numerous research works to address the design and challenges of GFDM systems have been reported in literature. These reported works usually address the challenges of GFDM systems based on QAM modulation scheme (i.e. GFDM/QAM). Only two papers [161, 162] have considered the design of GFDM schemes based on OQAM (GFDM/OQAM) in literature. There is no work, to the best of our knowledge, focused on channel estimation techniques for GFDM/OQAM-based systems in literature. In this dissertation, channel estimation techniques are presented for GFDM/OQAM-based system. Two linear and three adaptive channel estimation schemes have been proposed in this research as elaborately explained in Section 4.4 and the appendix of this dissertation. The performances of these estimation schemes are evaluated and compared with one another for both FBMC/OQAM waveforms (i.e. OFDM/OQAM and GFDM/OQAM) in terms of NMSE and BER at various levels of SNR. In this dissertation, the general system model block diagram of the proposed GFDM/OQAM-based system is shown in Fig. 4.7. Detailed system model description of this multicarrier waveform is presented in subsequent subsections.

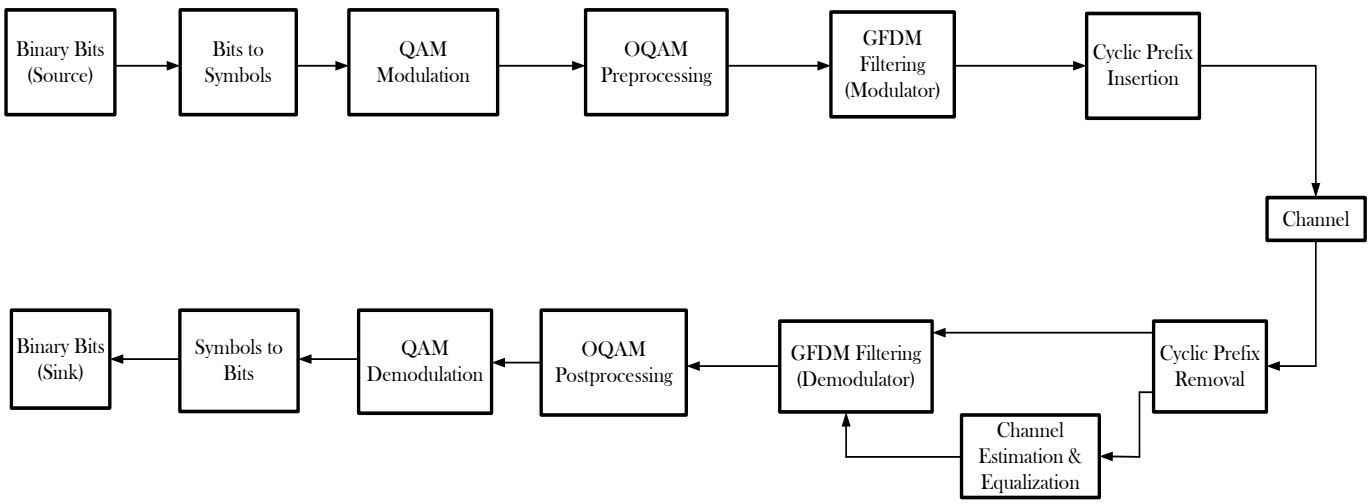

Fig. 4.7 System model block diagram of a GFDM/OQAM modem

4.3.1 TRANSMITTER STRUCTURE OF PROPOSED GFDM/OQAM SCHEME

In this subsection, the transmitter and receiver structures of the proposed GFDM/OQAM systems are presented. It is observed that the structure of this modem is eminently similar to that of OFDM/OQAM-based systems, however a significant difference between the two structures is found in the design of their respective filters banks. In addition, the GFDM/OQAM-based system adopts the use of short CP which gives the system extra robustness against ICI and ISI. The structure of the proposed GFDM/OQAM transmitter is shown in Fig. 4.8. The basic differences in this structure as compared to the proposed OFDM/OQAM transmitter of Fig. 4.2 are the design of the synthesis filter banks as well as the inclusion of cyclic prefix at the transmitter end. Cyclic prefix is added because there is loss of subcarrier orthogonality due to the modulation of subcarriers unto filter banks. The loss in orthogonality may consequently result in ISI or ICI, hence the added cyclic prefix is used to combat ISI that may arise from this process.

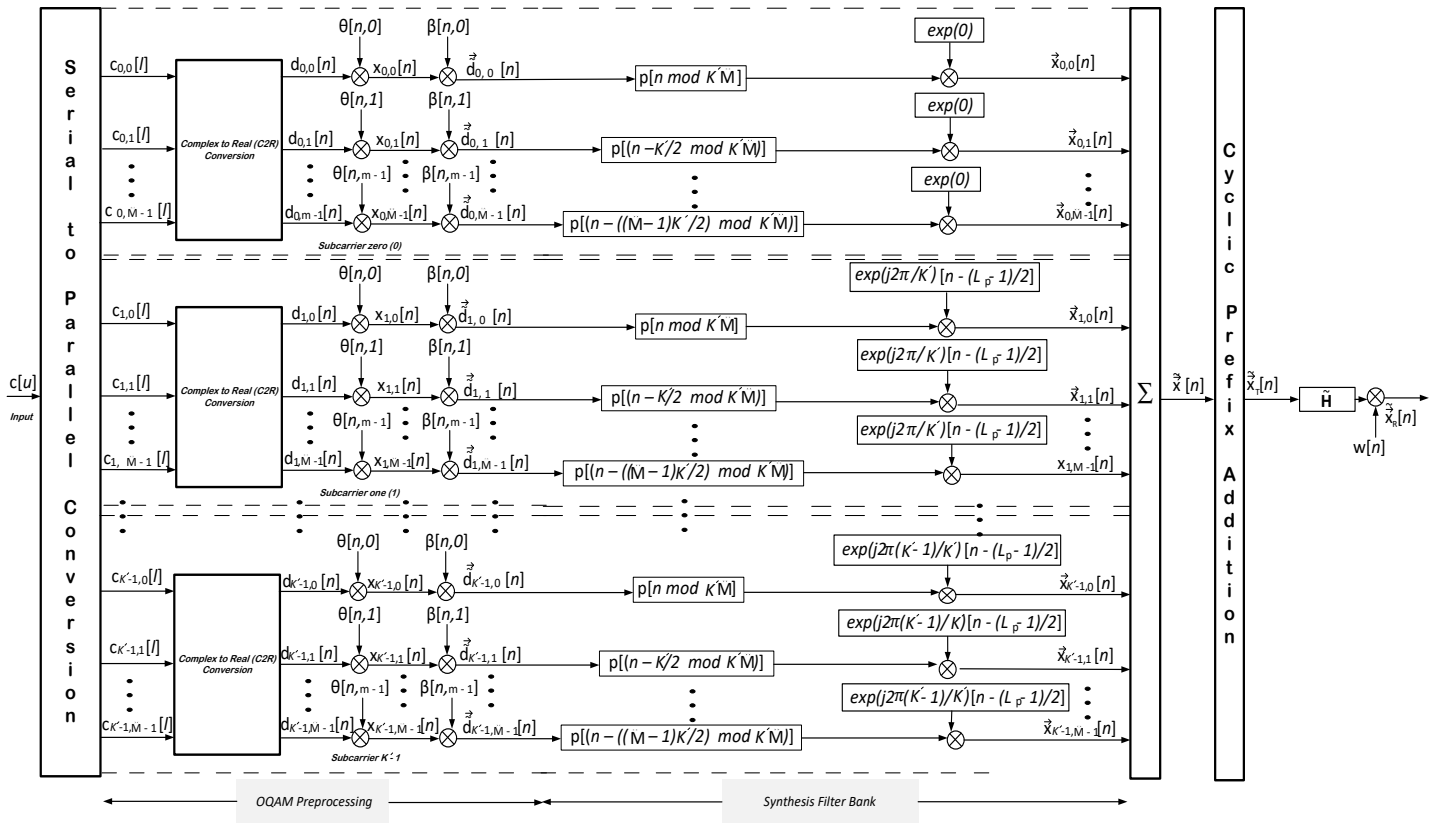

Fig. 4.8 Structure of GFDM/OQAM-based transmitter

In GFDM/OQAM-based transceivers, the real valued N data symbols generated at the transmitter are broken down (or decomposed) into $\ddot{M}$ subsymbols where the subsymbols are being carried on a subcarrier [126]. If K'represents the total number of subcarriers and $\ddot{M}$ is the total number of subsymbols per subcarrier, then the total number of data symbols to be transmitted is given as:

$$N = K'\ddot{M} \tag{4.40}$$

For this OQAM implementation of GFDM, let $\vec{\tilde{d}}_{k',\dot{m}}$ represent the real data obtained from the modulated QAM symbols (which consist of both real and imaginary components) where $\dot{m}$ is the subsymbol index at the k' th subcarrier of the GFDM/OQAM system, the entire symbols to be transmitted can be collected into a vector $\vec{\tilde{\mathbf{d}}}$ given as**:**

$$\vec{\tilde{\mathbf{d}}} = \left[\vec{\tilde{d}}_{0,0}\ \vec{\tilde{d}}_{1,0} \dots \vec{\tilde{d}}_{K\acute{}-1,0}\ \vec{\tilde{d}}_{0,1}\ \vec{\tilde{d}}_{1,1} \dots\ \vec{\tilde{d}}_{K\acute{}-1,1} \dots \vec{\tilde{d}}_{0,\ddot{M}-1}\ \vec{\tilde{d}}_{1,\ddot{M}-1}\ \vec{\tilde{d}}_{K\acute{}-1,\ddot{M}-1}\right]^{\boldsymbol{T}} \tag{4.41}$$

$k' = 0, 1, \dots, K\acute{} - 1$ and $\dot{m} = 0, 1, \dots, \ddot{M} - 1$

Each $\vec{\tilde{d}}_{k',\dot{m}}$ symbol of the GFDM system are transmitted with a corresponding pulse shape given as [161]:

$$g_{k',\dot{m}}[n] = p\left[n - \frac{\dot{m}K'}{2} \bmod K'\ddot{M}\right] \exp\left(j\frac{2\pi k'}{K'}\left(n - \frac{L_p - 1}{2}\right)\right) \tag{4.42}$$

where $n = 0, 1, \ldots, N-1$ and $g_{k',\dot{m}}[n]$ is the shifted version of the prototype filter p in time and frequency according to (4.7). L_p is the prototype filter length given by (4.5), hence the time domain transmit signal just before cyclic prefix insertion is given as:

$$x[n] = \sum_{k'=0}^{K'-1} \sum_{\dot{m}=0}^{\ddot{M}-1} \vec{\tilde{d}}_{k',\dot{m}}\, g_{k',\dot{m}}[n] e^{j\emptyset_{k',\dot{m}}} \tag{4.43}$$

where $e^{j\emptyset_{k',\dot{m}}}$ is used to ensure a $\pi/2$ difference in phase between the real valued data $\vec{\tilde{d}}_{k',\dot{m}}$ in time and frequency and $\emptyset_{k',\dot{m}}$ is given as:

$$\emptyset_{k',\dot{m}} = \frac{(k' + \dot{m})\pi}{2} \tag{4.44}$$

All the operations described in this subsection can be written in a matrix form $\vec{\tilde{x}}$ given as [5, 33]:

$$\vec{\tilde{x}} = \boldsymbol{A}\vec{\tilde{\mathbf{d}}} \tag{4.45}$$

where $\vec{\tilde{\mathbf{d}}}$ is given in (4.41), and $\boldsymbol{A}$ is an $N \times N$ transmitter modulation matrix containing elements of $g_{k',\dot{m}}[n]$ expressed as

$$\boldsymbol{A} = \left[\mathbf{g}_{0,0}\, \mathbf{g}_{1,0} \cdots \mathbf{g}_{K'-1,0}\, \mathbf{g}_{0,1}\, \mathbf{g}_{1,1} \cdots\, \mathbf{g}_{K'-1,1} \cdots \mathbf{g}_{0,\ddot{M}-1}\, \mathbf{g}_{1,\ddot{M}-1}\, \mathbf{g}_{K'-1,\ddot{M}-1}\right] \tag{4.46}$$

where $\mathbf{g}_{k',\dot{m}}$ are vectors given as:

$$\mathbf{g}_{k',\dot{m}} = \left[g_{k',\dot{m}}[n] e^{j\emptyset_{k',\dot{m}}}\right]^T \tag{4.47}$$

In (4.47), T is the transpose operator where $n = 0, 1, \ldots, N-1$. The matrix $\boldsymbol{A}$ can better be written as:

$$\boldsymbol{A} = \begin{bmatrix} g_{0,0}[0]e^{j\emptyset_{0,0}} & g_{1,0}[0]e^{j\emptyset_{1,0}} & \cdots & g_{2,0}[0]e^{j\emptyset_{2,0}} & \cdots & g_{K'-1,\ddot{M}-1}[0]e^{j\emptyset_{K'-1,\ddot{M}-1}} \\ g_{0,0}[1]e^{j\emptyset_{0,0}} & g_{1,0}[1]e^{j\emptyset_{1,0}} & \cdots & g_{2,0}[1]e^{j\emptyset_{2,0}} & \cdots & g_{K'-1,\ddot{M}-1}[1]e^{j\emptyset_{K'-1,\ddot{M}-1}} \\ \vdots & \vdots & & \vdots & & \vdots \\ g_{0,0}[N-1]e^{j\emptyset_{0,0}} & g_{1,0}[N-1]e^{j\emptyset_{1,0}} & \cdots & g_{2,0}[N-1]e^{j\emptyset_{2,0}} & \cdots & g_{K'-1,\ddot{M}-1}[N-1]e^{j\emptyset_{K'-1,\ddot{M}-1}} \end{bmatrix}$$

Cyclic prefix of length N_{CP} is then appended to $\tilde{\tilde{x}}$ so as to obtain the final transmit signal $\tilde{\tilde{x}}_T$ whose length is $(N + N_{CP})$.

4.3.2 CHANNEL DESCRIPTION OF THE GFDM/OQAM SCHEME

One important difference to note in the GFDM/OQAM and OFDM/OQAM filter bank waveforms is that the subcarriers required to transmit a given amount of data are fewer for GFDM/OQAM scheme as the symbols to be transmitted are grouped into sub-symbols which are then transmitted on a subcarrier. This improves the data rate of GFDM/OQAM system while also giving it an edge over filter bank OFDM/OQAM-based systems, especially when there is very large amounts of data to be transmitted. The channel model of the proposed GFDM/OQAM scheme is designed to be similar to that of filter bank OFDM/OQAM where the channel length (L_{ch}) is equal to the total number of subcarriers (K'). For this GFDM/OQAM system, it is assumed that the CIR over a frame are equal, hence the corresponding normalized discrete-time ACF is expressed by:

$$a[k'] = J_0\left(2\pi f_d T_s \left(\frac{M}{L_{ch}}\right)|k'|\right) \qquad k' = 0,1,2,\ldots,(L_{ch}-1) \tag{4.48}$$

where L_{ch} is the channel length and k' is the subcarrier index. f_d is the maximum Doppler frequency of the moving channel given as $f_d = \frac{v}{\lambda}$, v is the velocity of the moving mobile and λ is the wavelength of the carrier wave. The correlation matrix ($\boldsymbol{R}_{HH}[k']$) is given in expanded form in (4.49) as a function of ACF according to:

$$\boldsymbol{R}_{HH}[k'] = \begin{bmatrix} a[0] & a[1] & \cdots & a[(L_{ch}-1)] \\ a[1] & a[0] & \cdots & a[(L_{ch}-2)] \\ \vdots & \vdots & \ddots & \vdots \\ a[(L_{ch}-1)] & a[(L_{ch}-2)] & \cdots & a[0] \end{bmatrix} \tag{4.49}$$

The frequency domain fading channel coefficients $H[k']$ can be generated via an L_{ch}th order autoregressive (AR) process represented as AR (L_{ch}). This is given as:

$$H[k'] = \sum_{i=1}^{L_{ch}} z[i]H[k'-i] + \Omega[k'] \qquad k' = 0,1,2,\ldots,(L_{ch}-1) \tag{4.50}$$

where $H[k']$ represents the channel impulse response over the k'th subcarrier $\left(k' = 0,1,2,\ldots,(L_{ch}-1)\right)$ while $z[i]$ and $\varphi[i]$ are respectively expressed as:

$$z[i] = -\varphi[i] \tag{4.51}$$

$$\varphi[i] = \left[\varphi[1], \varphi[2], \ldots \varphi[L_{ch}]\right]^T \tag{4.52}$$

$\Omega[k']$ in (4.50) is a zero mean white Gaussian noise process with variance σ_Ω^2 given as:

$$\sigma_\Omega^2 = a[0] + \sum_{k=0}^{L_{ch}-1} \varphi[k']a[k'], \tag{4.53}$$

while $\varphi[k']$ are the coefficients of the AR model parameters and can be obtained by computing the Yule-Walker (YW) equation expressed as:

$$\varphi[k'] = -\boldsymbol{R}_{HH}{}^{-1}[k']b[k'], \tag{4.54}$$

where

$$b[k'] = \left[a[0]\ a[1] \ldots a[(L_{ch}-1)]\right]^T \tag{4.55}$$

Based on the channel expression in (4.50), the channel frequency coefficients are realized to have L_{ch} different values, i.e. $H[k'] = \left[H[0]\ H[1] \ldots H[L_{ch}-1]\right]$. This is then converted into time domain channel impulse response $h(n')$ through the use of IDFT as:

$$h(n') = IDFT\left[H[k']\right] \qquad n' = 0,1,\ldots,L_{ch}-1$$

$$= \sum_{k'=0}^{L_{ch}{}'-1} H[k']e^{j\frac{2\pi k'n'}{N}} \tag{4.56}$$

4.3.3 RECEIVER DESCRIPTION OF THE GFDM/OQAM SCHEME

After the transmitted symbols propagate through the wireless channel, the received signal can be expressed as

$$\tilde{\vec{x}}_R[n] = \widetilde{\ddot{\mathbf{H}}}\,\tilde{\vec{x}}_T[n] + w[n] \tag{4.57}$$

where $\tilde{\vec{x}}_T[n]$ is the transmitted signal with cyclic prefix. If CP is removed, the received signal is denoted as $\vec{x}_R[n]$. The symbol $w[n]$ is the complex additive white Gaussian noise vector with zero mean and variance ${\sigma_w}^2$, while $\widetilde{\ddot{\mathbf{H}}}$ is the circulant channel convolution matrix having a band diagonal structure based on the channel impulse responses obtained from (4.56) where

$$\widetilde{\ddot{\mathbf{H}}} = circ\big(h(n')\big) \tag{4.58}$$

Algorithm 4.2 presents a pseudo code that demonstrates how the circulant channel matrix (CCM) $\widetilde{\ddot{\mathbf{H}}}$ can be realized.

The received signal after equalization is given as:

$$x_R[n] = \vec{x}_R[n]{H^{-1}}_{chan}[n] \tag{4.59}$$

where $H_{chan}[n]$ are the fading coefficients obtained from channel estimation.

The demodulated signal is given as:

$$c_R[n] = \boldsymbol{B}x_R[n] \tag{4.60}$$

where $\boldsymbol{B}$ is the matched filter receiver matrix given as:

$$\boldsymbol{B} = \boldsymbol{A}^H \tag{4.61}$$

and $\boldsymbol{A}$ in (4.61) is given by (4.46) and H is the Hermitian transpose operator.

ALGORITHM 4.2: Circulant channel matrix realization for proposed GFDM/OQAM

01 **Start**
02 **Input**: L_{ch}, K', $\ddot{M}$, N_{cp}
03 **Output**: $\left\{\widetilde{\ddot{\mathbf{H}}}\right\}$
04 Compute N using (4.40)
05 Generate $H[k']$ vector using (4.50) % where length of $H[k'] = L_{ch}$.
06 Compute $h(n') = ifft(H[k'])$ according to (4.56). % $h(n')$ is of dimension $(1 \times L_{ch})$
07 Generate $\widetilde{\ddot{\mathbf{H}}} = zeros\left((N + N_{cp}), (N + N_{cp})\right)$ % Initialize CCM with all zero elements
08 $\widetilde{\ddot{\mathbf{H}}}\,(1, [1: L_{ch}]) = h(n')$ % put all $h(n')$ elements into 1st L_{ch} columns of $\widetilde{\ddot{\mathbf{H}}}$
09 ***for*** $ii \leftarrow 1:1:\left(size(\widetilde{\ddot{\mathbf{H}}}, 2) - 1\right)$
10 $\widetilde{\ddot{\mathbf{H}}}\,(ii + 1,1) = \widetilde{\ddot{\mathbf{H}}}\,(ii, end)$ % take last value of row ii and replace with 1st value of row $ii + 1$
11 $\widetilde{\ddot{\mathbf{H}}}\,(ii + 1, [2: end]) = \widetilde{\ddot{\mathbf{H}}}\,(ii, [1: end - 1])$
12 ***end for*** *(in line 09)*
13 ***return*** $\left\{\widetilde{\ddot{\mathbf{H}}}\right\}$
14 **Stop**

4.4 CHANNEL ESTIMATION FOR PROPOSED FILTER BANK WAVEFORMS

In this section, CE techniques that are used for estimating fading channel coefficients for the described filter bank OFDM/OQAM and GFDM/OQAM-based transceivers are presented. The proposed CE algorithms are least square, linear minimum mean square error, least mean square, normalized least mean square and recursive least square. The performances of these algorithms are analyzed and compared with one another in terms of mean square error and bit error rate for both waveforms.

4.4.1 CHANNEL ESTIMATION FOR FILTER BANK OFDM/OQAM

The performances of two linear and three adaptive-based channel estimation algorithms are selected for analysis in filter bank OFDM/OQAM-based transceivers. The linear algorithms are namely LS and LMMSE while the adaptive estimation schemes are LMS, NLMS and RLS-based channel estimation schemes. These algorithms are analyzed for this filter bank waveform subsequently.

4.4.1.1 LEAST SQUARES FOR OFDM/OQAM

The least square channel estimate is given as:

$$\widehat{\boldsymbol{H}}_{LS}[k] = \left[\widehat{H}_{LS}[0]\ \widehat{H}_{LS}[1]\ \widehat{H}_{LS}[2]\ldots\widehat{H}_{LS}[(L_{ch}-1)]\right]^{T} \qquad k = 0,1,2,\ldots,(L_{ch}-1)$$

$$= \left[\frac{L_{ch}}{M}\left(\sum_{k=0}^{\frac{M}{L_{ch}}-1}\left(\frac{s[n,k]}{x[n,k]}\right), \quad \sum_{k=\frac{M}{L_{ch}}}^{2\frac{M}{L_{ch}}-1}\left(\frac{s[n,k]}{x[n,k]}\right), \quad \sum_{k=2\frac{M}{L_{ch}}}^{3\frac{M}{L_{ch}}-1}\left(\frac{s[n,k]}{x[n,k]}\right) \ldots \sum_{k=\frac{M(L_{ch}-1)}{L_{ch}}}^{M-1}\left(\frac{s[n,k]}{x[n,k]}\right)\right)\right]^{T} \quad (4.62)$$

In (4.62), $s[n,k]$ are the output symbols received just before the channel estimation process as represented in (4.23) while $x[n,k]$ are the staggered OQAM symbols at the transmitter end.

4.4.1.2 LINEAR MINIMUM MEAN SQUARE ERROR FOR OFDM/OQAM

The simplified LMMSE channel estimate ($\widehat{\boldsymbol{H}}_{LMMSE}$) is generally given as [166 - 168]:

$$\widehat{\boldsymbol{H}}_{LMMSE}[n,k] = \mathbf{R}_{Hs}[n,k]\ \mathbf{R}_{ss}{}^{-1}[n,k]\ s[n,k] \quad (4.63)$$

where $\mathbf{R}_{Hs}[n,k]$ is the cross-covariance matrix between $\boldsymbol{H}[n,k]$ and $s[n,k]$, and $\mathbf{R}_{ss}[n,k]$ is the auto-covariance matrix of $s[n,k]$ and can both be expressed as:

$$\mathbf{R}_{Hs}[n,k] = E[Hs^{H}] = \boldsymbol{R}_{HH}[n,k]\boldsymbol{X}^{H}[n,k] \quad (4.64)$$

$$\mathbf{R}_{ss}[n,k] = E[ss^{H}] = \boldsymbol{X}[n,k]\mathbf{R}_{hh}[n,k]\boldsymbol{X}^{H}[n,k] + \sigma_{\eta}{}^{2}\boldsymbol{I}[m] \quad (4.65)$$

where

$$\boldsymbol{X}[n,k] = diag\ [\boldsymbol{x}[n,k]] = diag\ x[n,1]\ x[n,2]\ x[n,3]\ldots x[n,M] \quad (4.66)$$

Substituting (4.64) and (4.65) into (4.63) gives:

$$\widehat{\boldsymbol{H}}_{LMMSE}[n,k] = \frac{\boldsymbol{R}_{HH}[n,k]\ s[n,k]}{\boldsymbol{X}[n,k]\left[\boldsymbol{R}_{HH}[n,k] + (\boldsymbol{X}^{H}[n,k]\boldsymbol{X}[n,k])^{-1}\sigma_{\eta}{}^{2}\boldsymbol{I}[n,k]\right]} \quad (4.67)$$

where $\boldsymbol{R}_{HH}[n,k]$ is the autocorrelation matrix of the channel impulse response given by (4.15). $\sigma_{\eta}{}^{2}$ denotes the noise variance $E|\eta[n,k]|^{2}$ that is given as (4.25), $\boldsymbol{I}[n,k]$ is an identity matrix while E is the expectation notation. More details on the derivation of the LMMSE channel estimation as well as noise variance ($\sigma_{\eta}{}^{2}$) are given in Appendix A. Algorithm 4.3 presents a sequential procedure of realizing the average LMMSE channel estimate for OFDM/OQAM.

ALGORITHM 4.3: Average LMMSE channel estimation realization for OFDM/OQAM

01 **Start**
02 **Input**: $x[n,k], s[n,k], L_{ch}, M, \sigma_\eta^2, R_{HH}$
03 **Output**: $\{\widehat{\boldsymbol{H}}_{LMMSE}\}$
04 $\widehat{\boldsymbol{H}}_{LMMSE} = [\quad]$; % Creating empty matrix for $\widehat{\boldsymbol{H}}_{LMMSE}$ channel estimate
05 ***for*** $kk \leftarrow 0{:}\,1{:}\left(\frac{M}{L_{ch}} - 1\right)$
06 $\mathrm{x}(1,:) = x\left[n, \left(kk + 1{:}\frac{M}{L_{ch}}{:}\,M\right)\right]$ % Collecting input symbols per frame to form a vector
07 $\mathrm{s}(1,:) = s\left[n, \left(kk + 1{:}\frac{M}{L_{ch}}{:}\,M\right)\right]$ % Collecting corresponding received symbols per frame
08 $\boldsymbol{I} = ones\ (L_{ch}, L_{ch})$ % Creating Identity matrix so as to compute (4.65)
09 Calculate R_{Hs} using (4.64) % Cross covariance matrix
10 Calculate R_{ss} using (4.65) % Auto-covariance matrix
11 Obtain $\widehat{\boldsymbol{H}}_{LMMSE}\left[k = kk{:}\frac{M}{L_{ch}}{:}\,M\right]$ using (4.67)
12 $\widehat{\boldsymbol{H}}_{MAT} = \left[\widehat{\boldsymbol{H}}_{LMMSE};\ \widehat{\boldsymbol{H}}_{LMMSE}\right]$ % $\left(\frac{M}{L_{ch}} \times L_{ch}\right)$ matrix
13 ***end for*** *(in line 05)*
14 $\widehat{\boldsymbol{H}}_{LMMSE} = \frac{L_{ch}}{M} * \left[sum(\widehat{\boldsymbol{H}}_{MAT}, 1)\right]$ % Averaging $\widehat{\boldsymbol{H}}_{LMMSE}$ obtained from *line 12*
15 ***return*** $\{\widehat{\boldsymbol{H}}_{LMMSE}\}$
16 **Stop**

4.4.1.3 LEAST MEAN SQUARE FOR OFDM/OQAM

When employing adaptive channel estimation algorithm for estimating channel fading coefficients, a cost function is usually adopted for minimizing the MSE of the fading channel coefficients in order to obtain the best (or optimum) channel estimates of the channel impulse responses. This cost function for the LMS-based CE is expressed as

$$\boldsymbol{J}(\boldsymbol{n}) = E\{|\boldsymbol{e}[n,k]|^2\} = E\{\boldsymbol{e}[n,k]\boldsymbol{e}^*[n,k]\} \tag{4.69}$$

In (4.69), $E\{\cdot\}$ is the expectation operator, * denotes complex conjugation, $\boldsymbol{e}[n,k]$ is the channel estimation error given in (4.70) [118] while $\boldsymbol{J}(\boldsymbol{n})$ represents the cost function to be minimized.

$$\boldsymbol{e}[n,k] = s[n,k] - \widehat{H}^H[n,k]x[n,k] \tag{4.70}$$

where the term $\widehat{H}[n,k]x[n,k]$ is the inner product of the staggered OQAM symbols at the transmitter of the filter bank OFDM/OQAM-based system ($x[n,k]$) and the corresponding least square estimates as obtained from (4.62).

Substituting (4.70) into (4.69) yields:

$$\boldsymbol{J}(\boldsymbol{n}) = E\{(\boldsymbol{s}[n,k] - \widehat{H}^H[n,k]x[n,k])(s^*[n,k] - \hat{h}[n,k]x^H[n,k])\} \quad (4.71)$$

where $\boldsymbol{e}^*[n,k]$ is given as [37, 52, 166]:

$$\boldsymbol{e}^*[n,k] = s^*[n,k] - \widehat{H}[n,k]x^H[n,k] \quad (4.72)$$

The LMS (also known as *stochastic gradient*) based channel estimation scheme estimates CIR for the filter bank OFDM/OQAM-based on the following expression.

$$\widehat{\boldsymbol{H}}_{LMS}[n+1,k] = \widehat{H}[n,k] + \mu\boldsymbol{e}^*[n,k]x[n,k] \quad (4.73)$$

where μ is the fixed positive step size parameter that satisfies the condition $0 < \mu < 2$. The full derivation of LMS adaptive algorithm according to (4.73) is presented in Appendix B.

4.4.1.4 NORMALIZED LEAST MEAN SQUARE FOR OFDM/OQAM

In NLMS channel estimation, the estimation error is normalized by the power of the input signal. The channel impulse response (CIR) for this algorithm is represented as:

$$\widehat{\boldsymbol{H}}_{NLMS}[n+1,k] = \widehat{H}[n,k] + \frac{\mu\boldsymbol{e}^*[n,k]x[n,k]}{||x[n,k]||^2} \quad (4.74)$$

where $||x[n,k]||^2$ represents the Euclidean norm of the staggered input OQAM symbols, μ is the step size parameter, while the error $\boldsymbol{e}^*[n,k]$ is expressed as in (4.72).

4.4.1.5 RECURSIVE LEAST SQUARE FOR OFDM/OQAM

The index of performance to be minimized for RLS is:

$$\boldsymbol{J}(\boldsymbol{n}) = \sum_{k=0}^{n-1} \aleph[n,k]|\boldsymbol{e}[n,k]|^2 \quad (4.75)$$

In (4.75), $\aleph$ is the forgetting factor (or weighting factor) taking values in the range $0 << \aleph(n,k) < 1$ which is expressed as:

$$\aleph[n,k] = \lambda^{n-k} \qquad k = 0,1,2,\ldots,M-1 \quad (4.76)$$

In (4.76), λ is a positive constant that is close to but less than one. The inverse autocorrelation matrix ($\mathbf{R}^{-1}[n,k]$) of input vector $\boldsymbol{x}[n,k]$ is given as:

$$\mathbf{R}^{-1}[n,k] = \lambda^{-1}\mathbf{R}^{-1}[n-1,k] - \lambda^{-1}\,\tilde{\boldsymbol{g}}[n,k]x^{H}[n,k]\mathbf{R}^{-1}[n-1,k] \tag{4.77}$$

where $\tilde{\boldsymbol{g}}[n,k]$ is the gain vector expressed as:

$$\tilde{\boldsymbol{g}}[n,k] = \frac{\lambda^{-1}\mathbf{R}^{-1}[n-1,k]x[n,k]}{1 + x^{H}[n,k]\,\lambda^{-1}\mathbf{R}^{-1}[n-1,k]x[n,k]} \tag{4.78}$$

The RLS channel estimate can then be expressed as:

$$\hat{\boldsymbol{H}}_{RLS}[n,k] = \hat{H}[n-1,k] + \tilde{\boldsymbol{g}}[n,k]\boldsymbol{e}^{*}[n,k] \tag{4.79}$$

$\boldsymbol{e}^{*}[n,k]$ is given in (4.72). Comprehensive derivation of this algorithm can be found in Appendix C.

4.4.2 CHANNEL ESTIMATION FOR FILTER BANK GFDM/OQAM

Similar to the filter bank OFDM/OQAM-based system, the performances of two linear and three adaptive based channel estimation algorithms are selected for analysis in GFDM/OQAM-based transceivers. The linear algorithms are namely LS and LMMSE while the adaptive estimation schemes are namely LMS, NLMS and RLS-based channel estimation schemes. These algorithms (for GFDM/OQAM) have the same procedures as that of filter bank OFDM/OQAM as described in Subsection 4.4.1, except that their received and transmitted signals are different.

4.4.2.1 LEAST SQUARES FOR GFDM/OQAM

The least square channel estimate is given as:

$$\hat{\boldsymbol{h}}_{LS}[k'] = \left[\hat{h}_{LS}[0]\;\hat{h}_{LS}[1]\;\hat{H}_{LS}[2]\ldots\hat{h}_{LS}[(L_{ch}-1)]\right]^{T} \qquad k' = 0,1,2,\ldots,(L_{ch}-1)$$

$$= \left[\frac{L_{ch}}{M}\left(\sum_{k'=0}^{\frac{M}{L_{ch}}-1}\left(\frac{\vec{x}_R[n,k']}{\tilde{\vec{x}}[n,k']}\right)\sum_{k'=\frac{M}{L_{ch}}}^{2\frac{M}{L_{ch}}-1}\left(\frac{\vec{x}_R[n,k']}{\tilde{\vec{x}}[n,k']}\right)\sum_{k'=2\frac{M}{L_{ch}}}^{3\frac{M}{L_{ch}}-1}\left(\frac{\vec{x}_R[n,k']}{\tilde{\vec{x}}[n,k']}\right)\cdots\sum_{k'=\frac{M(L_{ch}-1)}{L_{ch}}}^{M-1}\left(\frac{\vec{x}_R[n,k']}{\tilde{\vec{x}}[n,k']}\right)\right)\right]^{T} \tag{4.80}$$

In (4.80), $\vec{x}_R[n,k']$ are the output symbols received after cyclic prefix removal while $\tilde{\vec{x}}$ are the transmitted QAM symbols without cyclic prefix.

4.4.2.2 LINEAR MINIMUM MEAN SQUARES FOR GFDM/OQAM

The simplified time-domain LMMSE channel estimate ($\widehat{\boldsymbol{h}}_{LMMSE}$) for GFDM/OQAM is given as:

$$\widehat{\boldsymbol{h}}_{LMMSE} = \frac{\boldsymbol{R}_{HH}[k']\,\vec{x}_R[n,k']}{\boldsymbol{X}[n,k']\left[\boldsymbol{R}_{HH}[k'] + (\boldsymbol{X}^H[n,k']\boldsymbol{X}[n,k'])^{-1}{\sigma_w}^2\boldsymbol{I}[m]\right]} \tag{4.81}$$

$$\boldsymbol{X}[n,k'] = diag\left[\tilde{\vec{x}}[n,k']\right] = diag\;\tilde{\vec{x}}[n,1]\,\tilde{\vec{x}}[n,2]\,\tilde{\vec{x}}[n,3]\ldots\tilde{\vec{x}}[n,M] \tag{4.82}$$

where $\boldsymbol{R}_{HH}[k']$ is the autocorrelation matrix of the channel impulse response given by (4.49). ${\sigma_w}^2$ denotes the noise variance $E|\eta[n,k]|^2$ that could be given as (4.57), $\boldsymbol{I}[m]$ is an identity matrix while E is the expectation notation.

4.4.2.3 LEAST MEAN SQUARE FOR GFDM/OQAM

The LMS adaptive CIR for the GFDM/OQAM symbols are estimated using

$$\widehat{\boldsymbol{h}}_{LMS}[n+1,k'] = \hat{h}[n,k'] + \mu\,ę^*[n,k']\,\tilde{\vec{x}}[n,k'] \tag{4.83}$$

where μ is the fixed positive step size parameter that satisfies the condition $0 < \mu < 2$ and the channel estimation error ($ę^*[n,k']$) for GFDM/OQAM is given as

$$ę^*[n,k'] = {\vec{x}_R}^*[n,k'] - \hat{h}[n,k']\tilde{\vec{x}}^H[n,k'] \tag{4.84}$$

4.4.2.4 NORMALIZED LEAST MEAN SQUARE FOR GFDM/OQAM

The NLMS channel estimate for the GFDM/OQAM system described in Subsection 4.3.1 is given as:

$$\widehat{\boldsymbol{h}}_{NLMS}[n+1,k'] = \hat{h}[n,k'] + \frac{\mu\,ę^*[n,k']\tilde{\vec{x}}[n,k']}{||\tilde{\vec{x}}[n,k']||^2} \tag{4.85}$$

where $||\tilde{\vec{x}}[n,k']||^2$ represents the Euclidean norm of the staggered input GFDM/OQAM symbols, μ is the step size parameter, $\hat{h}[n,k']$ is the discrete time-varying CIR while the error $ę^*[n,k']$ is expressed as shown in (4.84).

4.4.2.5 RECURSIVE LEAST SQUARE CHANNEL ESTIMATION FOR GFDM/OQAM

The inverse autocorrelation matrix ($\mathrm{R}^{-1}[n,k']$) for GFDM/OQAM with input vector $\tilde{\vec{x}}[n,k']$ is given as:

$$\mathrm{R}^{-1}[n,k'] = \lambda^{-1}\,\mathrm{R}^{-1}[n-1,k'] - \lambda^{-1}\,\tilde{\mathrm{g}}[n,k']\,\tilde{\vec{x}}^{H}[n,k']\,\mathrm{R}^{-1}[n-1,k'] \tag{4.86}$$

where λ is a positive constant that is close to but less than one while $\tilde{\mathrm{g}}[n,k']$ is the gain vector expressed as:

$$\tilde{\mathrm{g}}[n,k'] = \frac{\lambda^{-1}\,\mathrm{R}^{-1}[n-1,k']\,\tilde{\vec{x}}[n,k']}{1 + x^{H}[n,k']\,\lambda^{-1}\,\mathrm{R}^{-1}[n-1,k']\,\tilde{\vec{x}}[n,k']} \tag{4.87}$$

Hence, the RLS channel estimate for GFDM/OQAM system is given as

$$\hat{\boldsymbol{h}}_{RLS}[n,k'] = \hat{h}[n-1,k'] + \tilde{\mathrm{g}}[n,k']\,\mathrm{ę}^{*}[n,k'] \tag{4.88}$$

where $\mathrm{ę}^{*}[n,k']$ is given in (4.84).

4.5 CHAPTER SUMMARY

This chapter has presented an elaborate description of the two filter bank multicarrier waveforms under investigation (in this dissertation) which are called filter bank OFDM/OQAM and GFDM/OQAM-based transceivers. An introduction to the basic concepts and design of filter bank OFDM/OQAM assuming both NPR and Non-PR is presented while an elaborate description of the physical structure (of this waveform) as well as comprehensive mathematical analysis is given. The structure of the GFDM/OQAM system is also elaborated in this chapter where comprehensive mathematical analysis is used to describe every block of the system. The channel estimation algorithms proposed for estimating the fading channel coefficients for both filter bank multicarrier waveforms are elaborately described.

CHAPTER FIVE

SIMULATIONS AND RESULTS

5.1 INTRODUCTION

This chapter presents the simulation results obtained from implementing the proposed channel estimation techniques where the performances of two linear channel estimators, namely least squares and linear minimum mean square error-based estimators, as well as three adaptive channel estimators, namely least mean square, normalized least mean square and recursive least square based channel estimators are investigated for the two filter bank multicarrier-based transceivers in time-varying frequency selective Rayleigh fading channel. The two filter bank multicarrier-based transceivers are the orthogonal frequency division multiplexing with offset quadrature amplitude modulation and generalized frequency division multiplexing with offset quadrature amplitude modulation scheme as elaborately described in Chapter 4. For filter bank OFDM/OQAM system, the performances of these estimators are investigated under system design conditions of near perfect reconstruction and non-perfect reconstruction. In near perfect reconstruction, signal distortions resulting from aliasing is minimized as much as possible from accurate design of an FIR low-pass prototype filter which also minimizes the phase and amplitude distortions while in non-perfect reconstruction (i.e. imperfect reconstruction), aliasing and amplitude distortions are more prominent which may reduce system efficacy. The performances of these estimators are compared with one another as outlined.

This chapter is structured as follows. The performances of the proposed CE algorithms are presented in Section 5.2 for NPR and Non-PR filter bank OFDM/OQAM. A sequential procedure for implementing these estimation schemes as well as simulation results are also given in this section. Section 5.3 analyzes and documents the performances of all proposed channel estimation schemes for filter bank GFDM/OQAM waveforms while presenting sequential implementation procedures as well as simulation results obtained. In Section 5.4, the computational complexities of the CE schemes are analyzed while 5.5 summarize this chapter.

5.2 PERFORMANCE OF CHANNEL ESTIMATORS FOR OFDM/OQAM

This section evaluates and documents the performances of the proposed linear and adaptive channel estimation schemes under NPR and Non-PR filter bank OFDM/OQAM scheme as described in Chapter 4 of this dissertation. It presents a sequential procedure for implementing

these estimation algorithms while discussing the simulation procedure and parameters as well as the results obtained.

5.2.1 SEQUENTIAL PROCEDURE FOR IMPLEMENTING CE FOR OFDM/OQAM

A sequential procedure for implementing the channel estimation algorithms for the filter bank OFDM/OQAM system assuming NPR is shown in Algorithm 5.1.

ALGORITHM 5.1: LS AND LMMSE CHANNEL ESTIMATION FOR NPR OFDM/OQAM

01 **Start**
02 **Input**: M, K, $\boldsymbol{SNR}$, bps, T_s, f_d
03 **Output**: $\{\widehat{\boldsymbol{h}}_{LS}, \widehat{\boldsymbol{h}}_{LMMSE}\}$
04 ***for*** $esno = 1 : length(\boldsymbol{SNR})$
05 input = *randi*([0 1], ($M^2 \times$ bps), 1) Generate $M^2 \times bps$ random binary input bits
06 sym = *bi2de*(input) ← convert generated bits into ($M^2 \times$ bps)/bps symbols, [bps = bits/sym]
07 c[u] = *qammod*(sym) ← QAM modulate input symbols
08 Perform serial to parallel conversion to obtain c[l,k]
09 Interpolating from 1 to n: $n = 2l$
10 For all n
11 ***for*** $k \leftarrow 0 : M - 1$
12 ***if*** $k \leftarrow 0 : 2 : M - 1$ (even k), ***then***
13 $\boldsymbol{d}[n,k] \leftarrow$ [real($\boldsymbol{c}[l]$) imag($\boldsymbol{c}[l]$)]
14 ***else*** (for odd k)
15 $\boldsymbol{d}[n,k] \leftarrow$ [imag ($\boldsymbol{c}[l]$) real($\boldsymbol{c}[l]$)]
16 ***end for*** *(in line 11)*
17 ***for*** $k \leftarrow 0 : M - 1$, compute
18 $\boldsymbol{x}[n,k] \leftarrow \boldsymbol{d}[n,k] * (i)^{k+n}$
19 ***end for*** *(in line 17)*
20 Calculate $a[n,k]$ and $\boldsymbol{R}_{HH}[n,k]$ using (4.14) and (4.15) respectively
21 Obtain $\Omega[n,k]$ from σ_{Ω}^2 using (4.19)
22 Obtain $z[i]$ from (4.17) and construct $H[n,k]$ as in (4.16)
23 Obtain $g[n,k]$ using (4.6) and generate additive Gaussian noise $w[n,k]$
24 Compute $\eta[n,k]$ and $f[n,k]$ using (4.24) and (4.26) respectively
25 Obtain $\ddot{\boldsymbol{H}}[n,k]$ as described in Algorithm 4.1.
26 Compute the received signals $s[n,k]$ from $x[n,k]$, $\ddot{\boldsymbol{H}}[n,k]$ and $\eta[n,k]$ using (4.23)
27 **CHANNEL ESTIMATION COMPUTATION**
28 Obtain least square estimate $\widehat{\boldsymbol{h}}_{LS}$ using (4.62)
29 Calculate $\boldsymbol{X}[n,k]$ using (4.66)
30 Compute $LMMSE$ estimate $\widehat{\boldsymbol{H}}_{LMMSE}$ using (4.67) or (4.63) as described in Algorithm 4.3
31 ***end for*** *(in line 04)*
32 ***return*** $\{\widehat{\boldsymbol{h}}_{LS}, \widehat{\boldsymbol{h}}_{LMMSE}\}$
33 ***Stop***

In the simulation, the channel coefficients of the known channel are obtained using (4.16). The LS and LMMSE channel estimates are computed individually using (4.62) and (4.67) respectively. The channel coefficients obtained from these computations are then compared with that of the known channel after which the NMSE for each CE-based scheme is obtained by comparing the computed channel estimates of these proposed schemes with the channel estimates of the known channel. In simple mathematical expressions, the NMSE of the LS and LMMSE-based channel estimates are expressed in (5.1) and (5.2) respectively for these systems, where E is the expectation operation.

$$NMSE_{LS} = \frac{E\left[\left\|H[n,k] - \widehat{H}_{LS}[n,k]\right\|^2\right]}{E[\|H[n,k]\|^2]} \tag{5.1}$$

$$NMSE_{LMMSE} = \frac{E\left[\left\|H[n,k] - \widehat{H}_{LMMSE}[n,k]\right\|^2\right]}{E[\|H[n,k]\|^2]} \tag{5.2}$$

5.2.2 SIMULATION PARAMETERS FOR IMPLEMENTING THE ESTIMATORS

All simulations reported in this dissertation were implemented using MATLAB programming language where the pseudocode of Algorithm 5.1 is used as a guide for the implementation. Simulations for the filter bank OFDM/OQAM are implemented assuming NPR and Non-PR based on the system model described in Fig. 4.2 and 4.6 of Chapter 4. For the simulations, the performances of the linear estimators are analyzed and compared with one another as well as with the adaptive estimators through Monte-Carlo simulations with 10,000 trials per SNR. For this filter bank waveform, simulation parameters are indicated in Table 5.1. Uncoded 16-QAM modulation scheme is assumed for the OFDM/OQAM-based transceiver with $M = 512$ subcarriers under frequency selective Rayleigh fading channel with Doppler rates of 0.001 and 0.02, corresponding to both slow and fast fading channel conditions respectively, where the speed of the moving mobile is selected as 360 km/hr and 18 km/hr correlating with fast and slow channels respectively. The overlapping factor is chosen as $K = 4$, while the initial value of the filter coefficient $P[k]$ is selected to be $P[1] = 0.97195983$ as indicated in table (4.1) [46]. Cyclic prefix (CP) overhead is not considered for this system in contrast to the GFDM/OQAM system. For the adaptive algorithms, the positive step size parameter is selected as $\mu = 0.35$ while a regularization factor δ = 0.001 is chosen to initialize the inverse autocorrelation matrix

of (4.77). The forgetting factor λ is selected to be 0.998. Results obtained are shown and discussed in Subsection 5.2.3.

Table 5.1 Simulation parameters for filter bank OFDM/OQAM

Parameters	**Specifications**
No. of Subcarriers (M)	512
Signal Constellation Scheme	16-QAM/OQAM
Sampling Frequency (f_s)	10,000 MHz
Doppler Frequency (f_d)	10 and 200 (Hz)
Sampling Rate (T_s)	$\left(\frac{1}{10 \times 10^3}\right)$ s
Doppler Rate(s)	0.001 and 0.02
Pulse Shape	Non-rectangular
Overlapping Factor (K)	4
Filter Coefficient ($\tilde{P}[1]$)	0.97195983
Channel Type	Multipath fading
Cyclic Prefix Overhead	-

5.2.3 SIMULATION RESULTS OBTAINED FOR CE IN OFDM/OQAM

As shown in Fig. 5.1, the first 60 randomly generated 16-QAM symbols are plotted. Fig. 5.2 shows the constellation diagram of the transmitted signals (as employed in this dissertation). It clearly corresponds to the constellation of 16-QAM modulation scheme while a plot of the channel fading coefficients corresponding to Doppler rates of 0.001 is shown in Fig. 5.3. In this figure, it can be observed that the expectation of the channel coefficients, i.e. $(E\{H(k)\})$, is independent of SNR and same valued for all iterations. Similarly, when the channel fading coefficients corresponding to Doppler rates of 0.02 is plotted, it is observed that the average value of the channel coefficients is 1.24 for all SNR values considered.

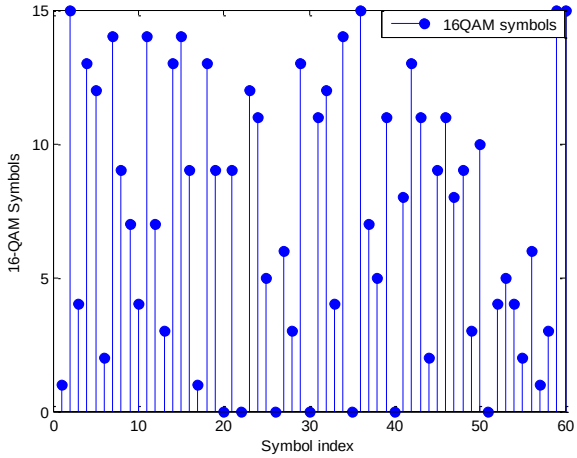

Fig. 5.1 Random 16-QAM symbols for the filter bank OFDM/OQAM systems

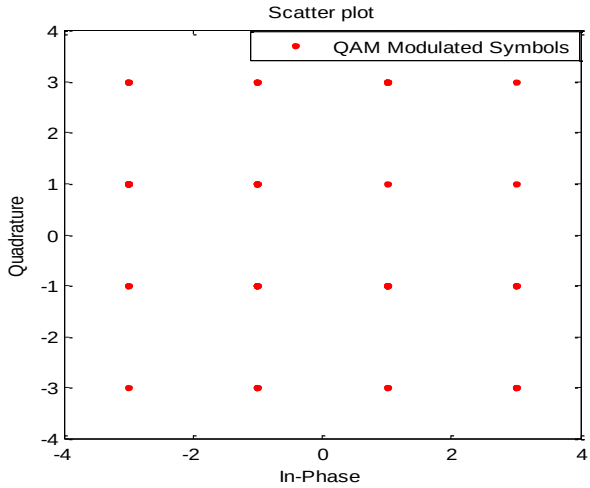

Fig. 5.2 Signal constellation of the 16-QAM OFDM/OQAM symbols

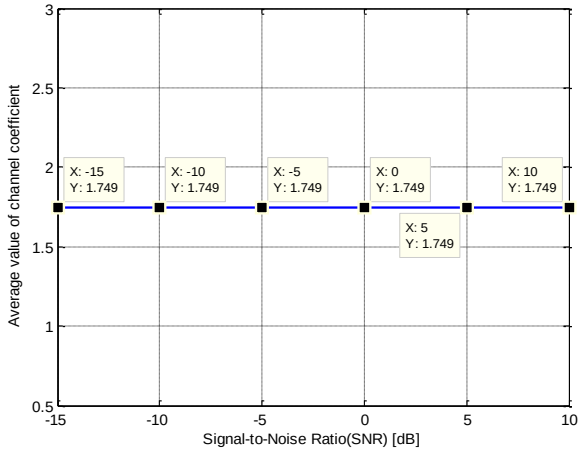

Fig. 5.3 A plot of channel impulse corresponding to $f_d T_s = 0.001$

The NMSE channel estimation performance for the proposed adaptive and linear estimators for NPR filter bank OFDM/OQAM system under slow fading channel conditions with Doppler rate $f_d T_s = 0.001$ is plotted as shown in Fig. 5.4 and 5.5 respectively while the BER curve at this rate is shown in Fig. 5.7 where the ideal channel is used to benchmark the performances of other estimators. An extension of the system performance at higher SNR is shown in Fig. 5.6.

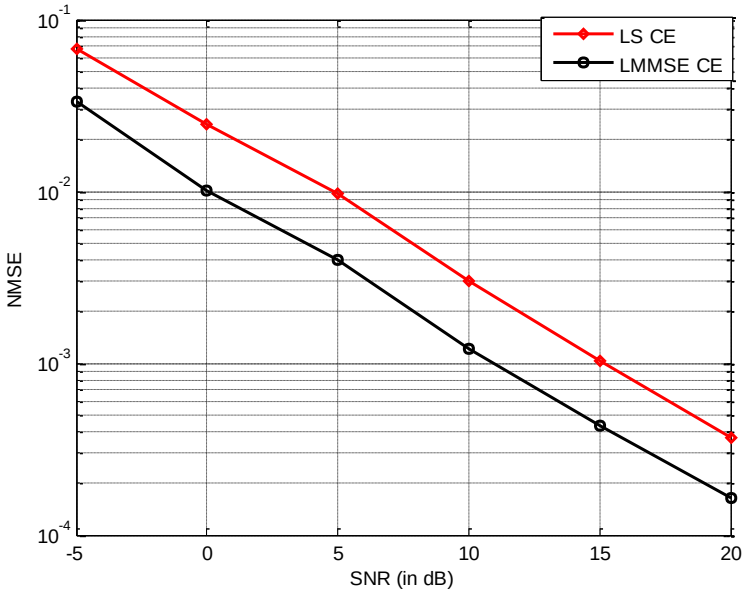

Fig. 5.4 NMSE performance of linear CE for NPR OFDM/OQAM under $f_d T_s = 0.001$

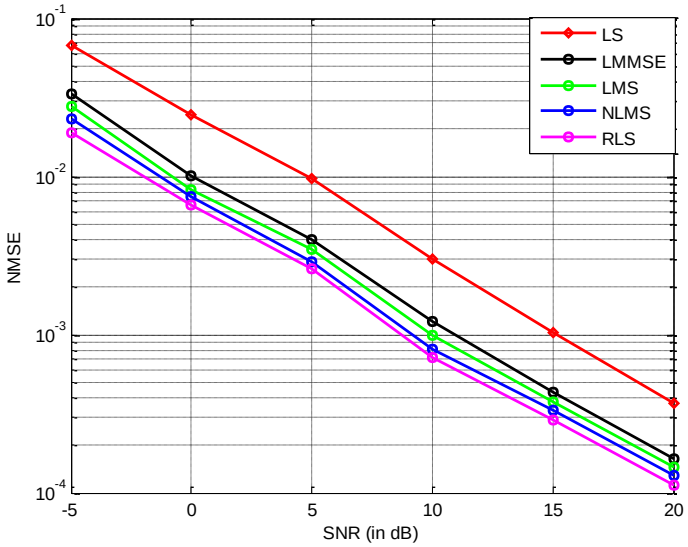

Fig. 5.5 NMSE of linear and adaptive CE schemes for NPR OFDM/OQAM $f_d T_s = 0.001$

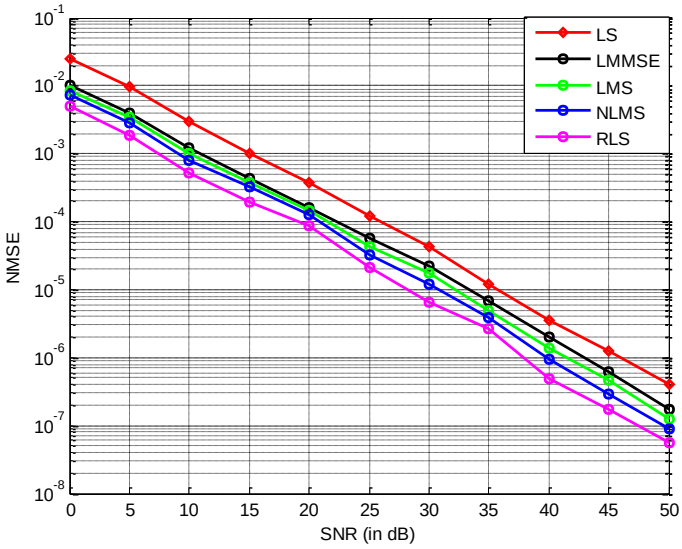

Fig. 5.6 NMSE of proposed estimators for NPR OFDM/OQAM $f_d T_s = 0.001$

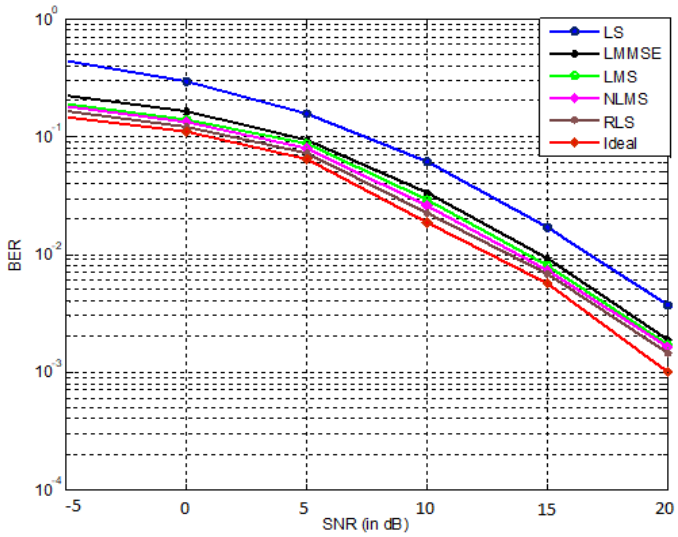

Fig. 5.7 BER of proposed estimators for NPR OFDM/OQAM $f_d T_s = 0.001$

Table 5.2 gives a comparison of the performances of the proposed CE schemes in terms of NMSE at various levels of SNR for NPR OFDM/OQAM waveform under $f_d T_s = 0.001$. It can be observed from Fig. 5.5 and this table that the adaptive channel estimators perform better than the linear channel estimates. For this Doppler rate, the basic LS channel estimate offers the worst NMSE performance for all SNR values. It is also observed from this table that the NMSE of all CE algorithms improves in performance (across a row) with corresponding increase in SNR.

Table 5.2 NMSE vs SNR for channel estimators assuming NPR with ($f_d T_s = 0.001$)

SNR (dB)	-5	0	5	10	15	20
NMSE (LS)	0.06699	0.0246	0.0096	0.0030	0.0010	0.0004
NMSE (LMMSE)	0.0333	0.0101	0.0040	0.0012	0.0004	0.0002
NMSE (LMS)	0.0277	0.0083	0.0035	0.0010	0.0004	0.0001
NMSE (NLMS)	0.0230	0.0739	0.0029	0.0008	0.0003	0.0001
NMSE (RLS)	0.0188	0.0067	0.0026	0.0007	0.0003	0.0001

The actual values of the correlation matrix used for this Doppler rate ($f_d T_s = 0.001$) are

$$\boldsymbol{R}_{HH}(n,k) = \begin{bmatrix} 1.0000 & 0.7708 & 0.3682 & \cdot & \cdot & 0.1355 \\ 0.7708 & 1.0000 & 0.7708 & \cdot & \cdot & 0.1276 \\ 0.3682 & 0.7708 & 1.0000 & \cdot & \cdots & 0.0317 \\ \vdots & \vdots & * & \cdot & \cdots & \vdots \\ & & * & * & & \\ 0.1355 & 0.1276 & 0.0317 & \cdot & \cdot & 1.0000 \end{bmatrix} \tag{5.3}$$

The NMSE performance of the linear estimators and all proposed estimators are shown in Fig. 5.8 and 5.9 respectively for NPR filter bank OFDM/OQAM scheme under fast fading channel with Doppler rate $f_d T_s = 0.02$ while Table 5.3 shows the corresponding performance comparison in terms of NMSE at various levels of SNR for the same Doppler rate. Fig. 5.11 gives the BER curve where the ideal channel is used to benchmark the performances of the estimators.

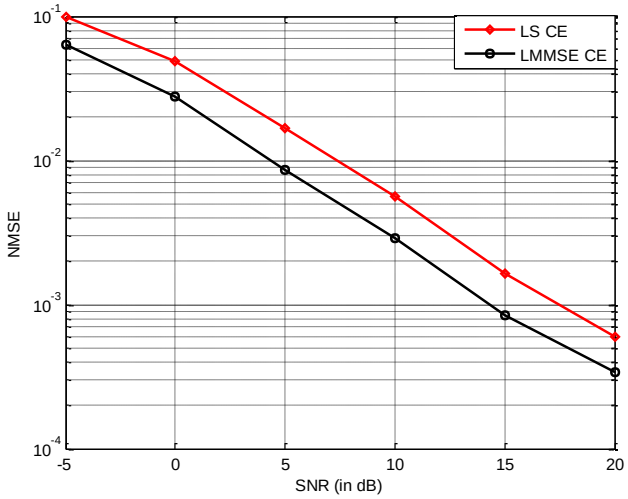

Fig.5.8 NMSE performance of LS vs LMMSE CE for NPR OFDM/OQAM $f_d T_s = 0.02$

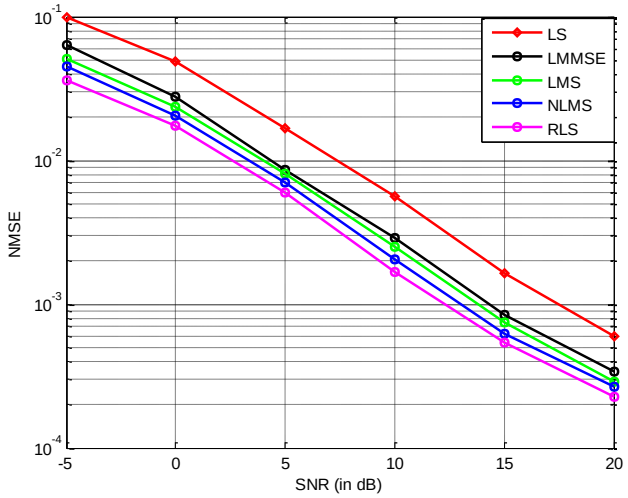

Fig. 5.9 NMSE performance of linear and adaptive CE for NPR OFDM/OQAM $f_d T_s = 0.02$

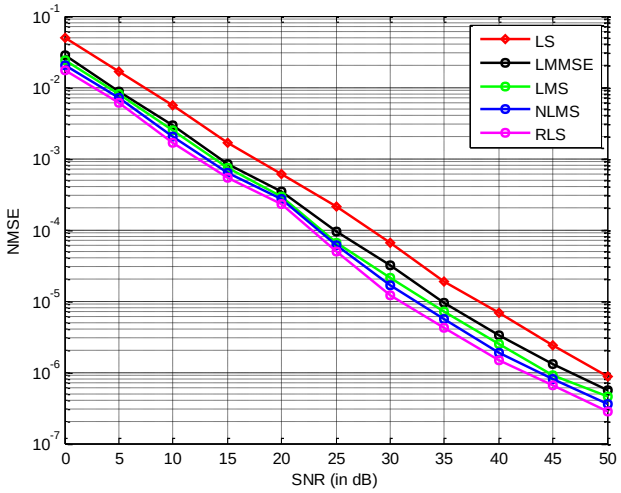

Fig. 5.10 Extended performance of linear and adaptive CE for NPR OFDM/OQAM $f_d T_s = 0.02$

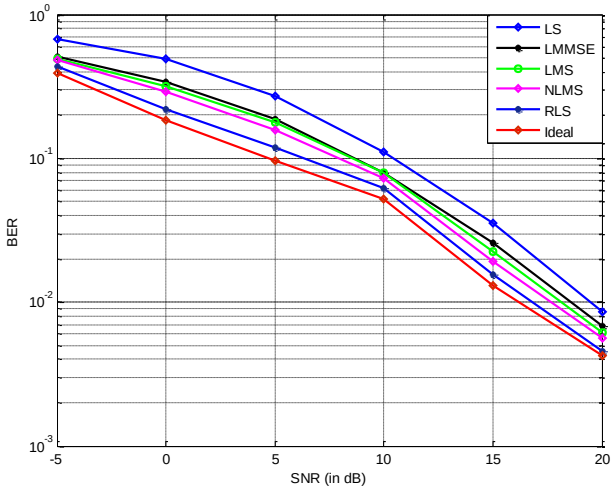

Fig. 5.11 BER performance of proposed estimators for NPR OFDM/OQAM $f_d T_s = 0.02$

Table 5.3 NMSE vs. SNR Performance NPR OFDM/OQAM $f_d T_s = 0.02$

SNR (dB)	-5	0	5	10	15	20
NMSE (LS)	0.0986	0.0487	0.0169	0.0056	0.0016	0.0006
NMSE (LMMSE)	0.0640	0.0279	0.0087	0.0029	0.0008	0.0003
NMSE (LMS)	0.0511	0.0237	0.0080	0.0025	0.0007	0.0003
NMSE (NLMS)	0.0451	0.0207	0.0071	0.0020	0.0006	0.0003
NMSE (RLS)	0.0360	0.0174	0.0060	0.0017	0.0005	0.0002

The correlation matrix used for this rate ($f_d T_s = 0.02$) is given in (5.4).

$$\boldsymbol{R}_{HH}(n,k) = \begin{bmatrix} 1.0000 & 0.1130 & 0.0330 & \cdots & 2.53 \times 10^{-14} \\ 0.1130 & 1.0000 & 0.1130 & \cdots & 6.42 \times 10^{-14} \\ 0.0330 & 0.1130 & 1.0000 & \cdots & 1.63 \times 10^{-13} \\ \vdots & \vdots & \vdots & \ddots & \vdots \\ 2.53 \times 10^{-14} & 6.42 \times 10^{-14} & 1.63 \times 10^{-13} & \cdots & 1.0000 \end{bmatrix} \quad (5.4)$$

It is observed (from Fig. 5.9 and 5.11 as well as Table 5.3) that the RLS channel estimate outperforms all other estimation schemes for all levels of SNR. The LS channel estimate offers the worst performance while having the lowest computational complexity. Hence, it can be concluded that RLS-based channel estimation scheme offers the best system performance for both slow and fast fading channel conditions in a filter bank OFDM/OQAM-based waveform, assuming NPR filter design whose performance gain is achieved at the expense of highest cost in computational complexity as compared with other estimators.

5.2.4 COMPARISON OF CE FOR NPR VS. NON-PR FILTER BANK OFDM/OQAM

In this subsection, performance comparisons of the proposed channel estimation schemes are made for NPR and Non-PR filter bank OFDM/OQAM system. A sequential procedure for implementing the estimation algorithms (assuming NPR conditions) is given in Algorithm 5.1. In Non-PR filter banks, the impulse response of the analysis filter bank FIR prototype filter is different from that of the synthesis filter bank, hence the analysis filter bank is not directly a time-reversed version of the corresponding synthesis filter bank due to the difference in prototype filter impulse response. This results into aliasing and amplitude distortions which may be detrimental to accurate signal reception. Fig. 5.12 compares the impulse response curve of the prototype filters as simulated in MATLAB assuming both NPR and Non-PR filter bank

OFDM/OQAM according to (4.7) and (4.30) respectively. The corresponding impulse response obtained from exponential modulation according to (4.6) is given in Fig. 5.13.

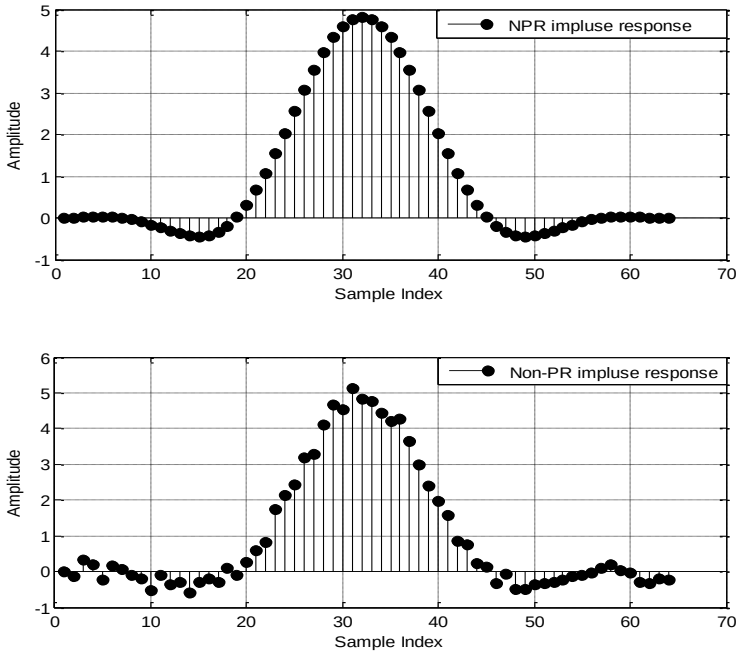

Fig. 5.12 Plot of prototype filter impulse responses assuming NPR and Non-PR, $K = 4$ and $M = 16$

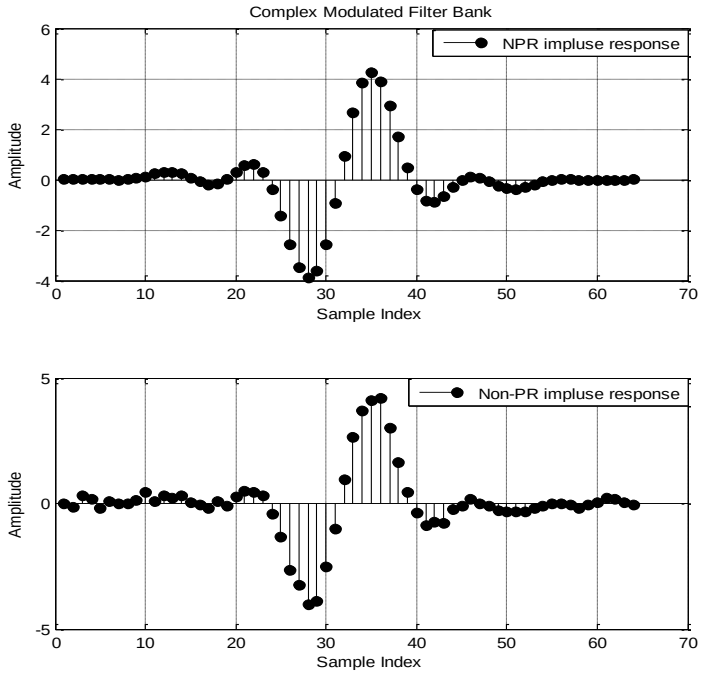

Fig. 5.13 Corresponding impulse responses plot using exponential modulation, $K = 4$ and $M = 16$

5.2.4.1 SEQUENTIAL PROCEDURE FOR IMPLEMENTING NON-PR OFDM/OQAM

Algorithm 5.2 displays a sequential procedure for implementing CE assuming Non-PR filter.

ALGORITHM 5.2 CHANNEL ESTIMATION FOR Non-PR OFDM/OQAM

01 **Start**
02 **Input**: M, K, $\boldsymbol{SNR}$, bps, T_s, f_d
03 **Output**: $\{\widehat{\boldsymbol{h}}_{LS}, \widehat{\boldsymbol{h}}_{LMMSE}\}$
04 ***for*** $esno = 1 : length(\boldsymbol{SNR})$
05 Repeat step 05 to 19 of Algorithm 5.1
06 Obtain $g[n,k]$ using (4.6) and compute $y[\dot{n},k]$ using (4.31)
07 Repeat step 20 to 22 of Algorithm 5.1 to obtain the channel impulse response
08 Compute $r[\dot{n},k]$ and $f'[\dot{n},k]$ using (4.33) and (4.32) respectively
09 Evaluate $s[n,k]$ from $r[\dot{n},k]$ and $f'[\dot{n},k]$ using $(4.35a)$
10 **CHANNEL ESTIMATION COMPUTATION**
11 Obtain least square estimate $\widehat{\boldsymbol{h}}_{LS}$using (4.62) and compare with that of NPR
12 Calculate $\boldsymbol{X}[n,k]$ using (4.66)
13 Compute $LMMSE$ estimate $\widehat{\boldsymbol{H}}_{LMMSE}$ using (4.67) and compare with that of NPR
14 ***end for*** *(in line 04)*
15 ***return*** $\{\widehat{\boldsymbol{h}}_{LS}, \widehat{\boldsymbol{h}}_{LMMSE}\}$
16 ***Stop***

5.2.4.2 SIMULATION PARAMETERS/RESULTS FOR NON-PR FILTER BANK

The simulation parameters used for Non-PR filter bank OFDM/OQAM are very similar to those of NPR as described in Subsection 5.2.2. Fig. 5.14 shows the NMSE vs. Non-PR error curve for different values of randomly introduced errors assuming an SNR of 5dB. When the error value is zero, the system assumes NPR. For other Non-PR simulations, the randomly introduced errors (with values between -0.1 and 0.1) are chosen to introduce imperfection as shown in (4.30). It is important to note that the higher the error value, the more the distortion. Results obtained from this performance comparison are shown for the linear and adaptive estimators as shown in Fig. 5.15 and. 5.16 respectively for Doppler rate of 0.001. Fig. 5.15 and 5.16 show the performance comparison of both the linear and adaptive channel estimation schemes for Doppler rate of 0.02.

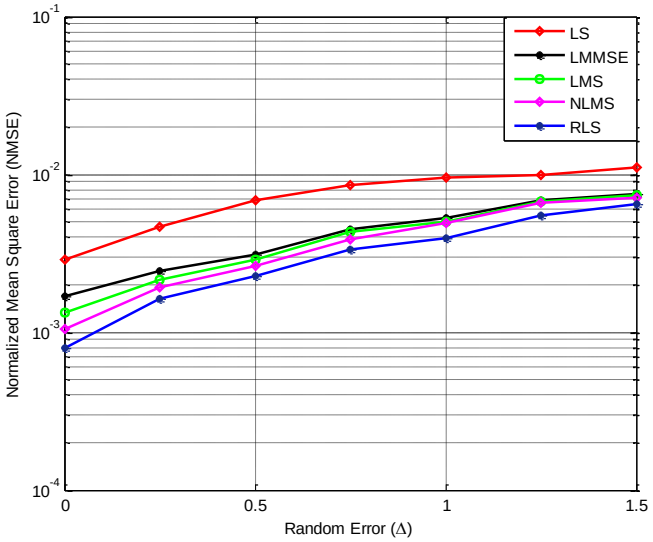

Fig. 5.14 NMSE vs introduced random errors (Δ) assuming Non-PR for SNR = 5dB

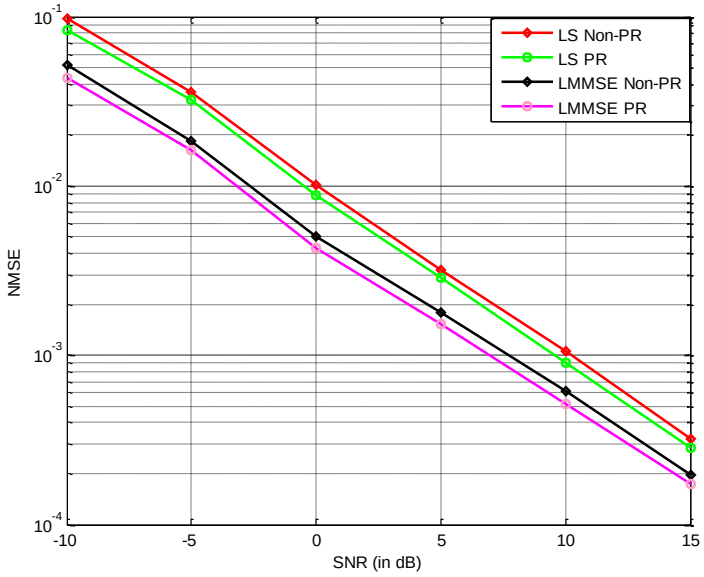

Fig. 5.15 Comparison of linear CE under NPR and Non-PR filter bank OFDM/OQAM for ($f_d T_s = 0.001$)

Results obtained from Fig. 5.15 indicate that the LMMSE estimation scheme performs better than the LS estimation scheme. The estimation schemes demonstrate superior performances under NPR condition in comparison to Non-PR filter bank systems.

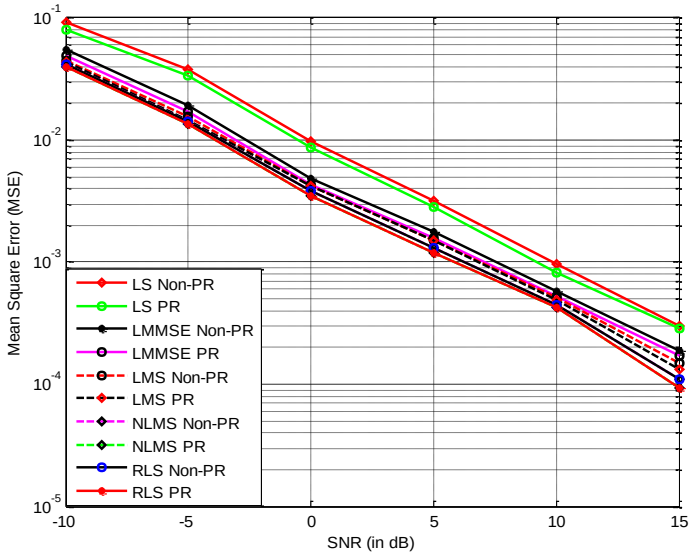

Fig. 5.16 Comparison of linear and adaptive CE under NPR/Non-PR OFDM/OQAM ($f_d T_s = 0.001$)

In Fig. 5.16, it is clear that all estimation schemes also demonstrate superior performances under NPR condition in comparison to Non-PR filter bank systems. RLS channel estimation offers the best system performance especially when applicable to NPR filter bank OFDM/OQAM while LS estimation offers the worst system performance especially when implemented in a Non-PR filter bank system. Table 5.4 shows the actual NMSE values for all estimation schemes under both NPR and Non-PR filter bank system for Doppler rates of 0.001 at various levels of SNR while Table 5.5 gives the MSE performance for Doppler rate = 0.02.

Table 5.4 NMSE vs. SNR Performance NPR and Non-PR OFDM/OQAM ($f_d T_s = 0.001$)

SNR (dB)	-10	-5	0	5	10	15
LS Non-PR	0.0931	0.0382	0.0097	0.0032	0.0010	0.0003
LS PR	0.0806	0.0334	0.0087	0.0028	0.0008	0.0003
LMMSE Non-PR	0.0550	0.0191	0.0049	0.0018	0.0006	0.0002
LMMSE PR	0.0486	0.0170	0.0043	0.0016	0.0005	0.0002
LMS Non-PR	0.0445	0.0156	0.0042	0.0015	0.0005	0.0001
LMS PR	0.0437	0.0146	0.0041	0.0013	0.0005	0.0001
NLMS Non-PR	0.0418	0.0141	0.0039	0.0011	0.0004	0.0001
NLMS PR	0.0400	0.0136	0.0035	0.0008	0.0004	0.0000
RLS Non-PR	0.0101	0.0069	0.0019	0.0005	0.0002	0.0000
RLS PR	0.0077	0.0056	0.0013	0.0003	0.0002	0.0000

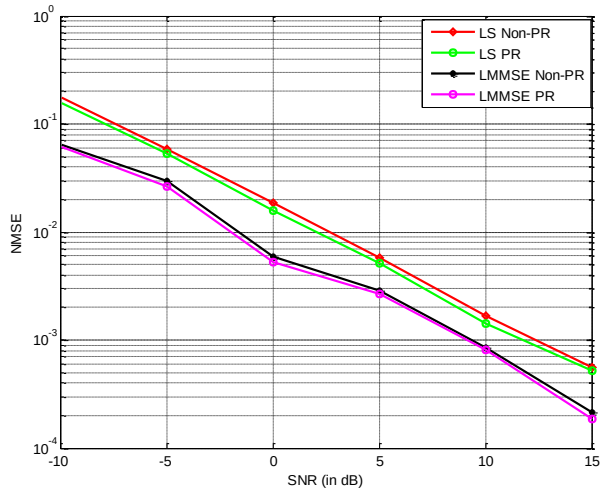

Fig. 5.17 Comparison of linear CE under NPR and Non-PR filter bank OFDM/OQAM for $f_d T_s = 0.02$

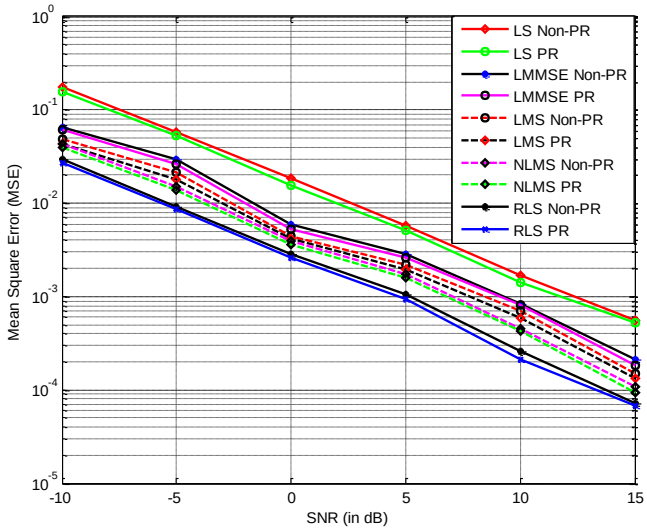

Fig. 5.18 Comparison of linear and adaptive CE under NPR/Non-PR OFDM/OQAM $f_d T_s = 0.02$

Table 5.5 NMSE vs. SNR Performance NPR OFDM/OQAM ($f_d T_s = 0.02$)

SNR (dB)	-10	-5	0	5	10	15
LS Non-PR	0.1760	0.0579	0.0184	0.0058	0.0017	0.0006
LS PR	0.1565	0.0533	0.0157	0.0051	0.0014	0.0005
LMMSE Non-PR	0.0647	0.0298	0.0059	0.0029	0.0008	0.0002
LMMSE PR	0.0616	0.0266	0.0052	0.0026	0.0008	0.0002
LMS Non-PR	0.0489	0.0213	0.0045	0.0022	0.0007	0.0001
LMS PR	0.0437	0.0178	0.0042	0.0020	0.0006	0.0001
NLMS Non-PR	0.0430	0.0150	0.0040	0.0017	0.0004	0.0001
NLMS PR	0.0400	0.0139	0.0036	0.0016	0.0004	0.0001
RLS Non-PR	0.0297	0.0092	0.0029	0.0011	0.0003	0.0001
RLS PR	0.0268	0.0088	0.0026	0.0009	0.0002	0.0001

The results obtained from Fig. 5.16 and Table 5.5 show that RLS channel estimation under NPR also offers the best NMSE performance while the LS channel estimation scheme assuming Non-PR offers the worst system performance for channel with Doppler rate of $f_d T_s = 0.02$.

5.3 CHANNEL ESTIMATION PERFORMANCE ANALYSIS FOR GFDM/OQAM

The proposed channel estimation algorithms are also analyzed for a GFDM/OQAM filter bank system. This section evaluates and documents the performances of the proposed linear and adaptive channel estimation schemes for the filter bank GFDM/OQAM scheme as described in Chapter 4 of this dissertation. It presents a sequential procedure for implementing the channel estimation schemes for the GFDM/OQAM system while also discussing the simulation procedure and parameters as well as the results obtained.

5.3.1 SEQUENTIAL PROCEDURE FOR IMPLEMENTING CE FOR GFDM/OQAM

In this dissertation, three adaptive channel estimation schemes namely LMS, NLMS, RLS and two linear schemes named LS and LMMSE are also implemented and analyzed for GFDM/OQAM-based transceivers under conditions of NPR of filters. Sequential procedures for implementing CE for the filter bank OFDM/OQAM is shown in Algorithm 5.3.

ALGORITHM 5.3: LS AND LMMSE CHANNEL ESTIMATION FOR GFDM/OQAM

01 **Start**
02 **Input**: M, K, $\boldsymbol{SNR}$, bps, T_s, f_d
03 **Output**: $\{\widehat{\boldsymbol{h}}_{LS}, \widehat{\boldsymbol{h}}_{LMMSE}\}$
04 ***for*** $ebno = 1 : length(\boldsymbol{SNR})$
05 input = *randi*([0 1], N, bps) Generate $N \times bps$ random binary input bits [bps = bits/sec]
06 sym = *bi2de*(input) ← convert generated bits into $N \times 1$ symbols
07 c[l] = *qammod*(sym) ← QAM modulate input symbols
08 ***for*** $n \leftarrow 0 : N-1$
09 ***if*** $n \leftarrow 0{:}\ 1 : N-1$ ***then***
10 $\boldsymbol{d}[n] \leftarrow$ [real($\boldsymbol{c}[l]$) imag($\boldsymbol{c}[l]$)]
11 ***end for*** *(in line 08)*
12 ***for*** $n \leftarrow 0 : M-1$, compute
13 $\vec{\tilde{d}}[n,k] \leftarrow \boldsymbol{d}[n] * (i)^n$
14 ***end for*** *(in line 12)*
15 Obtain $g_{k',\dot{m}}[n]$ using (4.42)
16 Collect coefficients of $g_{k',\dot{m}}[n]$ to form $(N \times N)$ modulation matrix $\boldsymbol{A}$ as in (4.46)
17 Calculate $\tilde{\vec{x}}[n]$ using (4.45)
18 Add cyclic prefix of length N_{CP} to the beginning of $\tilde{\vec{x}}[n]$ so as to yield $\tilde{\vec{x}}_T[n]$
19 Calculate $a[n,k']$ and $\boldsymbol{R}_{HH}[n,k']$ using (4.48) and (4.49) respectively
20 Obtain $\Omega[n,k']$ from σ_Ω^2 using (4.53)
21 Obtain $z[i]$ from (4.51) and calculate $H[n,k']$ and $h[n,k']$ using (4.50) and (4.56) respectively
22 Zero pad $h[n,k']$ by adding N_{CP} zeros to form $h_0[n,k']$ having length $(N + N_{CP}) \times 1$
23 Formulate circulant channel matrix $\widetilde{\ddot{\mathbf{H}}}$ according to (4.58).
24 Generate additive Gaussian noise $w[n]$
25 Compute the received signal $\tilde{\vec{x}}_R[n]$ (with cyclic prefix) using (4.57)
26 Remove the first N_{CP} elements of $\tilde{\vec{x}}_R[n]$ to obtain received signals $x_R[n]$
27 **CHANNEL ESTIMATION COMPUTATION**
28 Obtain least square estimate $\widehat{\boldsymbol{h}}_{LS}$ using (4.80)
29 Calculate $\boldsymbol{X}[n,k]$ using (4.82)
30 Compute $LMMSE$ estimate $\widehat{\boldsymbol{h}}_{LMMSE}$ using (4.81)
31 ***end for*** *(in line 04)*
32 ***return*** $\{\widehat{\boldsymbol{h}}_{LS}, \widehat{\boldsymbol{h}}_{LMMSE}\}$
33 ***Stop***

5.3.2 SIMULATION PARAMETERS FOR IMPLEMENTING GFDM ESTIMATORS

The simulations for the GFDM/OQAM-based system were also simulated using MATLAB programming language where the pseudocode of Algorithm 5.3 is used to describe the implementation procedure. Simulations for the filter bank GFDM/OQAM are implemented based on the system model described in Fig. 4.8 of Chapter 4. For the simulations, the performances of the linear estimators are analyzed and compared with one another, as well as with the adaptive estimators through Monte-Carlo simulations with 10,000 trials per SNR. For this filter bank waveform, simulation parameters are indicated in Table 5.6. Uncoded 16-QAM modulation scheme is also assumed for the GFDM/OQAM-based transceiver with $N = 512$ subcarriers under frequency selective Rayleigh fading channel with Doppler rates of 0.001 and 0.02, corresponding to both slow and fast fading channel conditions respectively, where the speed of the moving mobile is selected as 360 km/hr and 18 km/hr correlating with fast and slow channels respectively. The overlapping factor is chosen as $K = 4$, while the initial value of the filter coefficient $P[k]$ is selected to be $P[1] = 0.97195983$ as indicated in (4.7). Cyclic prefix overhead of length 25% of symbol duration is added in this system unlike in filter bank OFDM/OQAM system that does not consider the use of cyclic prefix. For the adaptive algorithms, the positive step size parameter is selected as $\mu = 0.35$ while a regularization factor δ = 0.001 is also chosen to initialize the inverse autocorrelation matrix of (4.67). The forgetting factor λ is selected to be 0.998. Results obtained are shown and discussed in Subsection 5.3.3.

Table 5.6 Simulation parameters for GFDM/OQAM system

Parameters	**Specifications (GFDM/OQAM)**
No. of Subcarriers (N)	512
Signal Constellation Scheme	Uncoded 16-QAM/OQAM
Sampling Frequency (f_s)	10,000 Hz
Doppler Frequency (f_d)	10 and 200 (Hz)
Sampling Rate (T_s)	(1/10,000) s
Doppler Rate(s)	0.001 and 0.02
Overlapping Factor (K)	4
Pulse Shape	Non-rectangular
Filter Coefficient ($\tilde{P}[1]$)	0.97195983
Channel Type	Multipath Rayleigh fading
Cyclic Prefix Overhead	25%

5.3.3 SIMULATION RESULTS OBTAINED FOR CE IN GFDM/OQAM

In this subsection, the simulation results obtained from analyzing the performances of all linear and adaptive channel estimation schemes are presented under the assumption of nearly perfect reconstruction of filters. The average channel impulse response corresponding to Doppler rates of 0.001 and 0.02 has values of 0.1052 and 0.0509 respectively while showing that the expectation of the channel impulse responses i.e. $(E\{H(k)\})$ is independent of SNR and same valued for all iterations.

The NMSE channel estimation performance of the proposed linear estimators in GFDM/OQAM system under slow fading channel conditions with Doppler rate $f_d T_s = 0.001$ is plotted as shown in Fig. 5.19, while the BER curve is given in Fig. 5.21 where the ideal channel is used as a bench mark for performance.

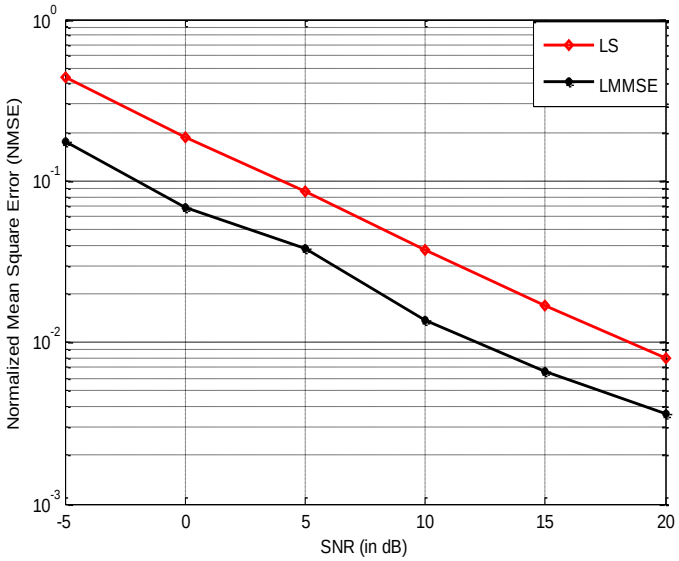

Fig. 5.19 NMSE performance of linear CE for GFDM/OQAM $(f_d T_s = 0.001)$

Table 5.7 shows a comparison of the performances of the proposed CE schemes in terms of NMSE at various levels of SNR for GFDM/OQAM waveform under $(f_d T_s = 0.001)$. It is observed from Fig. 5.20 and this table that the adaptive channel estimators perform better than the linear channel estimators. For this Doppler rate, the basic LS channel estimate offers the worst NMSE performance for all SNR values. It is also observed from this table that the NMSE of all CE algorithms improve in performance (across a row) with corresponding increase in SNR.

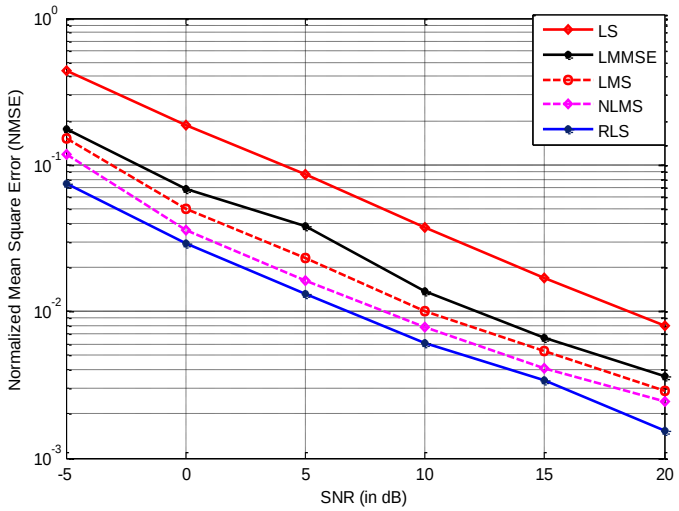

Fig. 5.20 NMSE of linear and adaptive CE schemes for GFDM/OQAM $f_d T_s = 0.001$

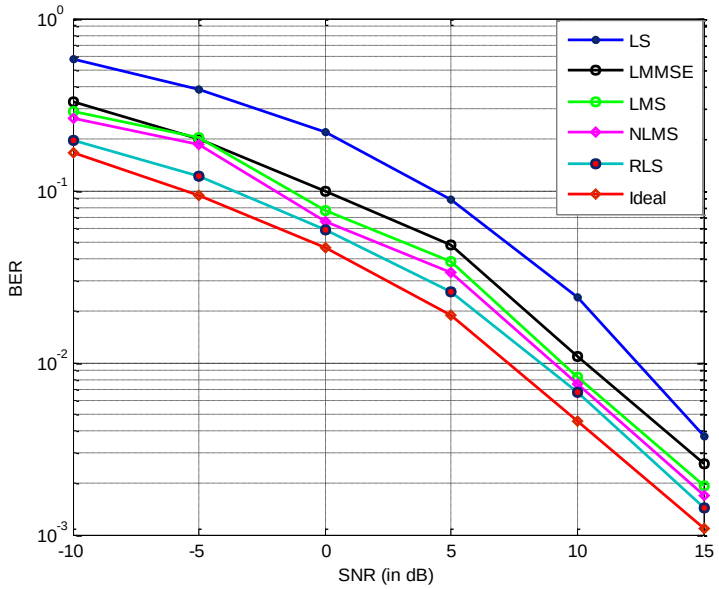

Fig. 5.21 BER curve of proposed estimators for GFDM/OQAM $f_d T_s = 0.001$

Table 5.7 NMSE vs. SNR of proposed channel estimators for GFDM/OQAM ($f_d T_s = 0.001$)

SNR (dB)	-5	0	5	10	15	20
NMSE (LS)	0.4388	0.1863	0.0860	0.0374	0.0169	0.0080
NMSE (LMMSE)	0.1757	0.0690	0.0382	0.0138	0.0066	0.0036
NMSE (LMS)	0.1514	0.0499	0.0229	0.0100	0.0053	0.0028
NMSE (NLMS)	0.1181	0.0359	0.0160	0.0077	0.0041	0.0024
NMSE (RLS)	0.0747	0.0289	0.0130	0.0061	0.0034	0.0015

The actual values of the correlation matrix used for this Doppler rate $f_d T_s = 0.001$ are given in (5.3). The NMSE performance of the linear and adaptive estimators are shown in Fig. 5.22 for filter bank GFDM/OQAM scheme under fast fading channel with Doppler rate $f_d T_s = 0.02$, while Table 5.8 gives the corresponding performance comparison in terms of NMSE at various levels of SNR for the same Doppler rate. Fig. 5.23 gives the BER curve where ideal channel is used as a benchmark to analyze the system performance.

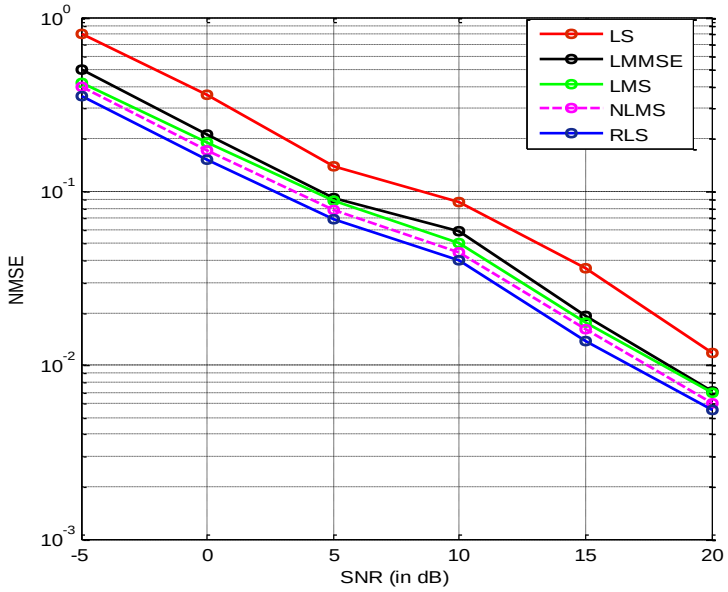

Fig. 5.22 NMSE of linear and adaptive CE schemes for GFDM/OQAM $(f_d T_s = 0.02)$

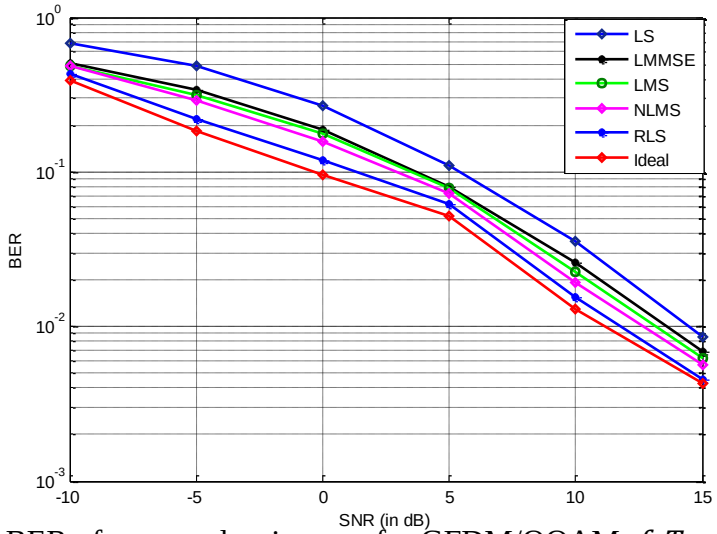

Fig. 5.23 BER of proposed estimators for GFDM/OQAM $f_d T_s = 0.02$

Table 5.8 NMSE vs. SNR of proposed channel estimators for GFDM/OQAM $f_d T_s = 0.02$

SNR (dB)	-5	0	5	10	15	20
NMSE (LS)	0.8070	0.3566	0.1397	0.0870	0.0360	0.0118
NMSE (LMMSE)	0.4967	0.2121	0.0912	0.0590	0.0192	0.0070
NMSE (LMS)	0.4212	0.1900	0.0876	0.0499	0.0175	0.0069
NMSE (NLMS)	0.3997	0.1727	0.0783	0.0444	0.0162	0.0060
NMSE (RLS)	0.3496	0.1523	0.0686	0.0400	0.0137	0.0055

5.4 COMPUTATIONAL COMPLEXITY ANALYSIS

The computational complexities per iteration of the proposed linear and adaptive based CE schemes are tabulated in Table 5.9. These complexities focuses on the amount of computing resources required for executing the channel estimates of the proposed algorithms assuming no repetition of channel values for a frame. From this table, it is calculated that the basic LS channel estimate is computed with $9M$ multiplications/Divisions and $6M$ additions/ subtractions. In a similar manner, LMMSE channel estimation scheme requires $(3M^3 + M^2 - M - 3)$ additions/subtractions while $(2M^3 + 2M^2 + 1)$ multiplications/Divisions are required to compute this channel estimate. The complexities of the adaptive schemes are tabulated above. Hence, RLS, NLMS, LMS, LMMSE and LS are the most complex estimators in decreasing order.

Table 5.9 Computational complexity analysis for the proposed channel estimators

Estimator	**Addition/Subtraction (+/-)**	**Multiplication/Division (×/÷)**
LS	$6M$	$9M$
LMMSE	$(3M^3 + M^2 - M - 3)$	$(2M^3 + 2M^2 + 1)$
LMS	$3(M^3 + 2)$	$4M^3$
NLMS	$(M^3 + 2M + 1)$	$(6M^3 + 4)$
RLS	$8M^3$	$(9M^3 + 5M^2 + 1)$

5.5 CHAPTER SUMMARY

In this chapter, the performances of LS, LMMSE, LMS, NLMS and RLS channel estimation schemes have been analyzed and documented for two filter bank multicarrier-based transceivers with offset quadrature amplitude modulation named GFDM/OQAM and filter bank OFDM/OQAM. The performances of the proposed channel estimation schemes are analyzed under the assumption of both NPR and Non-PR filter bank systems in slow and fast frequency selective Rayleigh fading channels with corresponding Doppler rates of 0.001 and 0.02 respectively. Results obtained demonstrate that all the presented channel estimation schemes performed better in NPR filter bank systems as compared to filter bank systems with imperfections (Non-PR). It is observed from these results that the RLS channel estimation scheme offers the best performance (as compared with all the other channel estimation schemes) in terms of NMSE with improvement in performance as the SNR increases. It is also observed that NLMS, LMS, LMMSE and LS channel estimation schemes demonstrate good performances (in decreasing order), with the basic LS channel estimation scheme exhibiting the worst estimation performance for all waveforms while having the simplest computational complexity. All simulations were performed using MATLAB programming language according to the system model that is described in Chapter 4 of this dissertation.

CHAPTER SIX

CONCLUSIONS & FUTURE WORKS

6.1 CONCLUSIONS

In this dissertation, the performances of LS, LMMSE, LMS, NLMS and RLS channel estimation schemes have been analyzed and documented for two filter bank multicarrier schemes with offset quadrature amplitude modulation (i.e. OFDM/OQAM and GFDM/OQAM-based transceivers). The performances of these estimation schemes are evaluated under the assumption of NPR and Non-PR design of the low-pass prototype filter with symbols propagated through both slow and fast frequency selective Rayleigh fading channels having corresponding Doppler rates of 0.001 and 0.02 respectively. Results obtained showed that all the channel estimation algorithms performed better in a near perfect reconstructed filter bank system as compared to non- perfect reconstructed systems for both slow and fast fading channels. The poor performance of Non-PR filter banks result from aliasing and amplitude distortions that are generated from the random introduction of errors which constitute the design of the low-pass prototype filter. It is observed that the RLS estimation scheme offered the best channel estimation performance (in terms of NMSE) with its estimation performance getting better as SNR increases while NLMS, LMS, LMMSE and LS estimation schemes also demonstrated good estimation performances (in decreasing order). In [112], the performances of the LS and LMMSE estimators are analyzed for OFDM systems where LMMSE showed better MSE performance in comparison to LS. The performances of LMMSE estimator is also shown to offer better performance than LS estimator in this dissertation. Similarly, in [166], the performances of adaptive CE are analyzed for multicarrier interleaves division multiple access (MC-IDMA) systems where NLMS offered better channel estimation performance than LMS. In a similar manner, NLMS is observed to perform better than LMS for all systems as investigated in this dissertation. All simulations are implemented using MATLAB programming language according to the system model described in Chapter 4. It can therefore be concluded, based on the research questions, that the RLS channel estimation scheme offers the best channel estimation performance in terms for NMSE at all levels of SNR in comparison to NLMS, LMS, LMMSE and LS (in decreasing order) for both investigated waveforms (i.e. filter bank OFDM/OQAM and GFDM/OQAM) assuming both NPR and Non-PR designs of the FIR low pass prototype filter impulse responses through frequency

selective Rayleigh fading channel. It can also be concluded that all the investigated channel estimation schemes perform better in a filter bank system designed with NPR under both slow and fast frequency selective Rayleigh fading channel as compared to filter bank systems designed with Non-PR assumption under same channel conditions.

6.2 FUTURE WORKS

During the course of this research, some problems are identified and suggested for future works. These problems are listed as follows:

- It is observed from the literature survey (to the best of our knowledge) that the performances of blind and semi-blind channel estimation schemes have not been analyzed for both waveforms analyzed in this dissertation (i.e. OFDM/OQAM and GFDM/OQAM). Adopting these channel estimation schemes may be used to boost bandwidth efficiency and improve signal detection for these waveforms.
- The performances of three adaptive and two linear CE schemes have been analyzed for OFDM/OQAM and GFDM/OQAM filter banks in this dissertation. The performances of these adaptive algorithms as well as the linear algorithms can also be investigated and analyzed for UFMC and BFDM-based transceivers as both waveforms are also considered as potential candidates for the emerging 5G networks.
- Since FBMC/OQAM-based systems are known to offer higher data rates and spectral efficiencies in comparison to the CP-based OFDM systems adopted for 4G networks, the proposed waveforms in this dissertation can be adopted to boost the spectral efficiency and data rates of terrestrial digital video broadcasting (DVB-T) networks.

REFERENCES

[1] A. Jain and D. Nagaria, "Filter bank spectrum sensing for Cognitive Radio oriented wireless network," *Communication, Control and Intelligent Systems (CCIS)*, Mathura, 2015, pp. 133-136.

[2] M. Narendar, A. P. Vinod, A. S. Madhukumar and A. K. Krishna, "A robust two-stage spectrum sensing method using filter bank based energy detector and fourth order cumulants for cognitive radios," *IEEE International Conference on Communication Systems (ICCS)*, Singapore, 2012, pp. 438-442.

[3] B. Farhang-Boroujeny, "Filter Bank Spectrum Sensing for Cognitive Radios," in *IEEE Transactions on Signal Processing*, vol. 56, no. 5, pp. 1801-1811, May 2008.

[4] I. F. Akyildiz , W.Lee and K. R. Chowdhury, "CRAHNs: Cognitive radio ad hoc networks", *Science Direct Journal on Ad Hoc Networks*, vol. 7, no. 5, pp. 810 – 836, Jan. 2009.

[5] Ian F. Akyildiz, Won-Yeol Lee, Mehmet C. Vuran and Shantidev Mohanty, "NeXt generation/dynamic spectrum access/cognitive radio wireless networks: A survey", *Science Direct Journal on computer Networks*, vol. 50, no. 13, pp. 2127-2159, May 2006.

[6] A. Mitra, "Lecture Notes on Mobile Communication", Dept. of Elect. and Comm. Eng., Indian Institute of Technology, India, Nov. 2009.

[7] S. Hara, R. Prasad, "Overview of multicarrier CDMA," *IEEE Communications Magazine*, vol. 35, no. 12, pp.126-133, Dec. 1997.

[8] S. Sun, S. Han, Q. Yu, W. Meng and C. Li, "A survey of two kinds of complementary coded CDMA wireless communications," *2014 IEEE Global Communications Conference*, Austin, TX, 2014, pp. 468 - 472.

[9] S. M. Alamouti and A. R. Sharafat, "Resource allocation for energy-efficient device-to-device communication in 4G networks," *Telecommunications (IST), 2014 7th International Symposium on*, Iran, 2014, pp. 1058-1063.

[10] Y. Chen, L. Duan and Q. Zhang, "Financial analysis of 4G network deployment," *2015 IEEE Conference on Computer Communications (INFOCOM)*, Kowloon, 2015, pp. 1607-1615.

[11] S. R. Qurat-ul-Ain, U. Hassnain, M. Shah and S. A. Mahmud, "An evaluation of scheduling algorithms in LTE based 4G networks," *2015 International Conference on Emerging Technologies (ICET)*, Peshawar, 2015, pp. 1-6.

[12] R. Vidhya and P. Karthik, "Coexistence of cellular IOT and 4G networks," *2016 International Conference on Advanced Communication Control and Computing Technologies (ICACCCT)*, Ramanathapuram, 2016, pp. 555-558.

[13] H. A. Salman, L. F. Ibrahim and Z. Fayed, "Overview of LTE-Advanced Mobile Network Plan Layout," *2014 5th International Conference on Intelligent Systems, Modelling and Simulation*, Langkawi, 2014, pp. 585-590

[14] E. Soltanmohammadi, K. Ghavami and M.Naraghi-Pour, "A Survey of Traffic Issues in Machine-to-Machine Communications Over LTE," in *IEEE Internet of Things Journal*, vol. 3, no. 6, pp. 865-884, Dec. 2016.

[15] A. Jassal and C. Leung, "H.265 video capacity over beyond-4G networks," *2016 IEEE International Conference on Communications (ICC)*, Kuala Lumpur, 2016, pp. 1-6.

[16] S. Zhang, Q. Wu, S. Xu and G. Y. Li, "Fundamental Green Tradeoffs: Progresses, Challenges, and Impacts on 5G Networks," in *IEEE Communications Surveys & Tutorials*, vol. 19, no. 1, pp. 33-56, First quarter 2017.

[17] M. Abu-Lebdeh, J. Sahoo, R. Glitho and C. W. Tchouati, "Cloudifying the 3GPP IP multimedia subsystem for 4G and beyond: A survey," in *IEEE Communications Magazine*, vol. 54, no. 1, pp. 91-97, Jan. 2016.

[18] Y. Ding, Y. Jin, L. Ren and K. Hao, "An intelligent self-organization scheme for the internet of things," in *IEEE Computational Intelligence Magazine*, vol. 8, no. 3, pp. 41-53, Aug. 2013.

[19] I. Gaspar, N. Michailow, A. Navarro, E. Ohlmer, S. Krone and G. Fettweis, "Low complexity GFDM receiver based on sparse frequency domain processing," in *2013 77th IEEE Vehicular Technology Conference (VTC Spring)*, Dresden, 2013, pp. 1-6.

[20] P. Fettweis, "The tactile internet: applications and Challenges," in *IEEE Vehicular Technology Magazine*, vol. 9, no. 1, pp. 64-70, Mar. 2014.

[21] N. Tadayon and S. Aissa, "Modeling and analysis of cognitive radio based IEEE 802.22 wireless regional area networks," in *IEEE Transactions on Wireless Communications*, vol. 12, no. 9, pp. 4363-4375, Sept. 2013.

[22] M. Danneberg, N. Michailow, I. Gaspar, D. Zhang and G. Fettweis, "Flexible GFDM Implementation in FPGA with Support to Run-Time Reconfiguration," in *2015 IEEE 82nd Vehicular Technology Conference, VTC Fall* 2015, Boston, MA, pp. 1-2.

[23] N. Michailow *et al*., "Generalized frequency division multiplexing for 5th generation cellular networks," in *IEEE Transactions on Communications*, vol. 62, no. 9, pp. 3045-3061, Sept. 2014.

[24] W. Cao, J. Zhu, X. Li, W. Hu and J. Lei, "Feasibility of multi-carrier modulation signals as new illuminators of opportunity for passive radar: orthogonal frequency division multiplexing versus filter-bank multi-carrier," in *IET Radar, Sonar & Navigation*, vol. 10, no. 6, pp. 1080-1087, Jul. 2016.

[25] D. S. Waldhauser, L. G. Baltar and J. A. Nossek, "MMSE subcarrier equalization for filter bank based multicarrier systems," in *2008 IEEE 9th Workshop on Signal Processing Advances in Wireless Communications*, Recife, 2008, pp. 525-529.

[26] V.S. Boyan, "Pilot patterns and power loading in NC-OFDM cognitive radios," Ph.D. dissertation, Dept. Elect. Eng., Univ. Cape Town, Cape Town, 2013.

[27] C. Sonntag, "Orthogonal frequency division multiplexing (OFDM) implementation as part of a software defined radio (SDR) environment," M.Sc. Thesis, Dept. Elect. & Elect Eng., University of Stellenbosch, Stellenbosch, 2005.

[28] B. B. Muyiwa, "Frequency Synchronization in multiuser OFDM-IDMA systems," M.Sc. Thesis, Dept. Elect. Elect., & Comp. Eng., University of Kwazulu-Natal, Durban, 2013.

[29] M. Zhu, "Low complexity channel estimation for OFDM based satellite systems," Ph.D. dissertation, Faculty of Eng. & Sciences, Uni. Of Surrey, Guildford (UK), 2011.

[30] E. T. Lagunas, "Sparse channel estimation based on compressed sensing theory for UWB systems," M.Sc. Thesis, Dept. of Signal Theory and Comm, Universitat Politencnica de Catalunya, Barcelona, 2010.

[31] A. Farhang, N. Marchetti and L. E. Doyle, "Low-Complexity Modem Design for GFDM," in *IEEE Transactions on Signal Processing*, vol. 64, no. 6, pp. 1507 - 1518, Mar. 2016.

[32] A. Farhang, N. Marchetti and L. E. Doyle, "Low complexity GFDM receiver design: A new approach," *2015 IEEE International Conference on Communications (ICC)*, London, 2015, pp. 4775-4780.

[33] L. Sendrei, S. Marchevský, N. Michailow and G. Fettweis, "Iterative receiver for clipped GFDM signals," in *2014 24th International Conference on Radioelektronika*, Bratislava, 2014, pp. 1- 4.

[34] B. Farhang-Boroujeny and H. Moradi, "Derivation of GFDM based on OFDM principles," in *IEEE International Conference on Communications, ICC 2015*, London, 2015, pp. 2680-2685.

[35] G. Fettweis, M. Krondorf and S. Bittner, "GFDM - Generalized frequency division multiplexing," in *IEEE 69th Vehicular Technology Conference, VTC Spring 2009*, Barcelona, 2009, pp. 1 - 4.

[36] H. Kim, J. Kim, S. Yang, M. Hong and Y. Shin, "An effective MIMO–OFDM system for IEEE 802.22 WRAN channels," in *IEEE Transactions on Circuits and Systems II: Express Briefs*, vol. 55, no. 8, pp. 821-825, Aug. 2008.

[37] V. Vakilian, T. Wild, F. Schaich, S. ten Brink and J. F. Frigon, "Universal-filtered multi-carrier technique for wireless systems beyond LTE," *in IEEE Globecom Workshops, GC Workshops 2013*, Atlanta, GA, 2013, pp. 223-228.

[38] R. Ayadi, M. Siala and I. Kammoun, "Transmit/receive pulse-shaping design in BFDM systems over time-frequency dispersive AWGN channel," in *IEEE International Conference on Signal Processing and Communications, ICSPC 2007*, Dubai, 2007, pp. 772-775.

[39] C. Siclet and P. Siohan, "Design of BFDM/OQAM systems based on biorthogonal modulated filter banks," in *IEEE Global Telecommunications Conference, GLOBECOM '00*, San Francisco, CA, 2000, vol. 2, pp. 701-705.

[40] G. Fettweis, M. Krondorf and S. Bittner, "GFDM-Generalized frequency division multiplexing," in *IEEE 69th Vehicular Technology Conference, VTC Spring 2009*, Barcelona, 2009, pp. 1-4.

[41] A. Jain and D. Nagaria, "Filter bank spectrum sensing for Cognitive Radio oriented wireless network," *Communication, Control and Intelligent Systems (CCIS)*, Mathura, 2015, pp. 133-136.

[42] M. Narendar, A. P. Vinod, A. S. Madhukumar and A. K. Krishna, "A robust two-stage spectrum sensing method using filter bank based energy detector and fourth order cumulants for cognitive radios," *IEEE International Conference on Communication Systems (ICCS)*, Singapore, 2012, pp. 438-442.

[43] B. Farhang-Boroujeny, "Filter Bank Spectrum Sensing for Cognitive Radios," in *IEEE Transactions on Signal Processing*, vol. 56, no. 5, pp. 1801-1811, May 2008.

[44] N. LaSorte, W. J. Barnes and H. H. Refai, "The History of Orthogonal Frequency Division Multiplexing," *IEEE Global Telecommunications Conference, GLOBECOM 2008,* New Orleans, LO, 2008, pp. 1 - 5.

[45] S. Zhang, J. Wang and S. Li, "A channel estimation method for NC-OFDM systems in cognitive radio context," in *11th IEEE Singapore International Conference on Communication Systems, ICCS 2008*, Guangzhou, 2008, pp. 208-212.

[46] A. Viholainen, T. Ihalainen, T. H. Stitz, M. Renfors and M. Bellanger, "Prototype filter design for filter bank based multicarrier transmission," in *2009 17th European Signal Processing Conference*, Glasgow, 2009, pp. 1359 - 1363.

[47] M. Mirahmadi, A. Al-Dweik and A. Shami, "BER reduction of OFDM based broadband communication systems over multipath channels with impulsive noise," in *IEEE Transactions on Communications*, vol. 61, no. 11, pp. 4602-4615, Nov. 2013.

[48] X. Gao *et al.*, "An efficient digital implementation of multicarrier CDMA system based on generalized DFT filter Banks," in *IEEE Journal on Selected Areas in Communications*, vol. 24, no. 6, pp. 1189-1198, June 2006.

[49] S. A. Fechtel and A. Blaickner, "Efficient FFT and equalizer implementation for OFDM receivers," in *IEEE Transactions on Consumer Electronics*, vol. 45, no. 4, pp. 1104-1107, Nov. 1999.

[50] J. Fang, Z. You, I. T. Lu, J. Li and R. Yang, "Comparisons of filter bank multicarrier systems," in *IEEE Long Island Systems, Applications and Technology Conference, LISAT 2013,* Farmingdale, NY, 2013, pp. 1-6.

[51] L. Chang, G. Y. Li, J. Li and R. Li, "Blind parameter estimation of GFDM signals over frequency-selective fading channels," in *IEEE Transactions on Communications,* vol. 64, no. 3, pp. 1120-1131, Mar. 2016.

[52] M. M. Rana, "An adaptive channel estimation technique for OFDM based cognitive radio systems," in *14th International Conference on Computer and Information Technology, ICCIT 2011,* Dhaka, 2011, pp. 315-320.

[53] H. Velamala, "Filter bank multicarrier modulation for spectrally agile waveform design", Msc. Thesis, Dept. Electrical & Computer Eng., Worcester Polytechnic Institute, Massachusetts.

[54] J. G. Proakis and D. G.Manolakis, "Digital signal processing*"*, Prentice-Hall Inc, 1996.

[55] P. P. Vaidyanathan, "Multirate systems and filter banks", Pearson Education, Inc, 1993.

[56] V. K.Madisetti and D.B.Williams, "The Digital Signal Processing Handbook: DSP Fundamentals", CRC Press, 2010.

[57] R. Kuc, "Introduction to Digital Signal Processing", McGraw-Hill, 1988.

[58] R. E. Crochiere and L. R. Rabiner, "Interpolation and decimation of digital signals - A tutorial review," in *Proceedings of the IEEE,* vol. 69, no. 3, pp. 300-331, March 1981.

[59] D. G. Manolakis and V. K. Ingle, "Applied digital signal processing", Cambridge University Press, 2011.

[60] R. Kumar, A. Kumar and S. P. Singh, "A review on decade of multi-rate filters," in *2nd International Conference on Electronics and Communication Systems, ICECS 2015,* Coimbatore, 2015, pp. 1615 - 1620.

[61] L. Milic, T. Saramaki and R. Bregovic, "Multirate filters: an overview," *in IEEE Asia Pacific Conference on Circuits and Systems, APCCAS 2006,* Singapore, 2006, pp. 912 - 915.

[62] P. P. Vaidyanathan, "Multirate digital filters, filter banks, polyphase networks, and applications: a tutorial," in *Proceedings of the IEEE,* vol. 78, no. 1, pp. 56-93, Jan. 1990.

[63] J. J. Shynk, "Frequency-domain and multirate adaptive filtering," in *IEEE Signal Processing Magazine*, vol. 9, no. 1, pp. 14-37, Jan. 1992.

[64] P. P. Vaidyanathan, "A tutorial on multirate digital filter banks," in *IEEE International Symposium on Circuits and Systems*, Espoo, 1988, vol. 3, pp. 2241-2248.

[65] T. Aach, "Comparative analysis of shift variance and cyclostationarity in multirate filter banks," in *IEEE Transactions on Circuits and Systems I: Regular Papers*, vol. 54, no. 5, pp. 1077-1087, May 2007.

[66] T. Chen and P. P. Vaidyanathan, "Multidimensional multirate filters and filter banks derived from one-dimensional filters," in *IEEE Transactions on Signal Processing*, vol. 41, no. 5, pp. 1749-1765, May 1993.

[67] R. Meyer and C. Burrus, "Design and implementation of multirate digital filters," in *IEEE Transactions on Acoustics, Speech, and Signal Processing*, vol. 24, no. 1, pp. 53-58, Feb. 1976.

[68] R. G. Shenoy, D. Burnside and T. W. Parks, "Linear periodic systems and multirate filter design," in *IEEE Transactions on Signal Processing*, vol. 42, no. 9, pp. 2242-2256, Sep. 1994.

[69] B. Farhang-Boroujeng, “Filter Bank Multicarrier Modulation: A Waveform Candidate for 5G and Beyond” *Hindawi Advances in Electrical Engineering*, vol. 2014, no. 482805, pp. 1–25, Dec. 2014.

[70] K. W. Martin, "Small side-lobe filter design for multitone data-communication applications," in *IEEE Transactions on Circuits and Systems II: Analog and Digital Signal Processing*, vol. 45, no. 8, pp. 1155-1161, Aug. 1998.

[71] Daniel Zhou, “A review of polyphase filter banks and their application” *In-House final technical report - Air Force Research Laboratory*, Newyork, pp. 1 – 29, Sept. 2006.

[72] Tensubam, B. Devi, and S. Singh, "A review on FBMC: an efficient multicarrier modulation system," *International Journal of Computer Applications,* vol. 98, no. 17, 2014.

[73] P. Zahradnik and M. Vlcek, "Perfect decomposition narrow-band FIR filter banks," in *IEEE Transactions on Circuits and Systems II: Express Briefs*, vol. 59, no. 11, pp. 805-809, Nov. 2012.

[74] M. Vetterli, "A theory of multirate filter banks," in *IEEE Transactions on Acoustics, Speech, and Signal Processing*, vol. 35, no. 3, pp. 356-372, Mar. 1987.

[75] L. R. Diniz and S. L. Netto, “Design of high-resolution cosine-modulated transmultiplexers with sharp transition band,” *IEEE Transactions on Signal Processing*, vol. 52, pp. 1278 – 1288, May 2004.

[76] T. Karp and N. J. Fliege, "MDFT filter banks with perfect reconstruction," in *IEEE International Symposium on Circuits and Systems, ISCAS '95*, Seattle, WA, 1995, vol. 1, pp. 744-747.

[77] M. Aldababseh and A. Jamoos, “Estimation of FBMC/OQAM Fading Channels Using Dual Kalman Filters” *The Scientific World Journal*, vol. 2014, no. 586403, pp. 1 – 9, Feb. 2014.

[78] M. Newinger, L. G. Baltar and J. A. Nossek, "MMSE training design for filter bank multicarrier systems with per-subcarrier channel estimation", in *IEEE 78th Vehicular Technology Conference, VTC Fall 2013*, Las Vegas, NV, Sept. 2013, pp. 1 - 5.

[79] Y. Wang and X. P. Zhang, "Filter-bank design for multicarrier modulation systems with MPSK based on symbol-error-rate evaluation," in *IEEE Proceedings- Communications*, vol. 153, no. 6, pp. 919-917, Dec. 2006.

[80] L. Vandendorpe, J. Louveaux, B. Maison and A. Chevreuil, "About the asymptotic performance of MMSE MIMO DFE for filter-bank based multicarrier transmission," in *IEEE Transactions on Communications*, vol. 47, no. 10, pp. 1472 - 1475, Oct. 1999.

[81] B. Farhang-Boroujeny and Lekun Lin, "Cosine modulated multitone for very high-speed digital subscriber lines," in *IEEE International Conference on Acoustics, Speech, and Signal Processing Proceedings, ICASSP '05*, vol. 3, pp. 345 - 348.

[82] M. K. Lakshmanan and H. Nikookar, “A Review of Wavelets for Digital Wireless Communication,” *International Journal on Wireless Personal Communications*, vol. 37, no. 3-4, pp. 387 - 420, May 2006.

[83] S. D. Sandberg and M. A. Tzannes, ‘Overlapped discrete multitone modulation for high speed copper wire communications’, *IEEE J. Sel. Areas Commun.*, vol. 13, no. 9, pp. 1571–1585, 1995.

[84] J. Alhava and M. Renfors, "Exponentially-modulated filter bank transmultiplexer with fine-coarse adaptive filtering," *3rd International Symposium on Communications, Control and Signal Processing, ISCCSP 2008,* St Julians, 2008, pp. 68 - 72.

[85] L. Lin and B. Farhang-Boroujeny, "Convergence analysis of blind equalizer in a filter-bank-based multicarrier communication system," in *IEEE Transactions on Signal Processing*, vol. 54, no. 10, pp. 4061-4067, Oct. 2006.

[86] B. Farhang-Boroujeny and L. Lin, "Analysis of post-combiner equalizers in cosine-modulated filterbank-based transmultiplexer systems," in *IEEE Transactions on Signal Processing*, vol. 51, no. 12, pp. 3249-3262, Dec. 2003.

[87] S. Mirabbasi and K. Martin, "Overlapped complex-modulated transmultiplexer filters with simplified design and superior stopbands," in *IEEE Transactions on Circuits and Systems II: Analog and Digital Signal Processing*, vol. 50, no. 8, pp. 456-469, Aug. 2003.

[88] J. Alhava, A. Viholainen and M. Renfors, "Efficient implementation of complex exponentially-modulated filter banks," *Proceedings of the 2003 International Symposium on Circuits and Systems, ISCAS '03*, 2003, vol. 4, pp. 157 – 160.

[89] T. Karp and N. J. Fliege, "Modified DFT filter banks with perfect reconstruction," *IEEE Transactions on Circuits and Systems II:Analog and Digital Signal Processing*, vol. 46, pp. 1404 – 1414, Nov. 1999.

[90] J. A.Viholainen and M. Renfors, "Efficient implementation of complex exponentially-modulated filter banks using cosine and sine modulated filter banks," *Journal on Applied Signal Processing EURASIP*, pp. 1 – 10, 2006.

[91] T. P. N. Heller and T. Q. Nguyen, "A general formulation of modulated filter banks," *IEEE Transactions on Signal Processing*, vol. 47, pp. 986–1002, Apr. 1999.

[92] Yuan-Pei Lin and P. P. Vaidyanathan, "Application of DFT filter banks and cosine modulated filter banks in filtering," in *IEEE Asia-Pacific Conference on Circuits and Systems, APCCAS '94*, Taipei, 1994, pp. 254-259.

[93] L. G. Baltar, I. Slim and J. A. Nossek, "Efficient filter bank multicarrier realizations for 5G," *IEEE International Symposium on Circuits and Systems, ISCAS 2015*, Lisbon, 2015, pp. 2608-2611.

[94] M. Aldababseh, “Channel estimation for FBMC/OQAM wireless system based on Kalman filter”, Msc. Thesis, Dept. Elect. and Comp. Eng. Eng., Al-Quds University, Jerusalem-Palestine, 2013.

[95] J. A. Viholainen and M. Renfors, “Efficient implementation of twice oversampled exponentially-modulated filter banks,” *IEEE Transactions on Circuits and Systems II: Express Briefs*, vol. 53, pp. 1138–1142, Oct. 2006.

[96] A. Viholainen, J. Alhava and M. Renfors, "Implementation of parallel cosine and sine modulated filter banks for equalized transmultiplexer systems," in *IEEE International Conference on Acoustics, Speech, and Signal Processing Proceedings, (ICASSP '01),* Salt Lake City, UT, 2001, vol. 6, pp. 3625 - 3628.

[97] R. Cox, “The design of uniformly and non-uniformly spaced pseudo-quadrature mirror filters”, *IEEE Transactions on Acoustics, Speech and Signal Processing*, vol. 34, pp. 1090 – 1096, Oct. 1986.

[98] J. Masson and Z. Picel, "Flexible design of computationally efficient nearly perfect QMF filter banks," in *IEEE International Conference on Acoustics, Speech, and Signal Processing, ICASSP '85*, 1985, pp. 541 - 544.

[99] T. A. Ramstad and J. P. Tanem, "Cosine-modulated analysis-synthesis filter bank with critical sampling and perfect reconstruction," in *International Conference on Acoustics, Speech, and Signal Processing, ICASSP-91,* Toronto, Ont., 1991, vol. 3, pp. 1789 - 1792.

[100] R. D. Koilpillai and P. P. Vaidyanathan, "New results on cosine-modulated FIR filter banks satisfying perfect reconstruction," in *International Conference on Acoustics, Speech, and Signal Processing, ICASSP-91,* Toronto, Ont., 1991, vol. 3, pp. 1793-1796.

[101] R. D. Koilpillai and P. P. Vaidyanathan, “Cosine-modulated fir filter banks satisfying perfect reconstruction,” *IEEE Transactions on Signal Processing*, vol. 40, pp. 770–783, Apr. 1992.

[102] S. Dhabal, S. M. L. Chowdhury and P. Venkateswaran, "A novel low complexity multichannel Cosine Modulated Filter Bank using IFIR technique for Nearly Perfect Reconstruction," *1st International Conference on Recent Advances in Information Technology, RAIT 2012,* Dhanbad, 2012, pp. 208-213.

[103] H. Bolcskei and F. Hlawatsch, “Oversampled cosine modulated filter banks with perfect reconstruction,” *IEEE Transactions on Circuits and Systems II: Analog and Digital Signal Processing*, vol. 45, pp. 1057–1071, Aug. 1998.

[104] Y. P. Lin and P. P. Vaidyanathan, “Linear phase cosine modulated maximally decimated filter banks with perfect reconstruction,” *IEEE Transactions on Signal Processing*, vol. 42, pp. 2525–2539, Nov. 1995.

[105] T. K. Sarkar, Zhong Ji, Kyungjung Kim, A. Medouri and M. Salazar-Palma, "A survey of various propagation models for mobile communication," in *IEEE Antennas and Propagation Magazine*, vol. 45, no. 3, pp. 51-82, June 2003.

[106] S. Güzelgöz, H. Arslan, A. Islam, and A. Domijan, “A review of wireless and PLC propagation channel characteristics for smart grid environments,” *Journal of Elect. and Comp. Eng*, pp. 1 – 12, Aug. 2011.

[107] T. S. Rappaport, “Wireless Communications: Principles and Practice,” 2nd Edition, Prentice-Hall Inc., New Jersey, 2002.

[108] B. Sklar, "Rayleigh fading channels in mobile digital communication systems. Part I. Characterization," in *IEEE Communications Magazine*, vol. 35, no. 9, pp. 136-146, Sep. 1997.

[109] D. Tse and P. Viswanath, “Fundamentals of Wireless Communications,” Cambridge University Press, New York, 2005.

[110] M. K. Ozdemir and H. Arslan, "Channel estimation for wireless ofdm systems," in *IEEE Communications Surveys & Tutorials*, vol. 9, no. 2, pp. 18-48, Second Quarter 2007.

[111] O. O. Oyerinde and S. H. Mneney, “Review of channel estimation for wireless communication systems” *IETE Technical Review Journal*, vol. 29 no. 4, Jul. -Aug. 2012.

[112] J.-J. Van de Beek, O. Edfors, M. Sandell, S.K. Wilson, P. Ola Borjesson, "On channel estimation in OFDM systems," *45th IEEE Vehicular Technology Conference, 1995*, 25 - 28 Jul 1995, vol. 2, pp. 815 – 819.

[113] S. Coleri, M. Ergen, A. Puri and A. Bahai, "Channel estimation techniques based on pilot arrangement in OFDM systems," in *IEEE Transactions on Broadcasting*, vol. 48, no. 3, pp. 223-229, Sep. 2002.

[114] A. R. James, R. S. Benjamin, S. John, T. M. Joseph, V. Mathai and S. S. Pillai, "Channel estimation for OFDM systems," *2011 International Conference on Signal Processing, Communication, Computing and Networking Technologies*, Thuckafay, 2011, pp. 587-591.

[115] M. Morelli and U. Mengali, "A comparison of pilot-aided channel estimation methods for OFDM systems," in *IEEE Transactions on Signal Processing*, vol. 49, no. 12, pp. 3065-3073, Dec. 2001.

[116] J. Min, G. Xue-mai and W. Qun, "An improved channel estimation method for NC-OFDM systems in Cognitive Radio context," *6th International ICST Conference on Communications and Networking in China (CHINACOM), 2011*, pp.147-150, 17-19 Aug. 2011.

[117] Chunhua Zhu and Shouyi Yang, "The Interference Constrained Pilot Design for NC-OFDM Systems in Cognitive Radios," *8th International Conference on Wireless Communications, Networking and Mobile Computing (WiCOM 2012),* 21-23 Sept. 2012, pp. 1-4.

[118] Jinnan Liu; Shulan Feng and Haiguang Wang, "Comb-Type Pilot Aided Channel Estimation in Non-Contiguous OFDM Systems for Cognitive Radio," *5th International Conference on Wireless Communications, Networking and Mobile Computing, 2009. WiCom '09.* pp. 1- 4, 24-26 Sept. 2009.

[119] Y. Zhang, X. Xu, B. Chen, X. Dai, "A suboptimal pilot design for NC-OFDM systems," *12th IEEE International Conference on Communication Technology (ICCT), 2010,* pp. 801 - 804, 11-14 Nov. 2010.

[120] E. Manasseh, S. Ohno, M. Nakamoto, "Pilot design for non-contiguous spectrum usage in OFDM-based cognitive radio networks," *Signal Processing Conference (EUSIPCO), 2012 Proceedings of the 20th European* , pp. 465 - 469, 27-31 Aug. 2012.

[121] C. R. Berger, Z. Wang, J. Huang and S. Zhou, "Application of compressive sensing to sparse channel estimation," *IEEE Communications Magazine,* vol. 48, no. 11, pp. 164 - 174, Nov. 2010.

[122] J. Min, L. Xin and G. Xue-mai, “Channel estimation algorithm based on compressive sensing for NC-OFDM systems in cognitive radio context,” *International Journal of Advancements in Computing Technology (IJACT)*, vol. 5, no. 1, Jan. 2013.

[123] E. Chen and C. Chu, "Channel estimation for NC-OFDM systems based on subspace pursuit algorithm," *IEEE 11th International Conference on Signal Processing (ICSP)*, pp. 88 - 91, 21-25 Oct. 2012.

[124] X. He, R. Song and W. P. Zhu, "Pilot Allocation for Sparse Channel Estimation in MIMO-OFDM Systems," in *IEEE Transactions on Circuits and Systems II: Express Briefs*, vol. 60, no. 9, pp. 612-616, Sept. 2013.

[125] H. Minn, N. Al-Dhahir and Y. Li, "Optimal training signals for MIMO OFDM channel estimation in the presence of frequency offset and phase noise," in *IEEE Transactions on Communications*, vol. 54, no. 10, pp. 1754-1759, Oct. 2006.

[126] H. Minn and N. Al-Dhahir, "Optimal training signals for MIMO OFDM channel estimation," in *IEEE Transactions on Wireless Communications*, vol. 5, no. 5, pp. 1158-1168, May 2006.

[127] I. Barhumi, G. Leus and M. Moonen, "Optimal training design for MIMO OFDM systems in mobile wireless channels," in *IEEE Transactions on Signal Processing*, vol. 51, no. 6, pp. 1615-1624, June 2003.

[128] W. Zhang, X. G. Xia and P. C. Ching, "Optimal Training and Pilot Pattern Design for OFDM Systems in Rayleigh Fading," in *IEEE Transactions on Broadcasting*, vol. 52, no. 4, pp. 505-514, Dec. 2006.

[129] D. S. Yoo and J. Lim, "MSE expression for transform-based decision-directed channel estimation schemes in M-PSK OFDM systems," in *Electronics Letters*, vol. 52, no. 5, pp. 363-365, Mar. 2016.

[130] S. Park, J. W. Choi, K. Lee and B. Shim, "Soft decision-directed channel estimation for multiuser MIMO systems," *2015 IEEE 26th Annual International Symposium on Personal, Indoor, and Mobile Radio Communications (PIMRC)*, Hong Kong, 2015, pp. 95-99.

[131] K. Mawatwal, D. Sen and R. Roy, "A Semi-Blind Channel Estimation Algorithm for Massive MIMO Systems," in *IEEE Wireless Communications Letters*, vol. 6, no. 1, pp. 70-73, Feb. 2017.

[132] M. L. Wang; C. P. Li; W. J. Huang, "Semi-Blind Channel Estimation and Precoding Scheme in Two-Way Multi-Relay Networks," in *IEEE Transactions on Signal Processing* , vol. PP, no. 99, pp. 1-12.

[133] Y. Ban, Q. Hu, Z. Mao and Z. Zhao, "Semi-blind pilot-aided channel estimation in uplink cloud radio access networks," in *China Communications*, vol. 13, no. 9, pp. 72-79, Sept. 2016.

[134] X. He, Z. Zhao and H. Zhang, "A pilot-aided channel estimation method for FBMC/OQAM communications system," in *International Symposium on Communications and Information Technologies, ISCIT, 2012*, Gold Coast, QLD, 2012, pp. 175-180.

[135] V. K. Valand, K. N. Patel, "A review of channel estimation techniques for OFDM," *International Journal for Scientific Research & Development I*, vol. 1, no. 12, pp. 2815 – 2817, 2014.

[136] C. H. Tseng, Y. C. Cheng and C. D. Chung, "Subspace-Based Blind Channel Estimation for OFDM by Exploiting Cyclic Prefix," in *IEEE Wireless Communications Letters*, vol. 2, no. 6, pp. 691-694, Dec. 2013.

[137] C. Qi and L. Wu, "A hybrid compressed sensing algorithm for sparse channel estimation in MIMO OFDM systems," in *Proc. IEEE Int. Conf. Acoust., Speech, Signal Process*., May 2011, pp. 3488–3491.

[138] Lélé Chrislin, J. P. Javaudin, R. Legouable, A. Skrzypczak and P. Siohan., "Channel estimation methods for preamble-based OFDM/OQAM modulations." *European Transactions on Telecommunications*, vol. 19, no. 7, pp. 741-750, 11 Sept. 2008.

[139] E. Kofidis and D. Katselis, "Improved interference approximation method for preamble-based channel estimation in FBMC/OQAM," in *19th European Signal Processing Conference*, Barcelona, 2011, pp. 1603 - 1607.

[140] E. Kofidis, "Short preamble-based estimation of highly frequency selective channels in FBMC/OQAM," *in IEEE International Conference on Acoustics, Speech and Signal Processing, ICASSP 2014*, Florence, 2014, pp. 8058 - 8062.

[141] L. G. Baltar, A. Mezghani and J. A. Nossek, "Spectral efficient channel estimation algorithms for FBMC/OQAM systems: A comparison," in *11th International Symposium on Wireless Communications Systems, ISWCS 2014*, Barcelona, Aug. 2014, pp. 707 - 711.

[142] Z. Zhao, N. Vucic and M. Schellmann, "A simplified scattered pilot for FBMC/OQAM in highly frequency selective channels," in *11th International Symposium on Wireless Communications Systems (ISWCS)*, Barcelona, Aug. 2014, pp. 819 - 823.

[143] L. G. Baltar, A. Mezghani and J. A. Nossek, "EM based Per-Subcarrier ML Channel Estimation for Filter Bank Multicarrier Systems," *Proceedings of the Tenth International Symposium on Wireless Communication Systems, ISWCS 2013,* Ilmenau, Germany, Aug. 2013, pp. 1-5.

[144] U. Vilaipornsawai and M. Jia, "Scattered-pilot channel estimation for GFDM," in *IEEE Wireless Communications and Networking Conference, WCNC 2014,* Istanbul, 2014, pp. 1053 - 1058.

[145] R. Zakaria and D. Le Ruyet, "A novel filter-bank multicarrier scheme to mitigate the intrinsic interference: application to MIMO systems," in *IEEE Transactions on Wireless Communications*, vol. 11, no. 3, pp. 1112-1123, March 2012.

[146] J. Fang, Z. You, I. T. Lu, J. Li and R. Yang, "Comparisons of filter bank multicarrier systems," in *IEEE Long Island systems, Applications and Technology Conference, LISAT 2013,* Farmingdale, NY, 2013, pp. 1-6.

[147] M. Danneberg, N. Michailow, I. Gaspar, D. Zhang and G. Fettweis, "Flexible GFDM Implementation in FPGA with Support to Run-Time Reconfiguration," in *2015 IEEE 82nd Vehicular Technology Conference, VTC Fall 2015*, Boston, MA, 2015, pp. 1 - 2.

[148] X. He, Z. Zhao and H. Zhang, "A pilot-aided channel estimation method for FBMC/OQAM communications system," in *2012 International Symposium on Communications and Information Technologies, ISCIT 2012,* 2-5 Oct. 2012, pp. 175-180.

[149] H. Saeedi-Sourck, Y. Wu, J. W. M. Bergmans, S. Sadri and B. Farhang-Boroujeny, "Complexity and performance comparison of filter bank multicarrier and OFDM in uplink of multicarrier multiple access networks," in *IEEE Transactions on Signal Processing*, vol. 59, no. 4, pp. 1907-1912, Apr. 2011.

[150] T. Ihalainen, A. Viholainen, T. H. Stitz and M. Renfors, "Generation of filter bank-based multicarrier waveform using partial synthesis and time domain interpolation," in *IEEE Transactions on Circuits and Systems I: Regular Papers*, vol. 57, no. 7, pp. 1767-1778, Jul. 2010.

[151] K. E. Baddour and N. C. Beaulieu, "Autoregressive models for fading channel simulation," in *IEEE Global Telecommunications Conference, GLOBECOM '01*, 2001, vol. 2, pp. 1187 - 1192.

[152] K. E. Baddour and N. C. Beaulieu, "Autoregressive modeling for fading channel simulation," in *IEEE Transactions on Wireless Communications*, vol. 4, no. 4, pp. 1650-1662, Jul. 2005.

[153] S. Haykin, “Adaptive filter theory”, Prentice hall, New Jersey, 1986.

[154] A. Jamoos, E. Grivel, N. Shakarneh and H. Abdel-Nour, "Dual optimal filters for parameter estimation of a multivariate autoregressive process from noisy observations," in *IET Signal Processing*, vol. 5, no. 5, pp. 471-479, Aug. 2011.

[155] L. Chang, J. Li and G. Y. Li, "Blind parameter estimation of GFDM signals over frequency-selective fading channels," *2015 IEEE Global Conference on Signal and Information Processing, GlobalSIP 2015*, Orlando, FL, 2015, pp. 275-279.

[156] N. Michailow, L. Mendes, M. Matthé, I. Gaspar, A. Festag and G. Fettweis, "Robust WHT-GFDM for the Next Generation of Wireless Networks," in *IEEE Communications Letters*, vol. 19, no. 1, pp. 106-109, Jan. 2015.

[157] R. Datta, D. Panaitopol and G. Fettweis, "Cyclostationary detection of 5G GFDM waveform in cognitive radio transmission," in *IEEE International Conference on Ultra-WideBand, ICUWB 2014*, Paris, 2014, pp. 108-112.

[158] P. S. Wang and D. W. Lin, "Maximum-Likelihood Blind Synchronization for GFDM Systems," in *IEEE Signal Processing Letters*, vol. 23, no. 6, pp. 790-794, June 2016.

[159] M. Matthe, I. Gaspar, D. Zhang and G. Fettweis, "Reduced complexity calculation of LMMSE filter coefficients for GFDM," in *IEEE 82nd Vehicular Technology Conference, VTC Fall 2015*, Boston, MA, 2015, pp. 1 - 2.

[160] R. Datta, N. Michailow, M. Lentmaier and G. Fettweis, "GFDM interference cancellation for flexible cognitive radio PHY design," in *Vehicular Technology Conference, VTC Fall 2012*, Quebec City, QC, pp. 1 - 5, 2012.

[161] S. K. Bandari, V. V. Mani and A. Drosopoulos, "OQAM implementation of GFDM," in *23rd International Conference on Telecommunications, ICT 2016*, Thessaloniki, 2016, pp. 1 - 5.

[162] I. Gaspar, M. Matthé, N. Michailow, L. Leonel Mendes, D. Zhang and G. Fettweis, "Frequency-Shift Offset-QAM for GFDM," in *IEEE Communications Letters*, vol. 19, no. 8, pp. 1454 - 1457, Aug. 2015.

[163] L. L. Scharf, "Statistical signal processing: Detection, estimation and time series analysis," *Addison-Wesley*, Jul. 1991.

[164] O. Edfors, M. Sandell, J.-J. van de Beek, S. K. Wilson, P. O. Borjesson, "OFDM channel estimation by singular value decomposition," in *1996 46th IEEE Vehicular Technology Conference on Mobile Technology for the Human Race*, 28 Apr - 1 May 1996, vol. 2, pp. 923 – 927.

[165] Meng-Han Hsieh, Che-Ho Wei, "Channel estimation for OFDM systems based on comb-type pilot arrangement in frequency selective fading channels," *IEEE Transactions on Consumer Electronics*, vol. 44, no. 1, pp. 217-225, Feb. 1998.

[166] O. O. Oyerinde and S. H. Mneney, "Adaptive algorithms based-time domain iterative channel estimation for MC-IDMA systems," in *3rd International Conference on Wireless Communications, Vehicular Technology, Information Theory and Aerospace & Electronic Systems, VITAE 2013*, Atlantic City, NJ, 2013, pp. 1-5.

APPENDIX

Appendix A*: Mathematical Derivation of LMMSE Channel Estimation Algorithm*

The input symbols $x[n,k]$ obtained from OQAM preprocessing output at the transmitter side are arranged to form a diagonal matrix $\boldsymbol{X}[n,k]$ given as:

$$\boldsymbol{X}[n,k] = diag\,[\boldsymbol{x}[n,k]] = diag\; x[n,1]\; x[n,2]\; x[n,3] \ldots x[n,M] \qquad (A.1)$$

The received symbols ($s[n,k]$) just before CE can be expressed as:

$$s[n,k] = \left[s[n,1]\; s[n,2]\; s[n,3] \ldots s[n,M]\right] \qquad (A.2)$$

Equation $(A.2)$ is generally represented as:

$$s[n,k] = \boldsymbol{X}[n,k]h[n,k] + \eta[n,k] \qquad (A.3)$$

where $\eta[n,k]$ is the Gaussian noise process with variance ${\sigma_{\eta,k}}^2$ expressed in (4.25). The variance (${\sigma_{\eta,k}}^2$) is be derived as follows. From (4.24),

$$\eta[n,k] = w[n,k] * f[n,k] \qquad (A.4)$$

According to standard convolution of two vectors,

$$\eta[n,k] = \sum_{l=-\infty}^{\infty} w[n-l,k]f[l,k]$$

$$\eta[n,k] = \sum_{l=0}^{L_p-1} w[n-l,k]f[l,k] \qquad (A.5)$$

But

$${\sigma_{\eta,k}}^2 = E\{\eta^2[n,k]\} \qquad (A.6)$$

where E is the expectation sign. Substituting $(A.5)$ into $(A.6)$ yields:

$${\sigma_{\eta,k}}^2 = E\left\{\left(\sum_{l=0}^{L_p-1} w[n-l,k]f[l,k]\right)^2\right\} \qquad (A.7)$$

$$= \sum_{l=0}^{L_p-1}\sum_{j=0}^{L_p-1} E\,\{w[n-l,k]w[n-j,k]f[l,k]f[j,k]\}$$

$$= \sum_{j=0}^{L_p-1} f[l,k]f[j,k]\, E\left\{\sum_{l=0}^{L_p-1}(w[n-l,k]w[n-j,k])\right\}$$

where

$$\sigma_{w,k}^2 = E\left\{\sum_{l=0}^{L_p-1}(w[n-l,k]w[n-j,k])\right\} \qquad (A.8)$$

Hence,

$$\sigma_{\eta,k}{}^2 = \sigma_{w,k}^2 \sum_{j=0}^{L_p-1} f^2[j,k] \qquad (A.9)$$

In order to derive the linear estimator which minimizes the MSE of the FBMC/OQAM symbols, we consider the equivalent channel representation for this multivariate normal problem as contained in Fig. A.1.

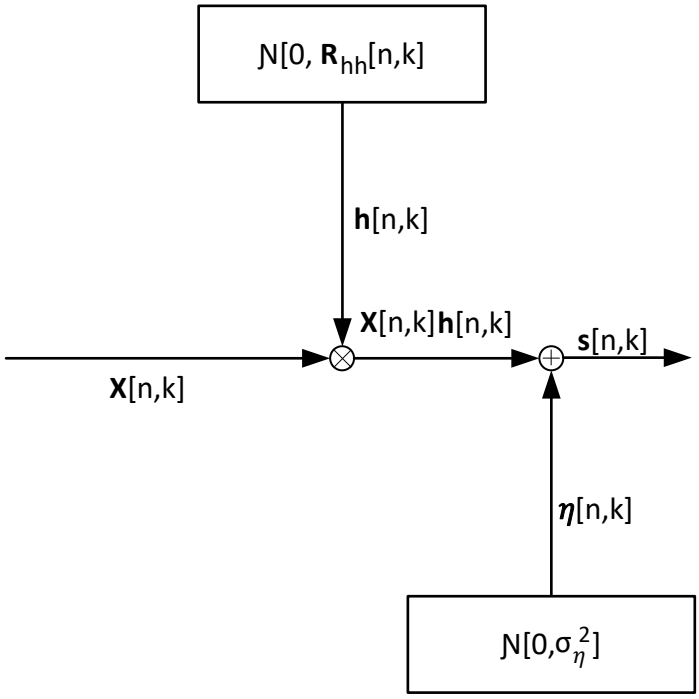

Fig. A.1 Channel representation for the waveform systems [163]

The possible auto- and cross-covariance matrices between the impulse response ($\boldsymbol{h}[n,k]$) and the output symbols ($\boldsymbol{s}[n,k]$) are defined as $\mathbf{R}_{hh}[n,k]$, $\mathbf{R}_{ss}[n,k]$, $\mathbf{R}_{hs}[n,k]$ and $\mathbf{R}_{sh}[n,k]$ respectively. $\mathbf{R}_{hh}[n,k]$ and $\mathbf{R}_{ss}[n,k]$ are the respective auto-covariance matrices of $\boldsymbol{h}[n,k]$ and $\boldsymbol{s}[n,k]$ while $\mathbf{R}_{hs}[n,k]$ and $\mathbf{R}_{sh}[n,k]$ are the two possible cross-covariance matrices between $\boldsymbol{h}[n,k]$ and $\boldsymbol{s}[n,k]$. The overall structured covariance matrix $\boldsymbol{R}[n,k]$ is given as:

$$\boldsymbol{R}[n,k] = \begin{bmatrix} \mathbf{R}_{hh}[n,k] & \mathbf{R}_{hs}[n,k] \\ W & W \\ \mathbf{R}_{sh}[n,k] & \mathbf{R}_{ss}[n,k] \end{bmatrix} \quad (A.10)$$

The inverse of the structured covariance matrix ($\boldsymbol{R}[n,k]$) can be obtained using the rule of "*inverse of a partitioned matrix*" and the "*Matrix inversion Lemma*" formula as given in [163]. In this rule, if $\boldsymbol{R}[n,k]$ is a partitioned matrix as represented in $(A.10)$, then $\boldsymbol{R}^{-1}[n,k]$ is generally given as:

$$\boldsymbol{R}^{-1} = \begin{bmatrix} \boldsymbol{A}^{-1} & \boldsymbol{B}\boldsymbol{D}^{-1} \\ W & W \\ \boldsymbol{D}^{-1}\boldsymbol{C} & \boldsymbol{D}^{-1} \end{bmatrix}$$

where

$$\boldsymbol{A} = \mathbf{R}_{hh}[n,k] - \mathbf{R}_{hs}[n,k]\mathbf{R}_{ss}{}^{-1}[n,k]\mathbf{R}_{sh}[n,k]$$

$$\boldsymbol{A}^{-1} = \mathbf{R}_{hh}{}^{-1}[n,k] + \boldsymbol{B}\boldsymbol{D}^{-1}\boldsymbol{C}$$

$$\mathbf{R}_{hh}[n,k]\boldsymbol{B} = -\mathbf{R}_{hs}[n,k] \quad (A.11)$$

$$\boldsymbol{C}\mathbf{R}_{hh}[n,k] = -\mathbf{R}_{sh}[n,k]$$

$$\boldsymbol{D} = \mathbf{R}_{hh}[n,k] - \mathbf{R}_{sh}[n,k]\mathbf{R}_{hh}{}^{-1}[n,k]\mathbf{R}_{hs}[n,k]$$

From the theorem of "partitioned matrix inverse",

$$\boldsymbol{R}^{-1}[n,k] = \begin{bmatrix} \mathbf{R}_{hh}{}^{-1}[n,k] & 0 \\ W & W \\ 0 & 0 \end{bmatrix} + \begin{bmatrix} \boldsymbol{B} \\ W \\ \boldsymbol{I}[m] \end{bmatrix} [\boldsymbol{D}^{-1}] \, [\boldsymbol{C} \quad \boldsymbol{I}[m]] \quad (A.12)$$

where $\boldsymbol{I}[m]$ is an $M \times M$ identity matrix. Direct substitution of all the expressions in $(A.11)$ into $(A.12)$ gives:

$$\boldsymbol{R}^{-1}[n,k] = \begin{bmatrix} \mathbf{R}_{hh}{}^{-1}[n,k] & 0 \\ W & W \\ 0 & 0 \end{bmatrix} + \begin{bmatrix} -\mathbf{R}_{hh}{}^{-1}[n,k]\mathbf{R}_{hs}[n,k] \\ W \\ I[m] \end{bmatrix} [\boldsymbol{D}^{-1}] \, [-\mathbf{R}_{sh}[n,k]\mathbf{R}_{hh}{}^{-1}[n,k] \quad \boldsymbol{I}[m]] \quad (A.13)$$

where in $(A.13)$, $\boldsymbol{D}$ is given as in $(A.11)$ and it is called the Schur component of $\mathbf{R}_{ss}[n,k]$. It also constitutes the noise variance $\sigma_\eta{}^2$. The linear expression given in $(A.3)$ can be represented in a matrix format as:

$$\begin{bmatrix} h[n,k] \\ W \\ s[n,k] \end{bmatrix} = \begin{bmatrix} \boldsymbol{I}[m] & 0 \\ W & W \\ \boldsymbol{X}[n,k] & \boldsymbol{I}[m] \end{bmatrix} \begin{bmatrix} h[n,k] \\ W \\ \eta[n,k] \end{bmatrix} \quad (A.14)$$

At this point, it is important to note that the structured covariance matrix is given as:

$$\boldsymbol{R}[n,k] = E\begin{bmatrix} h[n,k] \\ W \\ s[n,k] \end{bmatrix} [h^H[n,k] \quad s^H[n,k]] = \begin{bmatrix} \boldsymbol{I}[m] & 0 \\ W & W \\ \boldsymbol{X}[n,k] & \boldsymbol{I}[m] \end{bmatrix} \begin{bmatrix} \mathbf{R}_{hh}[n,k] & 0 \\ W & W \\ 0 & {\sigma_\eta}^2 \boldsymbol{I}[m] \end{bmatrix} \begin{bmatrix} \boldsymbol{I}[m] & \boldsymbol{X}^H[n,k] \\ W & W \\ \mathbf{0} & \boldsymbol{I}[m] \end{bmatrix}$$

$$= \begin{bmatrix} \mathbf{R}_{hh}[n,k] & \mathbf{R}_{hh}[n,k]\boldsymbol{X}^H[n,k] \\ W & W \\ \boldsymbol{X}[n,k]\mathbf{R}_{hh}[n,k] & \boldsymbol{X}[n,k]\mathbf{R}_{hh}[n,k]\boldsymbol{X}^H[n,k] + {\sigma_\eta}^2 \boldsymbol{I}[m] \end{bmatrix} = \begin{bmatrix} \mathbf{R}_{hh}[n,k] & \mathbf{R}_{hs}[n,k] \\ W & W \\ \mathbf{R}_{sh}[n,k] & \mathbf{R}_{ss}[n,k] \end{bmatrix} \quad (A.15)$$

where $(\cdot)^H$ denotes Hermitian transpose operator.

By comparing equations in $(A.15)$, the following equations are drawn up:

$$\mathbf{R}_{hs}[n,k] = E[hs^H] = \mathbf{R}_{hh}[n,k]\boldsymbol{X}^H[n,k] \quad (A.16)$$

$$\mathbf{R}_{sh}[n,k] = E[sh^H] = \mathbf{R}_{hh}[n,k]\,\boldsymbol{X}[n,k] \quad (A.17)$$

$$\mathbf{R}_{ss}[n,k] = E[ss^H] = \boldsymbol{X}[n,k]\mathbf{R}_{hh}[n,k]\boldsymbol{X}^H[n,k] + {\sigma_\eta}^2 \boldsymbol{I}[m] \quad (A.18)$$

From the Weiner-Hopf equation, the linear MMSE estimator of $\boldsymbol{h}[n,k]$ satisfies the orthogonality condition [163]:

$$E\left[(\boldsymbol{h}[n,k] - \boldsymbol{\Xi}[n,k]\boldsymbol{s}[n,k])\boldsymbol{s}^H[n,k]\right] = 0 \quad (A.19)$$

where $\boldsymbol{\Xi}[n,k]$ is a matrix that satisfies a Weiner-Hopf equation. In order to determine $\boldsymbol{\Xi}[n,k]$, the orthogonality condition given in $(A.19)$ may be expressed as [163]:

$$\mathbf{R}_{hs}[n,k] - \boldsymbol{\Xi}[n,k]\mathbf{R}_{ss}[n,k] = 0$$

$$\boldsymbol{\Xi}[n,k] = \mathbf{R}_{hs}[n,k]{\mathbf{R}_{ss}}^{-1}[n,k] \quad (A.20)$$

For a Gaussian and uncorrelated channel vector $h[n,k]$ with channel noise η as already defined, we can conclude by saying the linear estimator that minimizes the MSE is given as [163 - 165]:

$$\widehat{\boldsymbol{h}}_{LMMSE}[n,k] = \boldsymbol{\Xi}[n,k]\boldsymbol{s}[n,k] = \mathbf{R}_{hs}[n,k]\,{\mathbf{R}_{ss}}^{-1}[n,k]\,\boldsymbol{s}[n,k] \quad (A.21)$$

Substituting $(A.16)$ and $(A.18)$ into $(A.21)$ yields:

$$\widehat{\boldsymbol{h}}_{LMMSE}[n,k] = \mathbf{R}_{hh}[n,k]\boldsymbol{X}^H[n,k]\left[\boldsymbol{X}[n,k]\mathbf{R}_{hh}[n,k]\boldsymbol{X}^H[n,k] + {\sigma_\eta}^2\boldsymbol{I}[m]\right]^{-1}\boldsymbol{s}[n,k]$$

$$= \frac{\mathbf{R}_{hh}[n,k]\boldsymbol{X}^H[n,k]\boldsymbol{s}[n,k]}{\boldsymbol{X}[n,k]\mathbf{R}_{hh}[n,k]\boldsymbol{X}^H[n,k] + {\sigma_\eta}^2\boldsymbol{I}[m]}$$

$$= \frac{\mathbf{R}_{hh}[n,k]\boldsymbol{X}^{H}[n,k]\boldsymbol{s}[n,k]}{\boldsymbol{X}[n,k]\boldsymbol{X}^{H}[n,k]\left[\boldsymbol{R}_{hh}[n,k] + \ (\boldsymbol{X}^{H}[n,k]\boldsymbol{X}[n,k])^{-1}{\sigma_{\eta}}^{2}\boldsymbol{I}[m]\right]}$$

$$\widehat{\boldsymbol{h}}_{LMMSE}[n,k] = \frac{\boldsymbol{R}_{hh}[n,k]\ \boldsymbol{s}[n,k]}{\boldsymbol{X}[n,k]\left[\boldsymbol{R}_{hh}[n,k] + \ (\boldsymbol{X}^{H}[n,k]\boldsymbol{X}[n,k])^{-1}{\sigma_{\eta}}^{2}\boldsymbol{I}[m]\right]} \qquad (A.22)$$

Appendix B: *Mathematical Derivation of LMS Algorithm For FBMC/OQAM systems*

Equation $(B.1)$ is obtained from (4.71). This equation is expressed as:

$$\boldsymbol{J}(\boldsymbol{n}) = E\{(s[n,k] - \hat{h}^H[n,k]x[n,k])(s^*[n,k] - \hat{h}[n,k]x^H[n,k])\} \quad (B.1)$$

$$= E\left[(s[n,k]s^*[n,k]) - (s[n,k]\hat{h}[n,k]x^H[n,k]) - (s^*[n,k]\hat{h}^H[n,k]x[n,k]) + \hat{h}^H[n,k]x[n,k]\,\hat{h}[n,k]x^H[n,k]\right]$$

$$= E[(s[n,k]s^*[n,k])] - E\left[(s[n,k]\hat{h}[n,k]x^H[n,k])\right] - E\left[(s^*[n,k]\hat{h}^H[n,k]x[n,k])\right] + E\left[(\hat{h}^H[n,k]x[n,k]\,\hat{h}[n,k]x^H[n,k])\right]$$

$$= E[(s[n,k]s^*[n,k])] - \hat{h}[n,k]E[(s[n,k]x^H[n,k])] - \hat{h}^H[n,k]E[(s^*[n,k]x[n,k])] + \hat{h}^H[n,k]\hat{h}[n,k]E[(x[n,k]\,x^H[n,k])] \quad (B.2)$$

If the input symbols $x[n,k]$ and the FBMC/OQAM output $s[n,k]$ are jointly stationary, each expectation values in $\boldsymbol{J}(\boldsymbol{n})$ can be defined as [153]:

i) If $s[n,k]$ has zero mean, then

$$\sigma_s^2 = E[(s[n,k]s^*[n,k])] \quad (B.3)$$

ii) If $\boldsymbol{p}$ represents the $M \times 1$ cross-correlation vector between $x[n,k]$ and $s[n,k]$, then

$$\boldsymbol{p} = E[(s^*[n,k]x[n,k])] \quad (B.4)$$

iii) From $(B.4)$,

$$\boldsymbol{p}^H = E[(s[n,k]x^H[n,k])] \quad (B.5)$$

iv) The $M \times M$ correlation matrix between the input signals $x[n,k]$ is defined as:

$$\mathfrak{R}[n,k] = E\left[x[n,k]x^H[n,k]\right] \quad (B.6)$$

Substituting $(B.3) - (B.6)$ into $(B.2)$, the cost function to be minimized becomes

$$\boldsymbol{J}(\boldsymbol{n}) = \sigma_s^2 - \boldsymbol{p}^H\hat{h}[n,k] - \boldsymbol{p}\hat{h}^H[n,k] + \hat{h}^H[n,k]\hat{h}[n,k]\mathfrak{R}[n,k] \quad (B.7)$$

Differentiating the MSE (i.e. $(B.7)$) with respect to (wrt) $h[n,k]$, the gradient $\boldsymbol{\nabla}[n,k]$ is obtained as:

$$\boldsymbol{\nabla}[n,k] = \frac{d\boldsymbol{J}(\boldsymbol{n})}{d\hat{h}[n,k]} = -2\boldsymbol{p} + 2\boldsymbol{\mathfrak{R}}[k,n]\hat{h}[n,k] \qquad (B.8)$$

Equation $(B.8)$ is obtained from differentiation wrt a vector. The following expressions must be put to consideration when differentiating wrt a vector.

$$\frac{d(\boldsymbol{p}^H\hat{h}[n,k])}{d\hat{h}[n,k]} = 0 \qquad (B.9)$$

$$\frac{d(\boldsymbol{p}\hat{h}[n,k])}{d\hat{h}[n,k]} = 2\boldsymbol{p} \qquad (B.10)$$

$$\frac{d(\hat{h}[n,k]\hat{h}^H[n,k]\boldsymbol{\mathfrak{R}}[k,n])}{d\hat{h}[n,k]} = 2\boldsymbol{\mathfrak{R}}[k,n]\hat{h}[n,k] \qquad (B.11)$$

If we consider instantaneous estimates for $\boldsymbol{\mathfrak{R}}[k,n]$ and $\boldsymbol{p}$, then we define both as [153]:

$$\widehat{\boldsymbol{\mathfrak{R}}}[n,k] = x[n,k]\, x^H[n,k] \qquad (B.12)$$

$$\widehat{\boldsymbol{p}}[n,k] = x[n,k]\, s^*[n,k] \qquad (B.13)$$

From $(B.8)$, the instantaneous estimate of $\boldsymbol{\nabla}[n,k]$ is given as:

$$\begin{aligned}\widehat{\boldsymbol{\nabla}}[n,k] &= -2\widehat{\boldsymbol{p}}[n,k] + 2\widehat{\boldsymbol{\mathfrak{R}}}[n,k]\hat{h}[n,k] \\ &= -2x[n,k]\, s^*[n,k] + 2x[n,k]\, x^H[n,k]\hat{h}[n,k] \qquad (B.14)\end{aligned}$$

According to the method of steepest descent, the updated value of the channel impulse response vector at time $(n+1)$ is obtained using:

$$\widehat{\boldsymbol{h}}_{LMS}[n+1,k] = \hat{h}[n,k] + \frac{1}{2}\mu\left[-\widehat{\boldsymbol{\nabla}}[n,k]\right] \qquad (B.15)$$

where μ is the step size parameter that assumes a positive real-valued constant. It is important to note that the estimate expressed in $(B.14)$ is unbiased and also equals the true value of the gradient as expressed in $(B.8)$. Substituting $(B.14)$ into $(B.15)$ gives:

$$\widehat{\boldsymbol{h}}_{LMS}[n+1,k] = \hat{h}[n,k] + \frac{1}{2}\mu\left[2x[n,k]\, s^{*}[n,k] - 2x[n,k]\, x^{H}[n,k]\hat{h}[n,k]\right]$$

$$= \hat{h}[n,k] + \mu x[n,k]\, s^{*}[n,k] - \mu x[n,k]\, x^{H}[n,k]\hat{h}[n,k]$$

$$= \hat{h}[n,k] + \mu x[n,k]\left[s^{*}[n,k] - x^{H}[n,k]\hat{h}[n,k]\right] \qquad (B.16)$$

Substituting (4.72) into $(B.16)$ gives

$$\widehat{\boldsymbol{h}}_{LMS}[n+1,k] = \hat{h}[n,k] + \mu \boldsymbol{e}^{*}[n,k]x[n,k] \qquad (B.17)$$

This confirms the LMS algorithm as expressed in (4.73).

Appendix C: *Mathematical Derivation of RLS Algorithm For FBMC/OQAM systems*

As indicated in Appendix B, the $M \times M$ correlation matrix ($\mathfrak{R}[n,k]$) between the input signals $x[n,k]$ is defined in $(B.6)$. For RLS channel estimation, the product ($\boldsymbol{x}[n,k]\boldsymbol{x}^H[n,k]$) is weighed by the exponential factor λ^{n-k} to obtain $\mathfrak{R}[n,k]$ given as:

$$\mathfrak{R}[n,k] = \sum_{k=1}^{n} \lambda^{n-k} x[n,k] x^H[n,k] \qquad (C.1)$$

If the term corresponding to $n = k$ is isolated from the summation in $(C.1)$, the correlation matrix $\mathfrak{R}[n,k]$ is expressed as:

$$\mathfrak{R}[n,k] = \lambda \left[\sum_{k=1}^{n-1} \lambda^{n-k-1} x[n,k] x^H[n,k] \right] + x[n,k] x^H[n,k] \qquad (C.2)$$

Comparing $(C.2)$ and $(C.1)$, we can conclude that

$$\mathfrak{R}[n-1,k] = \sum_{k=1}^{n-1} \lambda^{n-k-1} x[n,k] x^H[n,k] \qquad (C.3)$$

From these expressions, the correlation matrix $\mathfrak{R}[n,k]$ is expressed as:

$$\mathfrak{R}[n,k] = \lambda\, \mathfrak{R}[n-1,k] + x[n,k] x^H[n,k] \qquad (C.4)$$

The expression in $(C.4)$ is used for updating the value of the deterministic correlation matrix. In order to obtain the RLS channel estimate ($\widehat{\boldsymbol{h}}_{RLS}[n,k]$), the inverse of the correlation matrix ($\mathfrak{R}^{-1}[n,k]$) must be obtained. To obtain the RLS channel estimates, the use of *matrix inversion lemma* (MIL) is employed. The MIL is summarized as follows:

If $\boldsymbol{Y}$ and $\boldsymbol{Z}$ are two positive-definite $M \times M$ matrices given by

$$\boldsymbol{Y} = \boldsymbol{Z^{-1}} + \boldsymbol{UV^{-1}U^H} \qquad (C.5)$$

where $\boldsymbol{V}$ is a small positive-definite $N \times N$ matrix and $\boldsymbol{U}$ is an $M \times N$ matrix, then from MIL, the inverse of $\boldsymbol{Y}$ is obtained as:

$$\boldsymbol{Y^{-1}} = \boldsymbol{Z} - \boldsymbol{ZU}(\boldsymbol{V} + \boldsymbol{U^H ZU})^{-1}\boldsymbol{U^H Z} \qquad (C.6)$$

where the product of $(C.5)$ and $(C.6)$ equals one (i.e. $\boldsymbol{YY^{-1}} = 1$) shows the proof of the MIL. This MIL can then be applied to $(C.4)$ so as to obtain the inverse correlation matrix $\mathfrak{R}^{-1}[n,k]$. The following substitutions are made [153]:

$\boldsymbol{Y} = \mathfrak{R}[n,k],\ \boldsymbol{U} = \boldsymbol{x}[n,k], \mathbf{Z}^{-1} = \lambda\,\mathfrak{R}[n-1,k], \boldsymbol{V} = 1.$ Therefore $\mathfrak{R}^{-1}[n,k]$ is given as:

$$\mathfrak{R}^{-1}[n,k] = \left[\lambda\,\mathfrak{R}[n-1,k]\right]^{-1} - \left(\left[\lambda\mathfrak{R}[n-1,k]\right]^{-1}\boldsymbol{x}[n,k]\left(1 + \boldsymbol{x}^H[n,k]\left[\lambda\mathfrak{R}[n-1,k]\right]^{-1}\boldsymbol{x}[n,k]\right)^{-1}\right)\boldsymbol{x}^H[n,k]\left[\lambda\mathfrak{R}[n-1,k]\right]^{-1}$$

$$= \lambda^{-1}\mathfrak{R}^{-1}[n-1,k] - (\lambda^{-1}\mathfrak{R}^{-1}[n-1,k]\boldsymbol{x}[n,k](1 + \boldsymbol{x}^H[n,k]\lambda^{-1}\mathfrak{R}^{-1}[n-1,k]\boldsymbol{x}[n,k])^{-1})\boldsymbol{x}^H[n,k]\lambda^{-1}\mathfrak{R}^{-1}[n-1,k]$$

$$= \lambda^{-1}\mathfrak{R}^{-1}[n-1,k] - \left[\frac{\lambda^{-1}\mathfrak{R}^{-1}[n-1,k]\boldsymbol{x}[n,k]\boldsymbol{x}^H[n,k]\,\lambda^{-1}\mathfrak{R}^{-1}[n-1,k]}{1 + \boldsymbol{x}^H[n,k]\,\lambda^{-1}\mathfrak{R}^{-1}[n-1,k]\boldsymbol{x}[n,k]}\right]$$

$$\mathfrak{R}^{-1}[n,k] = \lambda^{-1}\mathfrak{R}^{-1}[n-1,k] - \left[\frac{\lambda^{-2}\mathfrak{R}^{-1}[n-1,k]\boldsymbol{x}[n,k]\boldsymbol{x}^H[n,k]\,\mathfrak{R}^{-1}[n-1,k]}{1 + \boldsymbol{x}^H[n,k]\,\lambda^{-1}\mathfrak{R}^{-1}[n-1,k]\boldsymbol{x}[n,k]}\right] \qquad (C.7)$$

For computational convenience, the inverse correlation matrix $\mathfrak{R}^{-1}[n,k]$ is made to equal $\boldsymbol{\rho}[n,k]$ which is expressed as:

$$\boldsymbol{\rho}[n,k] = \mathfrak{R}^{-1}[n,k] \qquad (C.8)$$

$$\boldsymbol{\rho}[n-1,k] = \mathfrak{R}^{-1}[n-1,k] \qquad (C.9)$$

From $(C.7)$, let

$$\tilde{\boldsymbol{g}}[n,k] = \frac{\lambda^{-1}\mathfrak{R}^{-1}[n-1,k]\boldsymbol{x}[n,k]}{1 + \boldsymbol{x}^H[n,k]\,\lambda^{-1}\mathfrak{R}^{-1}[n-1,k]\boldsymbol{x}[n,k]}$$

$$= \frac{\lambda^{-1}\boldsymbol{\rho}[n-1,k]\boldsymbol{x}[n,k]}{1 + \boldsymbol{x}^H[n,k]\,\lambda^{-1}\boldsymbol{\rho}[n-1,k]\boldsymbol{x}[n,k]} \qquad (C.10)$$

where $\tilde{\boldsymbol{g}}[n,k]$ is the gain vector. Hence the inverse autocorrelation matrix is obtained by simple substitution of $(C.8)$, $(C.9)$ and $(C.10)$ into $(C.7)$ as:

$$\boldsymbol{\rho}[n,k] = \lambda^{-1}\boldsymbol{\rho}[n-1,k] - \lambda^{-1}\,\tilde{\boldsymbol{g}}[n,k]\boldsymbol{x}^{H}[n,k]\boldsymbol{\rho}[n-1,k] \qquad (C.11)$$

Equation $(C.11)$ is also given as:

$$\boldsymbol{\Re}^{-1}[n,k] = \lambda^{-1}\boldsymbol{\Re}^{-1}[n-1,k] - \lambda^{-1}\,\tilde{\boldsymbol{g}}[n,k]\boldsymbol{x}^{H}[n,k]\boldsymbol{\Re}^{-1}[n-1,k] \qquad (C.12)$$

From $(C.10)$,

$$\tilde{\boldsymbol{g}}[n,k](1 + \boldsymbol{x}^{H}[n,k]\,\lambda^{-1}\boldsymbol{\rho}[n-1,k]\boldsymbol{x}[n,k]) = \lambda^{-1}\boldsymbol{\rho}[n-1,k]\boldsymbol{x}[n,k]$$

$$\tilde{\boldsymbol{g}}[n,k] + \tilde{\boldsymbol{g}}[n,k]\boldsymbol{x}^{H}[n,k]\,\lambda^{-1}\boldsymbol{\rho}[n-1,k]\boldsymbol{x}[n,k] = \lambda^{-1}\boldsymbol{\rho}[n-1,k]\boldsymbol{x}[n,k]$$

$$\tilde{\boldsymbol{g}}[n,k] = \lambda^{-1}\boldsymbol{\rho}[n-1,k]\boldsymbol{x}[n,k] - \tilde{\boldsymbol{g}}[n,k]\boldsymbol{x}^{H}[n,k]\,\lambda^{-1}\boldsymbol{\rho}[n-1,k]\boldsymbol{x}[n,k]$$

$$\tilde{\boldsymbol{g}}[n,k] = \boldsymbol{x}[n,k]\left[\lambda^{-1}\boldsymbol{\rho}[n-1,k] - \tilde{\boldsymbol{g}}[n,k]\boldsymbol{x}^{H}[n,k]\,\lambda^{-1}\boldsymbol{\rho}[n-1,k]\right] \qquad (C.13)$$

Substituting $(C.11)$ into $(C.13)$ gives

$$\tilde{\boldsymbol{g}}[n,k] = \boldsymbol{\rho}[n,k]\boldsymbol{x}[n,k] \qquad (C.14)$$

The optimum RLS channel estimate is obtained when the performance index as in (4.75) attains its minimum value when $(C.15)$ is defined [153]:

$$\widehat{\boldsymbol{h}}_{RLS}[n,k] = \boldsymbol{\Re}^{-1}[n,k]\boldsymbol{\omega}[n,k] \qquad (C.15)$$

where $\boldsymbol{\omega}[n,k]$ is simply defined as the $M \times 1$ cross-correlation vector between the FBMC/OQAM symbols and its desired response $s[n,k]$ and can be compared to $(C.1)$ by:

$$\boldsymbol{\omega}[n,k] = \sum_{k=1}^{n} \lambda^{n-k} x[n,k]s^{*}[n,k] \qquad (C.16)$$

where * denotes complex conjugation. In a similar manner, $\boldsymbol{\omega}[n,k]$ can be similarly expressed in comparison to $\boldsymbol{\Re}[n,k]$ as in $(C.4)$, hence

$$\boldsymbol{\omega}[n,k] = \lambda\boldsymbol{\omega}[n-1,k] + x[n,k]s^{*}[n,k] \qquad (C.17)$$

Substituting $(C.17)$ into $(C.15)$, we obtain

$$\widehat{\boldsymbol{h}}_{RLS}[n,k] = \boldsymbol{\mathfrak{R}}^{-1}[n,k]\left[\lambda\boldsymbol{\omega}[n-1,k] + x[n,k]s^{*}[n,k]\right] \quad (C.18)$$

$$= \boldsymbol{\rho}[n,k]\left[\lambda\boldsymbol{\omega}[n-1,k] + x[n,k]s^{*}[n,k]\right]$$

$$= \lambda\boldsymbol{\rho}[n,k]\boldsymbol{\omega}[n-1,k] + \boldsymbol{\rho}[n,k]x[n,k]s^{*}[n,k] \quad (C.19)$$

Substituting $(C.11)$ into $(C.19)$,

$$\widehat{\boldsymbol{h}}_{RLS}[n,k] = \lambda\left[\lambda^{-1}\boldsymbol{\rho}[n-1,k] - \lambda^{-1}\,\widetilde{\boldsymbol{g}}[n,k]x^{H}[n,k]\boldsymbol{\rho}[n-1,k]\right]\boldsymbol{\omega}[n-1,k] + \boldsymbol{\rho}[n,k]x[n,k]s^{*}[n,k]$$

$$= \left[\boldsymbol{\rho}[n-1,k] - \widetilde{\boldsymbol{g}}[n,k]x^{H}[n,k]\boldsymbol{\rho}[n-1,k]\right]\boldsymbol{\omega}[n-1,k] + \boldsymbol{\rho}[n,k]x[n,k]s^{*}[n,k]$$

$$= \boldsymbol{\rho}[n-1,k]\boldsymbol{\omega}[n-1,k] - \widetilde{\boldsymbol{g}}[n,k]x^{H}[n,k]\boldsymbol{\rho}[n-1,k]\boldsymbol{\omega}[n-1,k] + \boldsymbol{\rho}[n,k]x[n,k]s^{*}[n,k]$$

$$= \boldsymbol{\mathfrak{R}}^{-1}[n-1,k]\boldsymbol{\omega}[n-1,k] - \widetilde{\boldsymbol{g}}[n,k]x^{H}[n,k]\boldsymbol{\mathfrak{R}}^{-1}[n-1,k]\boldsymbol{\omega}[n-1,k] + \boldsymbol{\rho}[n,k]x[n,k]s^{*}[n,k] \quad (C.20)$$

The following is derived similarly to $(C.15)$

$$\widehat{\boldsymbol{h}}[n-1,k] = \boldsymbol{\mathfrak{R}}^{-1}[n-1,k]\boldsymbol{\omega}[n-1,k] \quad (C.21)$$

Substituting $(C.21)$ into $(C.20)$ gives

$$\widehat{\boldsymbol{h}}_{RLS}[n,k] = \hat{h}[n-1,k] - \widetilde{\boldsymbol{g}}[n,k]x^{H}[n,k]\hat{h}[n-1,k] + \boldsymbol{\rho}[n,k]x[n,k]s^{*}[n,k] \quad (C.22)$$

Substituting $(C.14)$ into $(C.22)$ gives

$$\widehat{\boldsymbol{h}}_{RLS}[n,k] = \hat{h}[n-1,k] - \widetilde{\boldsymbol{g}}[n,k]x^{H}[n,k]\hat{h}[n-1,k] + \boldsymbol{\rho}[n,k]x[n,k]s^{*}[n,k]$$

$$= \hat{h}[n-1,k] - \widetilde{\boldsymbol{g}}[n,k]x^{H}[n,k]\hat{h}[n-1,k] + \widetilde{\boldsymbol{g}}[n,k]s^{*}[n,k]$$

$$= \hat{h}[n-1,k] + \widetilde{\boldsymbol{g}}[n,k]\left[s^{*}[n,k] - x^{H}[n,k]\hat{h}[n-1,k]\right] \quad (C.23)$$

Substituting (4.72) into $(C.23)$ gives:

$$\widehat{\boldsymbol{h}}_{RLS}[n,k] = \widehat{\boldsymbol{h}}[n-1,k] + \widetilde{\boldsymbol{g}}[n,k]\boldsymbol{e}^{*}[n,k] \qquad (C.24)$$

This is the expression for obtaining fading channel coefficients using RLS for the FBMC/OQAM based transceiver.